INTERACTIONS BETWEEN LONG AND SYNOPTIC-SCALE WAVES IN A SIMPLE MODEL

by

Wesley Nobuo Ebisuzaki

B.Sc. University of Toronto, Toronto
(1979)

Submitted to the Department of Earth, Atmospheric,
and Planetary Sciences in Partial Fulfillment
of the Requirements of the Degree of

Doctor of Philosophy

at the Massachusetts Institute of Technology

November 18, 1986

Signature of Author _____
Dept. of Earth, Atmospheric, and Planetary Sciences
November 1986

Certified by _____
R. M. Dole
Thesis Supervisor

Certified by _____
D. E. Harrison
Thesis Supervisor

Accepted by _____
Chairman, Department Committee on Graduate Students

INTERACTIONS BETWEEN LONG AND SYNOPTIC-SCALE WAVES IN A SIMPLE MODEL

by

Wesley Nobuo Ebisuzaki

Submitted to the Department of Earth, Atmospheric, and Planetary Sciences on November 18, 1986 in partial fulfillment of the requirements for the degree of Doctor of Philosophy.

ABSTRACT:

General circulation model (GCM) studies have examined the growth of disturbances in initially zonally symmetric basic states. Several studies (e.g. Gall et al. 1979b; MacVean 1985) used hemispheric GCMs which did not include orography, land-sea contrasts or any geographically fixed features. An unexpected finding in these studies was that after several days of model integration, long waves (i.e. scales of zonal wavenumbers k = 1 to 5) grew faster than predicted by linear theory. In some cases, the long waves grew more rapidly than any normal mode. Gall et al. and later MacVean suggested that this fast growth was caused by interactions with synoptic-scale waves (i.e. scales of zonal wavenumbers k $\simeq$ 8 to 20). In this thesis, we use both analytic and numerical methods to study the synoptic/planetary-scale interactions in an attempt to better understand the unexpectedly fast growth of long waves as found by the GCM experiments.

For our theoretical analysis, we employ a two-level quasi-geostrophic beta-plane model. In our model, we assume that the amplitude of the long wave varies on a time scale that is slow compared with the period of the more unstable synoptic-scale waves. In addition, we assume that the synoptic-scale waves are inviscidly unstable, but are rendered neutral by dissipation (i.e., a modified baroclinic adjustment holds). The model is then used to address the following sequence of questions: first, how a long wave spatially modulates a synoptic-scale wave; second, how the fluxes of that synoptic-scale wave vary on the planetary scale; and finally how those fluxes may themselves alter the evolution of the original transient long wave.

In the first part of the thesis, we examine a synoptic-scale wave growing in the presence of a fixed long wave. We find planetary-scale modulations of the amplitude, local wavelength, and vertical tilt of the synoptic-scale wave. Our results are consistent with previous findings, but since the parameter dependences are readily apparent in our analysis, we are to provide additional physical interpretations of the previous results.

In the second part of our analysis, we use the results from the first part to find heat and relative vorticity fluxes of the synoptic-scale wave. These fluxes, which have a planetary-scale modulation, can directly force the long wave. In the third part, we find that these fluxes may alter the vertical structure of the long wave which can then become more capable of extracting zonal available potential energy (ZAPE). (The synoptic-scale waves are essentially catalytic.) We conclude that by altering the

structure of the long wave, synoptic-scale waves can increase the growth rate of long waves. This provides a possible basis for the unexpectedly rapid growth of the long waves in the GCM experiments.

We then proceed to examine the results of a nonlinear time-dependent numerical model. The modeling results support our previous findings. In particular, the baroclinic adjustment hypothesis, a cornerstone of our analysis, was found to hold under conditions defined later. In addition, the energy fluxes of the long/synoptic-scale interactions compared favorably with the theory's predictions when the long waves were weaker than the synoptic-scale waves.

We have also examined the interaction of topographically forced waves with synoptic-scale waves. According to our model, non-resonant long waves are not sensitive to the synoptic-scale waves in the sense that small eddy fluxes produce only small changes in the long waves. Near resonance, however, the stationary long waves were sensitive to the synoptic-scale waves, as well as to all other factors.

Based on our analytic and modeling results, we conclude that the baroclinic adjustment hypothesis can be a good approximation, the effect of inviscidly unstable synoptic-scale waves on long waves can differ greatly from the effect of inviscidly neutral waves, and that the synoptic-scale waves can help destabilize transient long waves through a mutual interaction process.

Thesis Supervisor: Dr. Randall M. Dole
Title: Professor of Meteorology

Thesis Supervisor: Dr. D. E. Harrison
Title: Research Scientist

Acknowledgements

I happily acknowledge that this thesis would not have been possible without the help of my advisors, Drs. Harrison and Dole. This thesis had its genesis with Dr. Lorenz who started me thinking about the role of moisture in the large-scale circulation. Conversations with Dr. Lindzen were useful for they helped sharpen my thinking, and increased my understanding of the atmosphere and assumptions implicit in this thesis.

My fellow students were a pleasure to know. Discussions with Ted Shepherd, Peter Neilley, Rennie Selkirk, Steve Garner, and Bill Gutowski were always a source of stimulating ideas.

The research in this thesis was partially supported by NSF grant OCE 83-01787, NASA grant NAG5-322, and Air Force grant AF-ESD-C F19628-83-K-0012.

Table of Contents

Symbol List

β	beta, df/dy
Ψ	streamfunction, for two-layer model:
θ	thermal streamfunction, for two-layer model:
θ_e	radiative equilibrium thermal streamfunction
ε	length scale parameter, $L_{syn}/L_{ps} << 1$
δ	strength of basic-state wave, $\|U'\|/\|U\| << 1$
ρ	density
co	$\theta_{syn} / \Psi_{syn}$
coi	imag(co)
cor	real(co)
f	coriolis parameter
F	Froude number
Fr	friction
g	acceleration by gravity
H	density scale height
J	jacobian, $J(A, B) = \frac{dA}{dx}\frac{dB}{dy} - \frac{dA}{dy}\frac{dB}{dx}$
k,l	zonal and meridional wavenumbers
k_o	$2\pi / X$, smallest k in the model
K^2	$\langle k \rangle^2 + l^2$
ki	imag(k)
kr	real(k)
L_{syn}	synoptic length scale
L_{ps}	planetary length scale
l_o	π / Y, smallest l in the model
M	$K^2 (K^2 + 2F)$

N	Brunt-Vaisala frequency
p	pressure
q,Q	diabatic heating
t	time
t_d	time scale of dissipative processes
t_{rad}	time scale of radiative cooling
u	zonal wind
U	zonal wind of the basic state
<U>	zonally averaged U
Ut	thermal wind of the basic state
v	meridional wind
V	meridional wind of the basic state
w	frequency (complex)
ω	vertical velocity in pressure coordinates $\frac{Dp}{DT}$
wi	imag(w), growth rate
wr	real(w), frequency
x	distance along the zonal direction
X	length of the periodic beta-plane channel, or a slowly varying x variable
y	distance along the meridional direction
Y	width of the beta-plane channel
$\frac{\partial}{\partial x}$	partial derivative with respect to x
$\frac{D}{DT}$	derivative with respect to T
∇^2	Laplacian operator
$(..)_{ps}$	variable associated with the planetary scales
$(..)_{syn}$	variable associated with the synoptic scales

List of Figures

List of Tables

Chapter 1

Introduction

General circulation model (GCM) studies have examined the growth of disturbances on initially zonal symmetric basic states. Early work by **Gall et al.** (1979a, b) used a hemispheric GCM with neither mountains nor land-sea contrasts. The initial conditions were a zonal symmetric flow with small random perturbations. Initially, the fastest growing disturbances had wavenumbers between 5 and 20 - these have been frequently linked with baroclinically unstable synoptic-scale waves. The long waves ($k < 5$), on the other hand, initially tended to decay. After about 10 model days, however, the long waves grew faster than predicted by linear theory, and sometimes grew faster than any linear normal mode. These long waves were mid-latitude tropospheric disturbances with synoptic meridional scales (Gall et al., 1979b). We shall call these disturbances "planetary-scale waves" or "long waves."

These growing long waves could not be due to topography for the GCM had no mountains or oceans. The internal dynamics must somehow enhance the growth rate. **Gall et al.** (1979b) suggested that cyclone-scale disturbances could be forcing the long waves to grow faster than expected by linear theory. They stated, "[These cyclones are] manifestations of the portion of the spectrum that is growing by baroclinic instability." Generally, these cyclones will vary in strength and will be unequally spaced around a latitude circle. Hence, their heat flux will be unevenly distributed about the hemisphere, with maxima associated with stronger cyclones. This unsymmetric heat flux could directly force the planetary-scale waves. The strongest evidence was that the structure of the long waves was consistent

with forcing by the cyclones' heat fluxes. Unfortunately, their analysis was not complete. They did not show that the cyclones added APE to the long waves (i.e., force the waves), nor did they show that the response (long waves) had the frequency of the forcing (cyclones). Such calculations could either invalidate their hypothetical mechanism, or yield more supporting evidence for the mechanism as suggested by **Gall et al.**.

MacVean (1985) performed an experiment similar to **Gall et al.** (1979a, b). MacVean, however, could vary the horizontal resolution of the GCM. He found, to no great surprise, that the growth was initially linear with the most linearly unstable modes (i.e. synoptic-scale waves) growing fastest. By about day 15, however, the long waves were growing faster than predicted by linear theory. Moreover, MacVean found that the low-resolution model only predicted a slow growth for the long waves. Since the low-resolution GCM did not include synoptic-scale waves, MacVean concluded that the presence of synoptic-scale waves could enhance the growth of the long waves.

Young and Villere (1985) used a spherical GCM, and also found the long waves grew faster than predicted by linear theory. Moreover, when the GCM neglected the wave-wave interactions, the long waves grew slowly, at rates consistent with linear theory. They concluded that wave-wave interactions can be important for the growth of the long waves.

In all these GCM studies, the long waves grew faster than predicted by linear theory (until the flow began to 'equilibrate'). These long waves were mainly confined to the troposphere, and had synoptic-scale meridional lengths. In addition, Young and Villere (1985) suggested that wave-wave interactions were responsible for the growth of long wave, and MacVean (1985) suggested that the synoptic-scale waves were important. Unfortu-

nately, the GCM output has been insufficiently analyzed, and the analysis has neither fully confirmed nor disproved the mechanism suggested by **Gall et al.** (1979b). However, these GCM studies do suggest that the synoptic/planetary-scale interactions may be important for determining the growth and behavior of long waves.

The general goal of this thesis is to explain the interactions of the "planetary-scale" and the synoptic-scale waves. To accomplish this goal, we will use a simple model in hopes of understanding the first order effects of these interactions.

The problems we wish to consider are intrinsically nonlinear. To circumvent some of the primary problems associated with nonlinearity, we will use a simple model, the two-level quasi-geostrophic beta-plane model. We will also assume that the synoptic-scale waves have zonal scales shorter than the long waves. Furthermore, we will assume that the amplitude of the long wave varies on a time scale that is slow compared with the period of a synoptic-scale wave. These assumptions allow us to apply WKB techniques to find how the planetary-scale waves modulate the synoptic-scale waves. We use this result to parameterize the effects of the synoptic eddies, and then determine its effect on the linear growth of the long waves.

Basically, we will approach the problem of the synoptic/planetary-scale interactions using WKB and multiple-time-scale techniques. The latter requires that the synoptic-scale waves cannot grow on a fast time scale; otherwise, the synoptic-eddy fluxes would also change on the fast time scale, and ruin the time-scale separation. To avoid this problem, we will assume that the zonal flow has equilibrated to a state where the most unstable modes have a near zero growth rate. (This assumption is examined in chapter 5.) This zonal flow could be achieved by a modified

baroclinic adjustment (Stone, 1978). In Stone's adjustment, unstable modes would grow and eventually stabilize the zonal flow by their heat fluxes. On the other hand, if all modes were decaying, radiative forcing will eventually destabilize the flow, and allow unstable modes to neutralize the instability.

A specific goal of this thesis is to determine potential mechanisms by which the synoptic-scale waves could 'destabilize' the long waves in the GCM experiments. Based on our analysis, we conclude that a symbiotic, nonlinear interaction between synoptic- and planetary-scale waves can help destabilize the planetary-scale waves. On the fast time scale, the synoptic-scale waves see a "basic state" which consists of the zonal flow and a pre-existing long wave. This "basic state" will spatially modulate the synoptic-scale wave, and produce planetary-scale variations in the heat and relative-vorticity fluxes of the synoptic-scale wave. These fluxes can then alter the long wave on the slow time scale.

At first glance, the evidence for a symbiotic interaction between the synoptic-scale and long waves appears weak. For example, the atmospheric transient eddies reduce the APE in the stationary waves with time scale of 1.5 to 4.5 days (winter; Lau, 1979b). Holopainen et al. (1982) found that although the transient-eddy vorticity flux added energy to the stationary waves, the heat-flux terms appeared to dominate. Hence, they concluded that these eddies reduced the net energy in the stationary waves. But the direct effects of the transient eddy fluxes are not the only factor determining whether or not the synoptic-scale waves can destabilize the long waves. We will discuss two other mechanisms by which the synoptic-scale waves can influence the long waves. Both mechanisms do not directly change the energy in the long waves, but may alter their vertical structure

so that they can more efficiently extract ZAPE. These mechanisms could then provide an alternative explanation for why linear theory underestimated the growth of long waves in the GCM experiments.

A numerical model was developed to test the baroclinic-adjustment hypothesis and the synoptic-eddy parameterization. The model explicitly calculates all the non-linear interactions, and so it can be used to find the conditions for which our theory is valid. The model was also used to examine the effect of the transient eddies on stationary long waves. This was done by comparing the stationary long waves predicted by linear theory, by linear theory with synoptic-eddy fluxes, and by nonlinear theory (i.e. the time-mean solution of the numerical model).

The outline for the remainder of this thesis is as follows. Chapter 2 briefly reviews previous related studies. In chapter 3, we find the spatial structure of a normal-mode instability. From this, we get the eddy fluxes. Here, we implicitly assume that the synoptic-scale waves have properties like those of normal-mode instabilities. In chapter 4, we determine the effect of these eddy fluxes on the growth rate of a long wave. Using a perturbation analysis, we identify terms which influence the growth rate. Chapter 5 compares the results of our analytical theory with those of the numerical model. In addition, we also address the questions of baroclinic instability, and limitations of our theory. Chapter 6 examines the effects of the synoptic-scale waves on stationary long waves, and chapter 7 contains the summary and main conclusions of this thesis.

Chapter 2

2.0 Previous Work

The spatial modulation of the synoptic waves has been examined by C. A. Lin (1980a, b), Frederiksen (1978, 1979a, 1979b, 1980, 1982, 1983a, 1983b) and Niehaus (1980, 1981). Frederiksen and Niehaus examined the instability of non-zonal flows, and for specific flows they numerically found the most unstable modes which had synoptic scales. Niehaus (1981) found an analytical expression, but it too was numerically evaluated due to the complicated expression. These studies found solutions for specific flows, including the climatological-mean flow. However, the basic parameter dependences, and physical interpretation are not evident in these studies. On the other hand, we consider a simple model, and are able to obtain basic parameter dependences. Some relations were unexpected, and in some cases were different from published conjectures. Thus, the two approaches are complementary; we consider simple flows and find some basic parameter dependences; previous studies considered more realistic flows, but were unable to arrive at convincing physical interpretations.

The question of whether the synoptic eddies (de)stabilize the long waves has not been throughly examined. Some studies (e.g. Lin 1980a) have looked at energy transfers, but the energy fluxes of the synoptic eddies do not determine whether the synoptic eddies are themselves (de)stabilizing. Of more relevance are the GCM experiments discussed earlier which found that the long waves grew faster than predicted by linear theory (e.g. Gall et al., 1979a, b; MacVean, 1985; Young and Villere, 1985). MacVean's experiment, in particular, provides strong evidence that interactions between synoptic- and planetary-scale waves are responsible for destabilizing the planetary-scale waves. These GCM experiments are useful but they

do not explain the synoptic/planetary-scale interactions.

In this thesis, we examine the effects of the synoptic-scale waves on stationary waves by comparing linear theory, linear theory with parameterized synoptic-scale waves, and the time-mean solution from a nonlinear model. This approach is similar to that of Opsteegh and Vernekar (1982), Nigam (1983), and Nigam et al. (1986). A major difference with our study, however, is that the previously mentioned works used transient-eddy fluxes obtained from observations or model simulations which restricts the number of cases that may be considered.

2.1 Brief Review of Non-linear Theories

Few nonlinear theories analyze the problem of synoptic/planetary-scale interactions. We will briefly describe the results of the mixing-length hypothesis, and geostrophic-turbulence theory.

The mixing-length hypothesis assumes that smaller eddies mix conserved quantities similar to a strong molecular viscosity. This hypothesis is not based on the quasi-geostrophic equations, but it is used frequently to parameterize unresolved eddies in meteorological models. Mixing-length theory, by being diffusive, suggests that the synoptic-scale waves should stabilize the long waves (White and Green, 1982). This stabilization does not appear consistent with the results of GCM studies; therefore, mixing-length theory is probably poor for the problem at hand.

Geostrophic turbulence is based on the quasi-geostrophic equations and assumes that the fluid is nonlinear and quasi-random. Barotropic geostrophic turbulence theory probably doesn't apply to the GCM experiments for both the synoptic- and planetary-scale waves show strong conversions of

zonal to eddy baroclinic energy. Salmon's model (1982) for geostrophic turbulence in a two-layer flow is more relevant (figure 1). In this model, solar radiation adds baroclinic energy to the system which moves to smaller scales by turbulent processes. At the Rossby radius of deformation, baroclinic instability dominates, and converts baroclinic energy to barotropic energy. Finally, the barotropic energy flows into the low wavenumbers by a barotropic energy cascade. There is some evidence of such a process in the atmosphere; a barotropic energy cascade is observed, and so is a reverse cascade for APE (Boer and Shepherd, 1983).

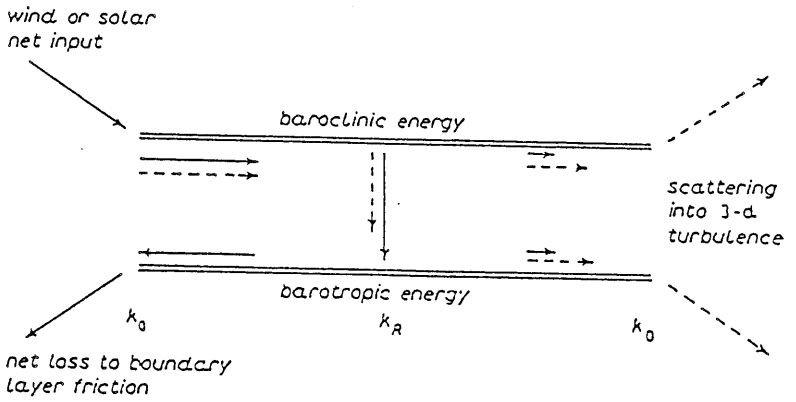

Fig. 1. The energy flow for a two-layer system. The solid arrows represent energy flow and the dashed arrows represent the potential-enstrophy flow (Salmon, 1982).

Chapter 3

3.0 The Model

In the GCM experiments, the long waves had synoptic meridional scales (Gall et al., 1979b). We will, therefore, use the QG1 quasi-geostrophic equations in our study. (The QG1 equations [White, 1982] are the commonly used quasi-geostrophic equations.) As a preliminary study, we analyze a model simpler than a GCM; we use the quasi-geostrophic equations for a two-level beta-plane channel. This system can, although crudely, model baroclinic instability and storm tracks. The former is important for both the synoptic- and planetary-scale waves gain much of their energy by converting ZAPE into EAPE. The storm tracks are important because they are regions of large heat fluxes due to synoptic-scale eddies. These fluxes can directly force long waves.

We rejected the one-level or barotropic model because it cannot model baroclinic instability. A model with more than two layers is more accurate, but it is harder to solve and may not give a better understanding.

There are two major differences between the two-level model and a continuously stratified model. The two-level model can only crudely reproduce the vertical structure of waves, and it cannot model the vertical energy propagation by waves. The latter flaw will produce artificial normal modes (Lindzen et al., 1968).

The top of the model is at 200 mb, and the bottom of the model is at 900 mb which are approximately the top of the troposphere and planetary-boundary layer, respectively.

pressure	level	primary	auxiliary variables
p_o = 200 mb	0	$\omega_0 = 0$	
p_1 = 375 mb	1	Ψ_1	Fr_1
p_2 = 550 mb	2	Q	Ψ_2, ω_2
p_3 = 725 mb	3	Ψ_3	Fr_3
p_4 = 900 mb	4	ω_4	

Where Ψ is the streamfunction

Fr is the friction

Q is the heating

ω is the vertical velocity in pressure coordinates

The equations for the two-level model in pressure coordinates are:

(See Yao, 1980)

$$\frac{\partial}{\partial t}\nabla^2\Psi_1 + J(\Psi_1, \nabla^2\Psi_1) + \beta \frac{\partial}{\partial x}\Psi_1 = f_o(\omega_2 - \omega_0) / dp + Fr_1 \quad (3.1)$$

$$\frac{\partial}{\partial t}\nabla^2\Psi_3 + J(\Psi_3, \nabla^2\Psi_3) + \beta \frac{\partial}{\partial x}\Psi_3 = f_o(\omega_4 - \omega_2) / dp + Fr_3 \quad (3.2)$$

$$\frac{\partial}{\partial t}(\Psi_1 - \Psi_3) + J(\Psi_2, \Psi_1 - \Psi_3) - dp \cdot Sp \cdot \omega_2 = dp \cdot R \cdot Q / (f_o \cdot Cp \cdot p_2) \quad (3.3)$$

Where $\omega = \frac{Dp}{Dt}$

dp = 350 mb

$$\Psi_2 = \frac{1}{2}(\Psi_1 + \Psi_3) \quad (3.4)$$

$$\omega_o = 0 \quad (3.5)$$

$$S_p = N^2 / f_o g^2 \rho (550 \text{ mb})^2 \quad (3.6)$$

Fr is the friction

Q is the heating

The equation for ω_2 can be found by taking ∇^2 of (3.3), subtracting (3.1) and adding (3.3).

$$(-2f_o/dp + dp\cdot Sp\ \nabla^2)\,\omega_2 = -\,J(\Psi_1,\ \nabla^2\Psi_1) + J(\Psi_3,\ \nabla^2\Psi_3) \qquad (3.7)$$
$$- \beta \frac{\partial}{\partial x}(\Psi_1 - \Psi_3) + \nabla^2 J(\Psi_2,\ \Psi_1 - \Psi_3)$$
$$- f_o\omega_4 \,/\, dp - R\cdot dp\ \nabla^2 Q \,/\, (f_o\cdot Cp\cdot p_2) + Fr_1 - Fr_3$$

The above equations were scaled. Time is measured in inertial periods ($1/f_o$), length is measured in units of the internal Rossby radius of deformation (NH/f_o), and pressure is measured in atmospheres (1000 mb).

$$\text{Time} = 1/f_o \ (\approx 6 \text{ hours}) \qquad (3.8)$$

$$L = NH \,/\, f_o \quad (\approx 1000 \text{ km}) \qquad (3.9)$$

$$N^2 = \frac{g}{\theta}\frac{\partial\theta}{\partial z} = -\,g^2\rho\ \frac{1}{\theta}\frac{\partial\theta}{\partial p} \qquad (3.10)$$

Primed variables are non-dimensional

$$t = t'/f_o \qquad (x,\ y) = (L\,x',\ L\,y')$$
$$\Psi_i = L^2 f_o\,\Psi_i' \qquad \omega = p_{oo} f_o \omega'$$
$$\beta = (f_o/L)\,\beta' \qquad dp' = \frac{350mb}{1000mb} = 0.35$$
$$Fr_i = f_o^2 Fr_i'$$

$$\text{Define } F = L^2\cdot f_o \,/\, Sp(550mb)\ dp^2 \qquad (3.11)$$

$$Q = f_o^3\ L^2\cdot Cp\cdot p_2\cdot Q' \,/\, R\cdot dp\cdot F \qquad (3.12)$$

$$\theta' = \frac{1}{2}(\Psi_1' - \Psi_3') \qquad (3.13)$$

θ' is proportional to the temperature

$$\Psi' = \frac{1}{2}(\Psi_1' + \Psi_3') \qquad (3.14)$$

$$Fr' = \frac{1}{2}(Fr_1' + Fr_3') \qquad (3.15)$$

After scaling, one-half of the sum of (3.1) and (3.2) is given by (3.16). One-half of the difference of (3.1) and (3.2) is given by (3.17), and (3.3) becomes (3.18).

$$\frac{\partial}{\partial t}\nabla^2\psi' + J(\psi', \nabla^2\psi') + \beta' \frac{\partial \psi'}{\partial x} + J(\theta', \nabla^2\theta') = \omega_4' / 2dp' + Fr' \qquad (3.16)$$

$$\frac{\partial}{\partial t}\nabla^2\theta' + J(\psi', \nabla^2\theta') + \beta' \frac{\partial \theta'}{\partial x} + J(\theta', \nabla^2\psi') = \qquad (3.17)$$
$$- \frac{1}{2dp'}(\omega_4' - 2\omega_2') + \frac{1}{2}(Fr_1' - Fr_3')$$

$$\frac{\partial \theta'}{\partial t} + J(\psi', \theta') - \omega_2' / 2F \cdot dp' = \frac{Q'}{2F} \qquad (3.18)$$

Using (3.17) and (3.18) to eliminate ω_2' gives (3.19).

$$\frac{\partial}{\partial t}(\nabla^2 - 2F)\theta' + J(\psi', (\nabla^2 - 2F)\theta') + J(\theta', \nabla^2\psi') = \qquad (3.19)$$
$$- \beta' \frac{\partial \theta'}{\partial x} - \omega_4' / 2dp' + \frac{1}{2}(Fr_1' - Fr_3') - Q'$$

The governing equations (3.16, and 3.19) have only two parameters when the flow is inviscid, adiabatic, and ω_4 is zero. These parameters, β' and F, are a scaled beta and a Froude number respectively. For our results, β' is set to one-quarter, and F is set to 3.7415 which is approximately the value when H is 9 km and the temperature at 550 mb is 250° K.

$$\beta' = (L/f_o)\,\beta \approx \frac{1}{4} \qquad (3.20)$$

Using (3.6), (3.11), and $dp \approx \rho \cdot g \cdot dz$, F can be rewritten as (3.21) or (3.22).

$$F = \left(\frac{f\,L}{N\,dz}\right)^2 \qquad (3.21)$$

$$F = (H \cdot g \cdot \rho / dp)^2 = (H \cdot g \cdot p)^2 \, (dp \cdot R \cdot T)^{-2} \qquad (3.22)$$

$dp = 350$ mb $= 3.5 \times 10^5$ pascal $\qquad p = p_2 = 5.5 \times 10^5$ pascal

$g = 9.8$ m s^{-2} $\qquad R = 287$ J deg^{-1} kg^{-1} for dry air

$H = 9$ km $\qquad T = 249.665$ K

Using the above values, $F = 3.7415$ (3.23)

For the rest of the thesis, these primes will be dropped.

Boundary Conditions

For the vertical boundary conditions, we must know ω at the top and bottom. At the top, ω is set to zero ($\omega_o = 0$). At the bottom (level 4), ω will be caused by Ekman pumping and orographic forcing.

The vertical velocity at the surface is given by (3.24) (Holton, 1972). His result can be converted into pressure coordinates (3.25) where 'd_o' is a function of the surface conditions and atmospheric stratification. The control run uses $d_o = 0.025$ which gives a decay time of 7 days for a barotropic wave. This Ekman pumping is weaker than Holton's (1972) suggested 4-day decay time.

$$\frac{Dz}{Dt} = c \, \nabla^2 \psi_{\text{top of boundary layer}} \qquad (3.24)$$

$$\frac{Dz}{Dt} \cong - \omega_4 / \rho \cdot g$$

$$\omega_4 = - d_o \, \nabla^2 \psi_3 + \omega_4(\text{due to orography}) \qquad (3.25)$$

$$d_o = 0.025 \quad \text{for control run} \qquad (3.26)$$

The model is periodic in 'x' (periodic beta-plane channel) and it has no flow through the meridional boundaries at y = 0, Y.

These meridional and vertical boundary conditions have been employed in many beta-plane models. The major effect of the boundary conditions is to "trap" the energy within the channel. This trapping can produce artificial vertical modes (Lindzen et al., 1968; Dickinson, 1968), and artificial meridional modes (Kasahara, 1980). This trapping definitely and significantly affects the stationary waves (Held, 1983), so one must interpret the results in chapter 6 with consideration to Held's results.

The effect of the boundary conditions on the transient waves is more uncertain. Perhaps, these effects may be minimal since we are only looking at the gross aspects of the wave interactions. Nevertheless, such speculations should be examined with a more realistic model.

Barotropic Dissipation

Fr includes the effects of viscosity and unresolved motions, and it will be modeled as a horizontal eddy viscosity. The coefficient of eddy viscosity (v) depends on many factors, including the horizontal resolution of the model. The term 'v' was chosen so that the shortest barotropic wave in our numerical model had a decay time of 7.5 days. The longer modes are less damped by the eddy viscosity, and the longest, widest mode had a decay time of roughly 90 days.

$$Fr = v \nabla^4 \psi \tag{3.27}$$

$$v = \frac{1}{125} \text{ for the control run} \tag{3.28}$$

Baroclinic Dissipation and Forcing

Many terms affect the baroclinic part of the flow (θ). These factors, which are listed below, are not independent. For example, the surface heat flux is forced by solar radiation, and depends on the vertical eddy fluxes.

Some Factors determining $\frac{1}{2}(Fr_1 - Fr_3)$ and Q

1. Solar forcing
2. Heat flux from the surface
3. Latent heat release
4. Radiative cooling
5. Fluxes of heat and momentum by unresolved motions

The factors determining $\frac{1}{2}(Fr_1-Fr_3)$ and Q are difficult to model accurately, especially in a two-level model. As our primary goal of this thesis is to understand the scale interactions, precise determination is not likely to be necessary. We, therefore, use a simple linear parameterization.

$$\frac{1}{2}(Fr_1-Fr_3) - Q' = 2F(\theta_e - \theta) / t_{rad} \qquad (3.29)$$

$\frac{1}{2F} t_{rad} (K^2 + 2F)$ is the decay time

t_{rad} = 40 for the control run (10 days) (3.30)

Note: t_{rad} includes the effects of unresolved eddy fluxes, so it should be smaller than the Newtonian-cooling time scale.

θ_e is the radiative equilibrium temperature (thermal forcing)

For most runs, $\theta_e = -0.3 (\frac{y}{Y} - \frac{1}{2})$ (3.31)

The radiative damping is stronger than determined by radiation calculations (t_{rad} = O(30 days)). We have used a strong radiative damping because we are implicitly including the effects of unresolved eddy fluxes which are presumably dissipative.

3.1 Theory Introduction

C. A. Lin (1980) calculated the linear instability properties of small- and large-amplitude planetary-scale waves, where large was determined by the ratio of the wave's meridional wind to its Doppler-shifted phase speed (i.e. $v/|c-U|$). The instability properties suggest some characteristics of the nonlinear flow.

When the basic state had a large-amplitude long wave, Lin found that the dominant linear instability consisted of long waves. This is a reason to suspect that long waves may dominate the flow and energetics. One may also expect nonlinear interactions among these planetary-scale waves to be important and perhaps a dominant process.

On the other hand, when the basic-state long wave was weak, the dominant linear instability consisted of synoptic-scale waves with a planetary-scale modulation. One could, therefore, expect that these modulated waves are important. In addition, the unstable waves, due to this planetary-scale modulation, could interact with the planetary-scale waves.

In our study, we anticipate that the flow containing a strong basic-state wave will differ greatly from a flow with a weak wave. We will focus on the latter case for we expect that the synoptic/planetary-scale interactions will be more important in that situation, and may prove more helpful to us in explaining the GCM results.

Strategy

The strategy for examining the synoptic/planetary-scale interactions is to assume that the synoptic-scale wave has a faster time scale than the

long wave. The time scale of a traveling planetary-scale wave is made longer by working in the frame of reference of that traveling wave. Hence, the slow time scale is that of the amplitude of the long wave, and the fast time scale is period of the synoptic-scale wave. The amplitude time scale of observed long waves needs to be evaluated; however, the ultra-long waves have a lifetime of roughly 20 days (Ahlquist, 1985) which is much longer than the period of synoptic-scale waves (2.5 to 6 days; Blackmon, 1976).

With this separation of time scales, the synoptic-scale wave only sees a wavy basic state that is unchanging on the fast time scale. We find the synoptic-scale wave by a linear, WKB analysis. This procedure determines the properties of the synoptic-scale wave up to a positive factor, the synoptic-eddy amplitude. In our study, this factor is either a free parameter or determined by the numerical model.

The zonal and planetary-scale flows, by assumption, vary slowly compared to the synoptic eddies, so that the large-scale flow only sees the 'time-averaged' flux due to the synoptic eddies. We determine these fluxes using the previous analysis. Basically, the effects of the synoptic eddies are now a linear function of the large-scale flow and the synoptic-eddy amplitude; i.e., the synoptic-scale waves are parameterized.

The evolution of the planetary-scale waves can be found using linear quasi-geostrophic equations and the linear synoptic-eddy parameterization. We can then find a linear growth rate of the long waves assuming that the zonal flow changes slowly.

The details of the analysis are broken into three parts. First, the growth of a synoptic-scale wave on a simple, wavy basic state is found. Using the WKB technique, the synoptic-scale wave is found to have a spatial modulation of its amplitude, local wavelength and vertical tilt. To keep

the synoptic-scale wave from growing on the fast time scale, the zonal flow is assumed to have equilibrated to where the growth rate of the most unstable modes is nearly zero. Basically, this is a form of baroclinic adjustment which is tested in chapter 5.

In this chapter, the fluxes of the modulated synoptic-scale wave are also found. These fluxes have a planetary-scale component which can directly force a long wave. These fluxes can then be parameterized in terms of the synoptic-eddy amplitude, zonal basic state, and the basic-state long wave.

In chapter 4, we examine the effect of the eddy fluxes on transient long waves. We find that the synoptic-eddy fluxes can increase the growth of the long waves. In addition, we identify the role of individual terms in the limit of small fluxes and dissipation.

3.2 Theory: Part A

In this section, the growth of a synoptic-scale wave on a wavy basic state is found. For our purposes, the large-scale basic state is invariant in time, and we will look for the normal-mode instabilities. In the next section, we will assume that the normal-mode instability is representive of the synoptic-scale waves, and will use it to find the eddy fluxes of the synoptic-scale waves.

This instability calculation has been done on a computer as an eigenvector problem (e.g. Frederiksen, 1978; Niehaus, 1980). Unfortunately, these results don't yield the insight required for our analysis, and are only valid for specific flows. Instead, we will apply the WKB technique because its results are more readily interpreted, and its results can be used to parameterize the synoptic eddies.

The first step in determining the synoptic modulation is to linearize the equations about a non-zonal basic state. For our theory, the basic state consists of a zonal flow with a single small-amplitude stationary long wave. This is a minor restriction since a zonal translation will make a traveling wave stationary, and, as our theory is linear, multiple waves can be handled separately.

Dissipation for the synoptic-scale waves is assumed to be linear in the potential vorticity (3.33). The dissipation can then be removed by a simple transformation (3.34). We used this dissipation for it simiplifies the calculations and probably doesn't change the largest order behavior of the synoptic-scale waves.

$$\frac{\partial q}{\partial t} + J(\Psi, q) + \beta \frac{\partial \Psi}{\partial x} = D(q) \qquad (3.32)$$

q is the potential vorticity, Ψ is the streamfunction

Let the dissipation $D(q) = - r \cdot q$ (3.33)

Let $\frac{\partial}{\partial t} = \frac{\partial}{\partial t} + r$ (3.34)

After using (3.16), (3.19), and (3.34), the governing equations are

$$\frac{\partial}{\partial t} \nabla^2\psi = - \beta \frac{\partial \psi}{\partial x} - J(\psi, \nabla^2\psi) - J(\theta, \nabla^2\theta) \quad (3.35)$$

$$\frac{\partial}{\partial t}(\nabla^2 - 2F)\,\theta = - \beta \frac{\partial \theta}{\partial x} - J(\psi, (\nabla^2 - 2F)\,\theta) - J(\theta, \nabla^2\psi) \quad (3.36)$$

Define $\psi(x,y,t) = \psi_o(x,y) + \psi'(x,y,t)$

$\theta(x,y,t) = \theta_o(x,y) + \theta'(x,y,t)$

ψ', θ' are the streamfunctions for the synoptic-scale wave

ψ_o, θ_o are the basic-state streamfunctions

Linearizing (3.35) and (3.36) gives:

$$\frac{\partial}{\partial t} \nabla^2\psi = - \beta \frac{\partial \psi'}{\partial x} - J(\psi', \nabla^2\psi_o) - J(\psi_o, \nabla^2\psi') - J(\theta', \nabla^2\theta_o) \quad (3.37)$$
$$- J(\theta_o, \nabla^2\theta')$$

$$\frac{\partial}{\partial t}(\nabla^2 - 2F)\theta' = -\beta \frac{\partial \theta'}{\partial x} - J(\psi_o, (\nabla^2 - 2F)\,\theta') \quad (3.38)$$
$$- J(\theta_o, (\nabla^2 + 2F)\psi') - J(\psi', \nabla^2\theta_o) - J(\theta', \nabla^2\psi_o)$$

The boundary conditions are that

ψ', θ' are periodic in x, and are zero at y = (0, Y).

Let the widest meridional wavenumber be $l_o = \pi / Y$

We will make the following assumptions. (1) The calculation is only for the most unstable modes because the nonlinear terms between the larger amplitude transients will dominate the equations governing the smaller amplitude transients. (2) The most unstable transient wave varies on the

synoptic scale which is much shorter than the basic-state wave (i.e., $\epsilon = L_{syn}/L_{ps} << 1$). (3) Last, the basic-state wave is weak (i.e., $\delta = |U'|/|U_o| << 1$).

We will look for solutions which have a sin(ly) structure, and we will ignore the interactions between different meridional modes. The Galerkin approximation (Gottlieb and Orszag, 1977) and a power expansion in ϵ are used to simplify the (3.37-3.38), giving (3.41) and (3.42). (Appendix H contains more details.)

Define $l = j \cdot l_o$

Let $\Psi'(x,y,t) = a(x,t)\sin(ly)$ (3.39)

$\theta'(x,y,t) = b(x,t)\sin(ly)$ (3.40)

$$\frac{\partial}{\partial t}(a_{xx} - l^2 a) = -\beta\, a_x + U(l^2 a - a_{xx})_x + Ut(l^2 b - b_{xx})_x + DU \cdot a_x + DUt \cdot b_x \quad (3.41)$$

$$\frac{\partial}{\partial t}(b_{xx} - l^2 b - 2Fb) = -\beta\, b_x + U\,[(2F + l^2)\, b - b_{xx}]_x - Ut\,[\,(2F - l^2)\, a + a_{xx}]_x + DU \cdot b_x + DUt \cdot a_x \quad (3.42)$$

The terms U(x), Ut(x), DU(x), and DUt(x) are defined below. They are the Galerkin approximations to the barotropic and thermal zonal winds, and the "curvature" of the barotropic and thermal zonal winds, respectively.

Define $\langle A \mid B \rangle = \frac{2}{Y} \int_0^Y A \cdot B \, dy$

$U(x) = \langle -\partial\psi_o/\partial y \sin(ly) \mid \sin(ly) \rangle$ is the zonal wind (3.43)

$Ut(x) = \langle -\partial\theta_o/\partial y \sin(ly) \mid \sin(ly) \rangle$ is the zonal thermal wind (3.44)

$DU(x) = \langle -\partial^3\psi_o/\partial y^3 \sin(ly) \mid \sin(ly) \rangle$ is the curvature of U(x) (3.45)

$DUt(x) = \langle -\partial^3\theta_o/\partial y^3 \sin(ly) \mid \sin(ly)\rangle$ is the curvature of Ut(x) (3.46)

For convenience, we assume <DU>, <DUt> are both $O(\delta)$

$V(x) = \langle \partial\Psi_o/\partial x \cos(ly) \mid \sin(ly)\rangle$

$Vt(x) = \langle \partial\theta_o/\partial x \cos(ly) \mid \sin(ly)\rangle$

$DV(x) = \langle \partial(\nabla^2\psi_o)/\partial x \cos(ly) \mid \sin(ly)\rangle$

$DVt(x) = \langle \partial(\nabla^2\theta_o)/\partial x \cos(ly) \mid \sin(ly)\rangle$

Note, the above quantities are a function of x and the meridional mode 'j.'

Equations 3.41 and 3.42 are ordinary differential equations, and can be solved using the WKB technique. The form of the WKB solution is given by (3.47) and (3.48). The range of validity of the solutions is examined in Appendix A.

$$\Psi(x,t) = \sin(ly)\exp\{i\cdot g_o(X)/\varepsilon + i\cdot g_1(X) + i\cdot\varepsilon\cdot g_2(X) + .. - i\cdot w_o\cdot t - i\cdot\varepsilon\cdot w_1\cdot t - ..\} \quad (3.47)$$

$$\theta(x,t) = (co(X) + \varepsilon\cdot c_1(X) + ..)\,\Psi \quad (3.48)$$

A local wavenumber is defined by $k(X) = \frac{1}{\varepsilon}\frac{\partial}{\partial x}g_o(X)$

Using the local wavenumber, (3.47) becomes

$$\Psi = \exp\left(i\int^x k(x)dx + i\cdot g_1(X) + \ldots - i\cdot w_o\cdot t + \ldots\right) \quad (3.49)$$

Equations 3.48 and 3.49 can be combined with (3.41) and (3.42). Ignoring terms of $O(\varepsilon)$, the results are two third-order polynomials in k. These two polynomials can be manipulated to find an expression for co.

$$co(x) = \frac{[(w - U(x)\cdot k(x))\,(k(x)^2 + l^2) + (\beta - DU(x))\,k(x)]}{[Ut(x)\cdot k(x)\cdot(k(x)^2 + l^2) + DUt(x)\cdot k(x)]} \qquad (3.50)$$

Using these two polynomials to eliminate co, one gets a sixth order polynomial in k (3.51). (See appendix H for more details.)

$$H(k,w) = \sum_{o}^{6} a_n k^n = 0 \qquad (3.51)$$

where $a_6 = U^2 - Ut^2$

$a_5 = -2Uw$

$a_4 = w^2 + 2U^2(l^2 + F) - 2\beta_{eff}U + 2Ut^2(F - l^2) - 2Ut\cdot DUt$

$a_3 = 2\beta_{eff}w - 4wU\cdot(l^2 + F)$

$a_2 = -l^2(l^2 - 2F)\,Ut^2 - DUt^2 - 2(l^2 - F)\,Ut\,DUt + 2w^2(l^2 + F) + \beta_{eff}^2 - 2(l^2 + F)\,\beta_{eff}U + l^2(l^2 + 2F)\,U^2$

$a_1 = 2w\,[\beta_{eff}(l^2 + F) - U\cdot l^2(l^2 + 2F)]$

$a_0 = w^2 l^2(l^2 + 2F)$

and $\beta_{eff} = \beta - DU$ is the effective beta

Frequency, and Growth Rate

Co (3.50) and H(k,w) (3.51) govern the synoptic-scale wave. Co determines the vertical structure of this wave, while H fixes the wave's growth rate, frequency, and local wavenumber. H is a 6th order polynomial in k with two unknowns, k and w. If we were to solve for k using a predetermined w, we would find six values of k(x), which correspond to the six possible roots. We would then have to find the roots which correspond to physical solutions. [Pierrehumbert (1984) found the local instabilities by this procedure.]

A simpler method uses the zonal average of H (3.51). Since the zonal

asymmetries of U, Ut, DU, and DUt are O(o), they can be neglected. If the zonal asymmetry of k(x) is $O(\delta)$, it too can be ignored. (After completing the analysis, one should verify that $|k'| < O(\delta)$.) The final result is an equation for the O(1) frequency (3.52). Here, the frequency is a function of the zonal-mean wavenumber.

$$w_o = \langle U\rangle\langle k\rangle - \beta \frac{\langle k\rangle}{M} (K^2 + F) \pm i\frac{\langle k\rangle}{M} [-(\beta F)^2 + \langle Ut\rangle^2 M\cdot K^2 (2F - K^2)]^{1/2} \quad (3.52)$$

Where $K^2 = \langle k\rangle^2 + l^2$ (3.53)

$M = K^2 (K^2 + 2F)$ (3.54)

Where $\langle..\rangle$ is the zonal average,

and $(..)'$ is the perturbation from the zonal mean.

The $O(\delta)$ correction to the frequency is zero. This result comes from expressing H in a Taylor series of the zonal asymmetries, k', U', Ut', DU', and DUt'. On zonally averaging this Taylor series, the linear perturbation terms disappear leaving quadratic perturbation terms of $O(\delta^2)$. Thus, the correction to w is $O(\delta^2)$ which implies that changes in the frequency and growth rate can be ignored.

Local Wavelength

In our analysis, the local wavenumber is complex and a function of location. This is different from the analysis of zonal and nonzonal **stable** flows which have real wavenumbers. The imaginary part of the wavenumber is extremely important for it creates O(1) spatial variations in the eddy amplitude, and eddy fluxes. This, in turn, allows strong interactions

between the synoptic- and planetary-scale waves, and may help explain the strength and locations of storm tracks.

The variations of the local wavenumber, k, can be found by a Taylor's expansion of H (3.55). In this equation, the partial derivatives are evaluated at the zonal-mean state, and are given by (3.56-3.61).

$$\frac{\partial H}{\partial k} k' + \frac{\partial H}{\partial U} U' + \frac{\partial H}{\partial Ut} Ut' + \frac{\partial H}{\partial DU} DU' + \frac{\partial H}{\partial DUt} DUt' = 0 \qquad (3.55)$$

As shown in appendix I,

$$\frac{\partial H}{\partial U} = -2i\langle k\rangle \cdot \mathrm{imag}(w) \cdot M \qquad (3.56)$$

$$\frac{\partial H}{\partial Ut} = -2\langle k\rangle^2 \langle Ut\rangle K^2 (K^2 - 2F) \qquad (3.57)$$

$$\frac{\partial H}{\partial DUt} = -2\langle k\rangle^2 \langle Ut\rangle (K^2 - F) \qquad (3.58)$$

$$\frac{\partial H}{\partial DU} = 2 \frac{\beta}{M} \langle k\rangle^2 F^2 - 2i \cdot \mathrm{imag}(w) \langle k\rangle (K^2 + F) \qquad (3.59)$$

$$\mathrm{imag}\left(\frac{\partial H}{\partial k}\right) = 2 \cdot \mathrm{imag}(w) \left[- U \cdot M + \beta \cdot (K^2 + F) - 2\beta \langle k\rangle^2 - 4 \frac{\beta}{M} \langle k\rangle^2 F^2 \right] \qquad (3.60)$$

$$\mathrm{real}\left(\frac{\partial H}{\partial k}\right) = - 4\langle k\rangle (K^2 + F)\, \mathrm{imag}(w)^2 + 2\langle k\rangle \langle Ut\rangle^2 \left[2\langle k\rangle^2 (F - K^2) - K^2(K^2 - 2F)\right] + 2 \frac{\langle k\rangle}{M} \beta^2 F^2 \left[-1 + \frac{2}{M} \langle k\rangle^2 (K^2 + F) \right] \qquad (3.61)$$

In our analysis, the synoptic-scale wave has one free parameter, its mean wavenumber. Knowing the mean wavenumber, the wave's frequency (3.52), local wavenumber (3.55) and vertical structure (3.50) are determined.

An important and special case occurs when the synoptic-scale wave has the most unstable zonal wavelength. It is an important because one might expect that this wave will have a large amplitude. It is special because a $\partial w/\partial k$ is real, and $\partial H/\partial k$ has a simple form. Because of the simple form of $\partial H/\partial k$ (3.63), this case is often considered in the following analyses.

Special Case: k_c = most unstable zonal wavenumber

$$\frac{\partial H}{\partial w} = 2i \cdot M \cdot \text{imag}(w) \qquad \text{from 3.51 and 3.52.} \tag{3.62}$$

Since $H(k, w) = 0$

then $\frac{\partial H}{\partial k} = -\left(\frac{\partial H}{\partial w}\right)\left(\frac{\partial w}{\partial k}\right)$

But at the most zonal unstable wavelength, $\text{imag}\left(\frac{\partial w}{\partial k}\right) = 0$

and $\text{real}\left(\frac{\partial w}{\partial k}\right) = c_g$, where c_g is the 'group velocity'

$$\text{Therefore } \frac{\partial H}{\partial k} = -2i \cdot M \cdot \text{imag}(w) \cdot c_g \tag{3.63}$$

at the most unstable zonal wavenumber

Co

Co is the ratio of the baroclinic and barotropic components of the synoptic-scale wave (3.48). This term is complex valued because there are phase shifts between the baroclinic and barotropic components. As a result, co is important for determining the local vertical phase tilt, and heat flux.

Co' can be determined from (3.50); however, (3.68) will be used instead. This equation includes the small terms, V, Vt, DV, and DVt which are formally of $O(\varepsilon)$. However, using these small terms is not inconsistent because the exact value of co never enters into the calculations. The smaller terms do not significantly increase the computational costs, and they do make a minor improvement in the results.

$$\text{cor} = \text{real}(\text{co}) \tag{3.64}$$

$$\text{coi} = \text{imag}(\text{co}) \tag{3.65}$$

$$\langle cor \rangle = \frac{\beta \cdot F}{M \langle Ut \rangle} \tag{3.66}$$

$$\langle coi \rangle = \frac{imag(w)}{\langle k \rangle \langle Ut \rangle} \tag{3.67}$$

Note that <coi> is proportional to the meridional heat flux, and not surprisingly, <coi> is also proportional to the (inviscid) growth rate.

$$co' = \left\{ \frac{[2\langle k \rangle (w - U\langle k \rangle) + \beta]}{[\langle k \rangle Ut K^2]} - \frac{\langle U \rangle}{\langle k \rangle \langle Ut \rangle} - \frac{2\langle co \rangle \langle k \rangle}{K^2} - \frac{\langle co \rangle}{\langle k \rangle} \right\} k' \tag{3.68}$$

$$- \frac{(U' + \langle co \rangle Ut')}{\langle Ut \rangle} + \frac{il\,(V' + \langle co \rangle Vt')}{\langle k \rangle \langle Ut \rangle}$$

$$- \frac{(DU + \langle co \rangle DUt)}{\langle Ut \rangle K^2} + \frac{il\,(DV + \langle co \rangle DVt)}{\langle k \rangle Ut K^2}$$

3.3 Theory Part B:

Spatial Modulation

The imaginary part of k(x), ki, controls the local eddy amplitude and the planetary-scale modulation of the synoptic-eddy fluxes. When ki is negative, the amplitude of the synoptic-scale wave is larger to the east (3.69). This condition will be called 'spatial growth downstream', or 'spatial growth.' Downstream is unambiguous for reasonable mid-latitude flows; the phase and group velocities of most unstable synoptic-scale wave, and the zonal-mean flow are all eastward. (For atypical flows, downstream is in the direction of the group velocity of the synoptic-scale wave.)

The synoptic-eddy amplitude is given by $|\Psi| = \Psi_{oo}\, e^{\int^{x} -ki(x)\cdot dx}$ (3.69)

-ki = spatial growth, -ki > 0 implies spatial growth downstream

Effects of Ut'

The zonal asymmetries of the zonal thermal wind, Ut', will modulate synoptic-scale waves by (3.70). Basically, a strong Ut' produces spatial growth downstream, as illustrated by figure 3.

$$\frac{dk}{dUt} = -\frac{dH}{dUt} \Big/ \frac{dH}{dk}$$

$$\frac{dki}{dUt} = 2\langle k\rangle^2 \langle Ut\rangle K^2 (K^2 - 2F)\, \mathrm{imag}\left(\frac{dH}{dk}\right) \left|\frac{dH}{dk}\right|^{-2} \qquad (3.70)$$

Note that baroclinically unstable waves must have $K^2 < 2F$

and $\mathrm{imag}\left(\frac{dH}{dk}\right) =$ (from 3.60)

$$= 2\cdot \mathrm{imag}(w)\, [-\langle U\rangle M + \beta (K^2 + F) - 2\beta \langle k\rangle^2 - 4 \frac{\beta}{M} \langle k\rangle^2 F^2] \qquad (3.71)$$

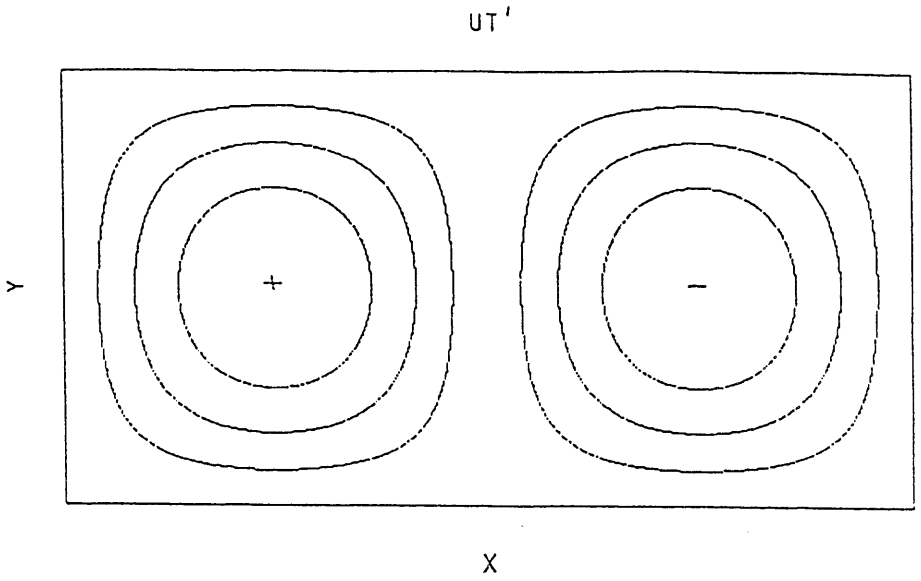

Fig. 2. The Ut' for figures 3-5. Ut' is the zonally asymmetric thermal wind of the basic-state flow. U' is zero.

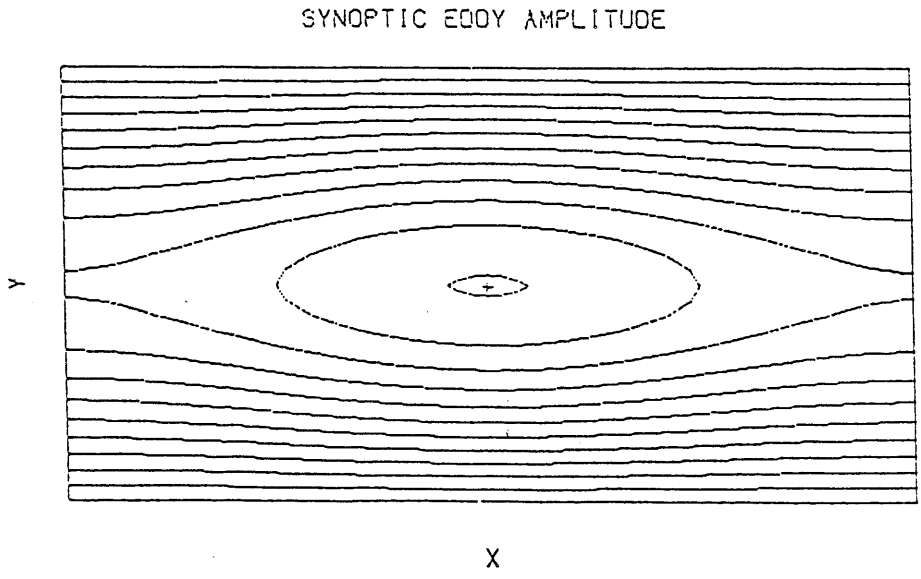

Fig. 3. The synoptic-eddy amplitude as determined by theory.

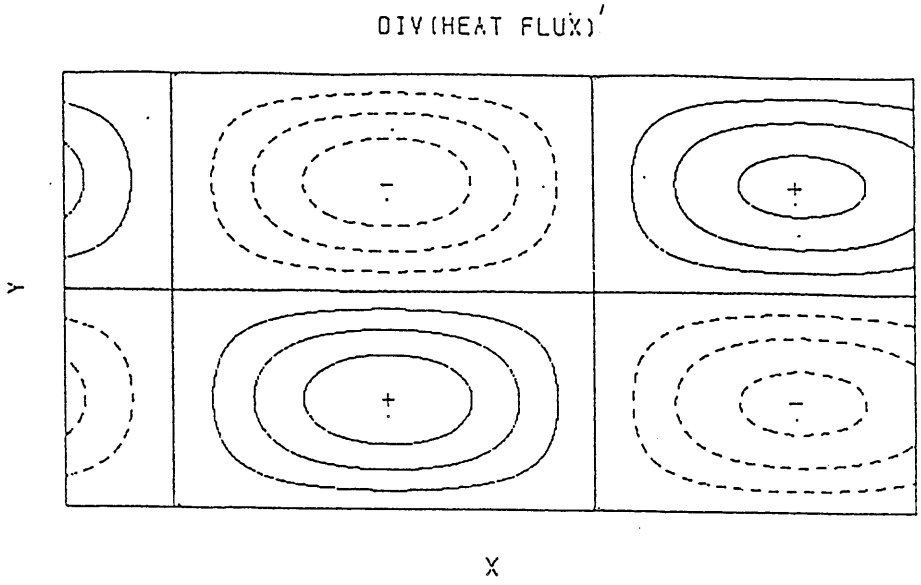

Fig. 4. $J(\Psi_{syn}, \theta_{syn})$ The divergence of the eddy heat flux as determined by theory. (Deviation from the zonal mean is shown.)

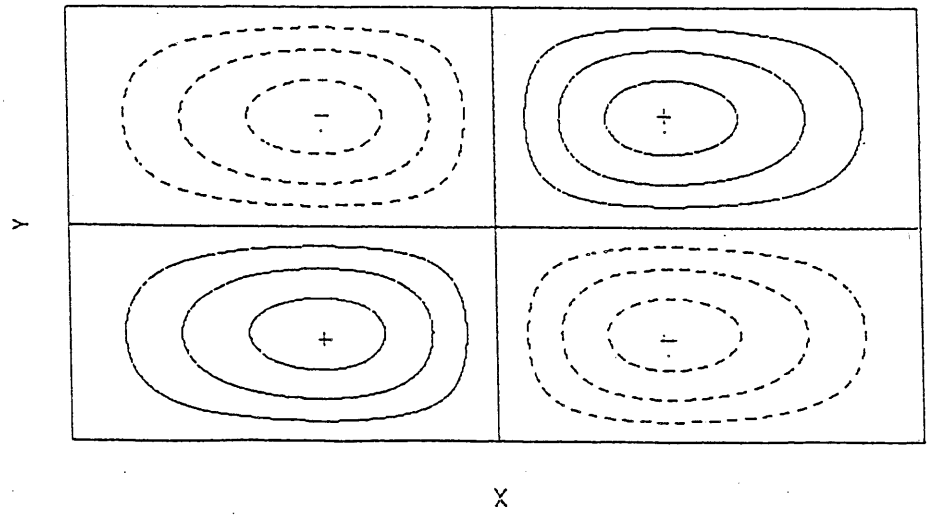

Fig. 5. $J(\Psi_{syn}, \nabla^2\Psi_{syn})$ The divergence of the vorticity flux as determined by theory. (For levels 1, 2, and 3.)

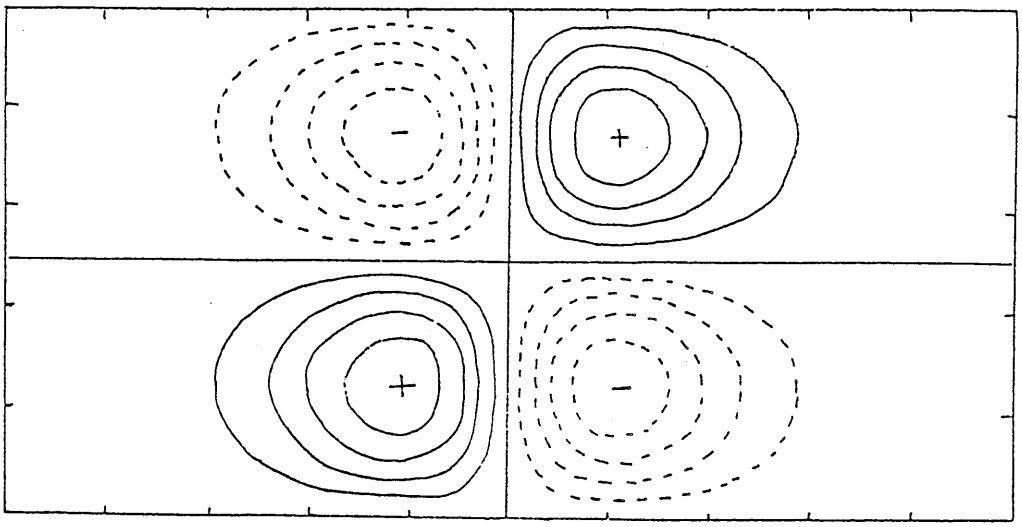

Fig. 6. Like fig. 5 except the spatial growth rate (or length of the channel) is 10 times larger.

Using 3.52, one can find that

$$M \cdot \mathrm{real}\left(\frac{\partial w}{\partial k}\right) = \langle U \rangle M - \beta (K^2 + F) - 2\beta \langle k \rangle^2 + 4 \frac{\beta}{M} \langle k \rangle^2 (K^2 + F)^2$$

$$= \langle U \rangle M - \beta (K^2 + F) - 2 \frac{\beta}{M} \langle k \rangle^2 [M - 2 (K^2 + F)^2]$$

$$= \langle U \rangle M - \beta (K^2 + F) - 2 \frac{\beta}{M} \langle k \rangle^2 (-M - 2F^2)$$

$$= \langle U \rangle M - \beta (K^2 + F) + 2\beta \langle k \rangle^2 + 4 \frac{\beta}{M} \langle k \rangle^2 (K^2 + F)^2$$

$$= - \mathrm{imag}\left(\frac{\partial H}{\partial k}\right) / 2 \cdot \mathrm{imag}(w)$$

Thus $$\mathrm{imag}\left(\frac{\partial H}{\partial k}\right) = -2 \cdot \mathrm{imag}(w) \cdot M \cdot \mathrm{real}\left(\frac{\partial w}{\partial k}\right) \qquad (3.72)$$

Using (3.70) and (3.72), $\frac{\partial ki}{\partial Ut} < 0$ when $\mathrm{real}\left(\frac{\partial w}{\partial k}\right) > 0$

The term $\frac{\partial ki}{\partial Ut}$ is negative when $\mathrm{real}\left(\frac{\partial w}{\partial k}\right)$ is positive. For this typical case, a stronger than average thermal wind (Ut' > 0), implies that ki is negative. Hence, regions of large Ut' should show spatial growth downstream. If the variations were sinusoidal, then the eddy amplitude should

peak $\frac{1}{4}$ wavelength (or 90^{o}) downstream of the strongest thermal winds.

The perturbation thermal wind (Ut') affects the spatial growth in a predictable way. Where Ut' is positive, the local baroclinic instability is larger than average. A cyclone moving in this more unstable region, will grow as it moves downstream. If one calculates the average amplitude of many cyclones as a function of position, one would expect to see spatial growth in the more unstable regions.

Ut:	Ut' > 0		Ut' < 0	
w:	strong local instability		weak local instability	
ki:	ki < 0		ki > 0	
	spatial growth to east		spatial decay to east	
|Ψ|:	mean	large	mean	small

<---------- x ---------->

Equation 3.70 is simpler when the synoptic-scale wave has the most unstable zonal wavelength (3.63 and 3.70 give 3.73). Here, the spatial growth is inversely proportional to the group velocity.

$$\frac{\partial ki}{\partial Ut} = - \frac{\langle k \rangle^2 \langle Ut \rangle K^2 (2F - K^2)}{M \cdot \mathrm{imag}(w) \cdot c_g} \qquad (3.73)$$

(at most unstable zonal wavelength)

$c_g = \frac{\partial w}{\partial k}$ is the group velocity (The group velocity for the most unstable wave is its wave packet velocity.)

The term ki (from 3.73) blows up when the group velocity is zero. For this situation, the spatial modulation is undefined because the waves do not 'move' in a wave-tracing sense (Yeh, 1949). The waves in one region do not influence those in other regions; hence, the spatial modulation is unconstrained.

The term ki also blows up when the inviscid growth rate (i.e. ignoring dissipation) is zero. When 'wi' is small, ∂(wi)/∂Ut is very large because the growth rate has a square root dependence on the thermal wind (3.52). Thus, a small change in the perturbation thermal wind will produce a larger change in the local growth rate, and consequently the spatial modulation.

$$dk = -\left(\frac{\partial H}{\partial Ut} \Big/ \frac{\partial H}{\partial k}\right) dUt \qquad \text{(most unstable wave)}$$

$$dk = \left[\frac{\partial H}{\partial Ut} \Big/ \left(\frac{\partial w}{\partial k}\,\frac{\partial H}{\partial w}\right)\right] dUt$$

$$\text{Therefore,}\quad dk = -\left[\frac{\partial w}{\partial Ut} \Big/ c_g\right] dUt \qquad (3.74)$$

note: $\frac{\partial w}{\partial Ut}$ is imaginary

$$|\Psi| \simeq \exp \frac{\int^{x} \frac{\partial w}{\partial Ut}\, Ut'(x)\, dx}{c_g} \qquad (3.75)$$

The term ∂w/∂Ut is imaginary for the most unstable wave, and determines the effect of Ut' on the local growth rate.

Equation 3.74 has a simple interpretation. Consider a synoptic eddy moving into a region of strong thermal wind (Ut = <Ut> + Ut'). Its inviscid growth rate is imag(w + (∂w/∂Ut)Ut'). Its real growth rate, however, is only imag((∂w/∂Ut)·Ut') since its 'global' growth is zero (baroclinic adjustment hypothesis). As a result, the eddy's amplitude grows like $e^{\text{imag}(\partial w/\partial Ut)\cdot Ut'\cdot t}$. The eddy also travels at its group velocity. Suppose the eddy's position is given by the equation $x = c_g t$.

Then, the eddy's amplitude, which is a function of time, is also a function of position, $e^{\text{imag}(\partial w/\partial Ut)\cdot Ut'\cdot x/c_g}$. This is like (3.75). Hence, we have given both wave and particle interpretations to the Ut' effects.

Ut' can also change the local wavelength (3.76). Waves longer (shorter) than the most unstable wave, have their local wavelength reduced (increased).

$$\frac{\partial kr}{\partial Ut} = -2\langle k\rangle^2 \langle Ut\rangle K^2 (K^2 - 2F)\, \text{real}\left(\frac{dH}{dk}\right) \left|\frac{dH}{dk}\right|^{-2} \qquad (3.76)$$

Effects of U'

The most direct effect of U' is to change the local wavelength of the synoptic-scale wave. When the zonal wind is stronger than average, the local wavelength is longer so that the frequency remains constant. (See 3.77 and 3.78.) This wavelength modulation is easily seen in Frederiksen (1980).

$$\frac{\partial k}{\partial U} = -2i \langle k\rangle \,\text{imag}(w)\, M \,/\, \frac{dH}{dk} \qquad \text{from (3.55)} \qquad (3.77)$$

The zonal wind perturbation can influence the spatial growth of the synoptic-scale wave. This may seem surprising since the zonal wind does not alter the baroclinic stability in the Phillips' model (e.g. Pedlosky, 1979). The barotropic zonal wind controls the spatial growth indirectly. When the zonal wind (U' > 0) is stronger than average, the local wavelength is longer to keep the frequency constant. (This is true only when real($\partial w/\partial k$) > 0.) In turn, the larger local wavelength changes the local instability, and can produce spatial growth.

When U' is positive, the synoptic-scale waves will have a longer local wavelength. Waves that are longer than the most unstable wave will become more stable and experience spatial decay, and shorter waves will show spatial growth.

$$\frac{\partial k}{\partial U} = - \langle k \rangle / c_g \qquad \text{at the most unstable wave number} \qquad (3.78)$$

U:	$U' > 0$	$U' < 0$
kr:	$kr' < 0$	$kr' > 0$
k:	$k < \langle k \rangle < k_o$	$\langle k \rangle < k < k_o$
w:	weaker local instability	stronger local instability
	spatial decay downstream	spatial growth downstream
ki:	$ki > 0$	$ki < 0$

Effect of U' on longer synoptic-scale waves

k_o = most unstable zonal wavenumber

Effects of DU'

DU' ($\partial^2 U'/\partial y^2$) is the curvature of the basic-state wave's zonal wind. This term modulates the synoptic-scale wave by changing the effective beta. A strong effective beta reduces the instability (3.52); therefore, regions of a strong effective beta should show spatial decay downstream.

$$\beta_{eff} = \beta - U_{yy} = \beta - DU'$$

$$\frac{\partial k}{\partial DU'} = - \frac{\partial H}{\partial DU} / \frac{\partial H}{\partial k} \qquad (3.79)$$

$$= [- 2\beta \langle k \rangle^2 F^2 + 2i \cdot \text{imag}(w) \langle k \rangle (K^2 + F)] / M \cdot \frac{dH}{dk}$$

When the synoptic-scale wave has the most unstable zonal wavenumber,

(3.79) can be simplified by using $dH/dk = -2i\ \mathrm{imag}(w)\ M\ c_g$.

$$\frac{\partial k}{\partial DU'} = - \frac{i\beta \langle k \rangle^2 F^2}{M^2 \cdot \mathrm{imag}(w) \cdot c_g} - \frac{\langle k \rangle (K^2 + F)}{M \cdot c_g} \qquad (3.80)$$

(for the most unstable zonal wavelength)

Effects of DUt'

The curvature of the basic-state wave's thermal zonal wind, DUt', can modulate the synoptic-scale wave. For the most unstable zonal wavelength, (3.82) suggests that the effect of DUt' is opposite to that of DU' (when $K^2 > F$). This opposite effect is reasonable since a positive DUt' increases the effective beta in the lowest layer unlike DU'. The lowest layer tends to control baroclinic instability for it is easier to change the sign of the potential vorticity gradient in that layer.

$$\frac{\partial k}{\partial DUt} = - \frac{\partial H}{\partial DUt} \Big/ \frac{\partial H}{\partial k}$$
$$= 2\langle k \rangle^2 \langle Ut \rangle (K^2 - F) \Big/ \frac{\partial H}{\partial k} \qquad (3.81)$$

At the critical wavenumber, (3.81) can be simplified by using

$$\frac{\partial H}{\partial k} = -2i \cdot \mathrm{imag}(w) \cdot M \cdot c_g$$

giving $$\frac{\partial k}{\partial DUt} = \frac{i \langle k \rangle^2 \langle Ut \rangle (K^2 - F)}{M \cdot \mathrm{imag}(w) \cdot c_g} \qquad (3.82)$$

(for the most unstable zonal wavelength)

Effects of <U>, Beta

The zonal-mean barotropic wind, <U>, has a direct effect on the spatial modulation of the synoptic-scale waves. A large <U> increases the wave's group velocity. By (3.74), (3.78), (3.80), and (3.82), a larger group velocity decreases the spatial modulation. Basically, a large c_g implies the cyclones move faster. Consequently, the cyclones spend less time in regions of strong thermal winds before entering regions of weak thermal winds. Therefore, the are less influenced by zonal asymmetries, and show a smaller spatial modulation.

$$\frac{\partial w}{\partial k} = \langle U \rangle - \frac{\beta}{M}(K^2 + F) + 2\frac{\beta}{M}\langle k \rangle^2 + 4\beta \langle k \rangle^2 \left(\frac{F}{M}\right)^2 \qquad (3.83)$$

= group velocity at the most unstable zonal wavelength

One must remember that <U> is measured relative to phase speed of the long wave. A different zonal wind will alter both the phase speed of the transient long wave and the group velocity of the synoptic-scale wave. Since <U> alters both velocities by similar amounts, the changes cancel each other. Hence, the interactions between synoptic-scale and transient long waves should be relatively insensitive to the zonal-mean barotropic winds.

Beta is important since it helps determine the relative group velocity (3.83). A small beta makes the medium weakly dispersive, and increases the effect of the synoptic eddies. For example, our analysis blows up on an f-plane, suggesting strong eddy effects.

For stationary planetary-scale waves, <U> is measured relative to the ground. Thus, the zonal wind is important for determining the group velocity of the synoptic-scale wave, and consequently the spatial modulation.

A stronger zonal wind will decrease the interaction between the stationary long and synoptic-scale waves for typical situations.

Effects of <Ut>

Increasing the zonal-mean thermal wind, <Ut>, decreases the term <Ut>/imag(w) (except on an f-plane). As a result, the spatial amplitude modulation that is caused by Ut', and DUt' is reduced (3.73, and 3.81). Of course, in the real world, changes in <Ut> are likely to be associated with changes in the synoptic-eddy amplitudes, which may counteract the direct effect of <Ut>.

Summary

In summary, we looked at the spatial modulation of a synoptic-scale wave, and found some terms which affect the amplitude modulation. We found that the equations lead to some physical interpretations, particularly at the most unstable zonal wavelength.

Regions where the basic-state thermal wind is larger than average (Ut' > 0) show spatial growth downstream. If one only considers Ut', then the amplitude of the synoptic-scale wave should peak 90^{o} downstream of the strongest thermal winds.

The thermal wind modulates the synoptic-scale wave by changing the local instability. When the thermal wind is larger than average, the wave is more locally unstable, and the wave shows spatial growth downstream. At the most unstable wavenumber, this spatial growth is proportional to the local growth rate ($\frac{\partial wi}{\partial Ut} \cdot Ut'$) and inversely proportional to the 'group

velocity' (3.74).

U' can also modulate the synoptic-scale wave. It changes the local wavelength for the frequency must be independent of location. A differing local wavelength will consequently change the local growth rate. If the local growth rate is positive, we find spatial growth downstream.

The curvature of the zonal flow modulates the synoptic-scale wave by changing the local effective beta. Where the effective beta is weak, the local instability is strong and the region shows spatial growth downstream.

<U> is important for stationary planetary-scale waves. A larger <U> increases the group velocity of the synoptic-scale wave, and consequently reduces the spatial modulation of the synoptic-scale wave. Thus, the effects of the synoptic-eddy fluxes are reduced. Fortunately, the exact value of <U> is not critical because it only changes the magnitude and not the phase of the eddy fluxes.

Beta has an important role for transient planetary-scale waves because it is proportional to the group velocity. (The group velocity is measured relative to the planetary-scale wave.) As a result, a more dispersive medium shows less interaction between the synoptic- and planetary-scale waves.

3.4 Theory: Part C

In Part B, we described the spatial structure of synoptic-scale waves. In this section, we use those results to find the large-scale variations of the waves' heat and (relative) vorticity fluxes. We find that the heat flux tends to reduce, and the vorticity fluxes tend to enhance the energy in the long waves. This is similar to observations (stationary waves: Holopainen et al., 1982) and to calculations (f-plane: Niehaus, 1980).

Our analysis is based on the separation of length and time scales. With the scale separations, the equations governing the slowly varying, large-scale flow are (3.84) and (3.85). The variables without subscripts denote the slowly varying, large-scale flow. The last two jacobians in (3.84) and (3.85) are the effect of synoptic eddies on the large-scale flow. We evaluate these jacobians using the previous results.

$$\frac{\partial}{\partial t}\nabla^2\psi = -\beta\frac{\partial\psi}{\partial x} - J(\psi, \nabla^2\psi) - J(\theta, \nabla^2\theta) - J(\psi_{syn}, \nabla^2\psi_{syn}) - J(\theta_{syn}, \nabla^2\theta_{syn}) + g \tag{3.84}$$

$$\frac{\partial}{\partial t}(\nabla^2 - 2F)\,\theta) = -\beta\frac{\partial\theta}{\partial x} - J(\psi, (\nabla^2 - 2F)\,\theta) - J(\theta, \nabla^2\psi) - J(\psi_{syn}, (\nabla^2 - 2F)\,\theta_{syn}) - J(\theta_{syn}, \nabla^2\psi_{syn}) + h \tag{3.85}$$

ψ is the large scale, slowly varying barotropic streamfunction

θ is the large scale, slowly varying baroclinic streamfunction

g, and h are dissipative effects from radiative cooling, friction and Ekman pumping.

Eddy Heat Flux

The divergence of the eddy heat flux (DHF) is calculated using our analytical solution (3.48 and 3.49). The growth rate can be ignored by the baroclinic adjustment hypothesis, so after some manipulation one can get (3.86) which is illustrated in figure 4.

$$J(\Psi_{syn}, \theta_{syn}) = \frac{1}{2}\, l \cdot \sin(2ly) \cdot kr \cdot coi\ A(x)^2 + \text{smaller terms} \qquad (3.86)$$

$$= DHF$$

Where $A(x) = A_o\, e^{\int^x -ki(x)\cdot dx}$ is the local eddy amplitude

The above equations can be linearized in the zonal asymmetries.

$$\langle J(\Psi_{syn}, \theta_{syn})\rangle = \frac{1}{2}\, l \cdot \sin(2ly)\ \langle k\rangle\ \langle coi\rangle\ A_o^2 \qquad (3.87)$$

$$J(\Psi_{syn}, \theta_{syn})' = \frac{1}{2}\, l \cdot \sin(2ly)\ A_o^2 \qquad (3.88)$$

$$\{ \int^x -2\langle coi\rangle \cdot \langle k\rangle \cdot ki(x) \cdot dx + \langle coi\rangle \cdot kr' + \langle k\rangle \cdot coi' \}$$

Note: A strong DHF in the southern region indicates a strong poleward heat flux.

Equation 3.88 can be simplified using (3.66-3.68).

$$J(\Psi_{syn}, \theta_{syn})' = \frac{1}{2}\, l \cdot \sin(2ly)\ A_o^2 \{ \int^x -2\langle coi\rangle \cdot \langle k\rangle \cdot ki(x) \cdot dx$$

$$- \left[\langle U\rangle - \frac{\beta\,(K^2 + F)}{M} + \frac{2\beta\,\langle k\rangle^2}{K^4} \right] \frac{ki}{\langle Ut\rangle} - \frac{\langle coi\rangle\ \langle k\rangle\ Ut'}{\langle Ut\rangle}$$

$$+ \frac{l\,(V' + \langle cor\rangle\ Vt')}{\langle Ut\rangle} - \frac{\langle k\rangle\ \langle coi\rangle\ DUt'}{\langle Ut\rangle\ K^2} + \frac{l \cdot (DV' + \langle cor\rangle\ DVt')}{\langle Ut\rangle\ K^2} \}$$

Using (3.52) gives:

$$J(\Psi_{syn}, \theta_{syn})' = \frac{1}{2}\, l \cdot \sin(2ly)\ A_o^2 \{ \int^x -2\langle coi\rangle\ \langle k\rangle\ ki(x) \cdot dx \qquad (3.89)$$

$$- \left(\frac{\text{real}(w)}{\langle k \rangle} + \frac{2\beta \langle k \rangle^2}{K^4} \right) \frac{ki}{\langle Ut \rangle} - \frac{\langle coi \rangle \langle k \rangle Ut'}{\langle Ut \rangle} + \frac{(V' + \langle cor \rangle Vt')}{\langle Ut \rangle}$$

$$- \frac{\langle k \rangle \langle coi \rangle DUt'}{\langle Ut \rangle K^2} + \frac{1 \cdot (DV' + \langle cor \rangle DVt')}{\langle Ut \rangle K^2} \Bigg\}$$

Note: by convention $\langle k \rangle > 0$, $\langle coi \rangle > 0$, and usually $\text{real}\left(\frac{w}{k}\right) > 0$

Ut' and ki are two major factors in (3.89). By this equation, a large eddy amplitude (i.e., $\int^{x} -ki \cdot dx$ is large) produces a large poleward heat flux. In addition, regions of strong spatial growth ($ki < 0$) have strong poleward heat fluxes.

The term $\langle coi \rangle \cdot \langle k \rangle \cdot Ut' / Ut$ (3.89) suggests that a stronger thermal wind will decrease the heat flux. However, a perturbation thermal wind also increases the spatial growth. The latter dominates when $\text{imag}(w)/\langle Ut \rangle$ is small. Hence, a positive perturbation of the thermal wind usually implies stronger a poleward heat flux.

In summary, the strongest poleward heat fluxes should occur where the eddy amplitude and spatial growth are large, and these two factors will combine in an intermediate location. Since the eddy amplitude peaks downstream of the largest spatial growth, both factors will combine downstream of the largest spatial growth, and upstream of the largest eddy amplitude. Since one expects the spatial growth to be in phase with Ut', the DHF should reduce the baroclinic energy in the long waves.

The synoptic eddies affect the barotropic flow through the divergence of their vorticity fluxes (DVFBT, 3.90). The DVFBT was calculated using (3.48) and (3.49), and it is roughly proportional to the spatial growth (see figure 5).

Equation 3.90 is flawed, for the zonal-mean DVFBT is zero at leading order. This result, unlike in the atmosphere, is a consequence of using a solution that is separable in x and y. This solution only introduces an $O(\delta)$ error in the DVFBT; however, this error is the largest term in the zonal-mean DVFBT. Our analysis, thus, cannot predict the zonal-mean barotropic flow. Fortunately, the $O(\delta)$ error has no great bearing on the interactions between the synoptic- and planetary-scale waves for the larger terms are not neglected. Therefore, the separable solution is formally justified in our problem.

The vorticity fluxes which affect the barotropic flow (DVFBT) are:

$$J(\Psi_{syn}, \nabla^2\Psi_{syn}) + J(\theta_{syn}, \nabla^2\theta_{syn}) \qquad (3.90)$$
$$= \frac{1}{2} J(\Psi_{syn,1}, \nabla^2\Psi_{syn,1}) + \frac{1}{2} J(\Psi_{syn,3}, \nabla^2\Psi_{syn,3})$$
$$= -1 \cdot ki \cdot kr^2 \, |1 + co|^2 \, A(x)^2 \sin(2ly)$$

where $\Psi_{syn,1} = \Psi_{syn} + \theta_{syn}$ = is streamfunction at level 1

$\Psi_{syn,3} = \Psi_{syn} - \theta_{syn}$ = is streamfunction at level 3

$A(x) = A_o \, e^{\int^x -ki(x)\cdot dx}$ is the synoptic eddy amplitude

Linearizing (3.90) in the zonal asymmetries gives

$$J(\Psi_{syn}, \nabla^2\Psi_{syn}) + J(\theta_{syn}, \nabla^2\theta_{syn}) \qquad (3.91)$$
$$= - ki(x) \cdot 1 \cdot \langle k \rangle^2 \, |1 + \langle co \rangle|^2 \, A_o^2 \sin(2ly)$$

In regions of spatial growth (ki < 0), the DVFBT has the form sin(2ly) (see 3.91). Here, the DVFBT enhances the poleward barotropic-vorticity gradient. Now consider a typical planetary-scale wave; its baroclinic and barotropic components are almost in phase (i.e. equivalent barotropic). Regions of strong barotropic winds (U' > 0, $\partial\Psi'/\partial y$ < 0) are also regions of strong thermal wind (Ut' > 0, $\partial\theta'/\partial y$ < 0). This strong thermal wind implies spatial growth (ki < 0). In addition, $\partial\Psi'/\partial y$ < 0 suggests that $\partial^3\psi'/dy^3$ > 0. However in regions of spatial growth, the synoptic eddies enhance the poleward barotropic-vorticity gradient (3.91). Therefore, the synoptic eddies tend to enhance the existing meridional vorticity gradients ($\partial^3\psi'/dy^3$).

Since the DVFBT typically enhances the existing meridional vorticity gradients, the DVFBT adds barotropic energy to the long wave. Roughly, equal amounts of energy comes from the baroclinic and barotropic components of the synoptic eddies. (The ratio is $|co|^2$.)

The linearized divergence of the vorticity fluxes (3.92) shows that the structure of vorticity fluxes are identical in each layer. The magnitude of these fluxes increases with height.

$$J(\Psi_{syn,i}, \nabla^2\Psi_{syn,i}) = -ki \cdot l \cdot \langle k\rangle^2 \, C^2 \, A_o^{\,2} \sin(2ly) \qquad (3.92)$$

Where C = $|1 + \langle co\rangle|$, 1, $|1 - \langle co\rangle|$ for levels 1, 2, and 3 respectively

Note that real$\langle co\rangle = \beta \cdot F \,/\, M \cdot \langle Ut\rangle > 0$

Vorticity Flux-Baroclinic

The synoptic eddies can affect the baroclinic flow through the

divergence of their vorticity fluxes (DVFBC, 3.93). The DVFBC was calculated using (3.48) and (3.49), and has the same structure as the DVFBT. Since the DVFBT enhances the barotropic component of the planetary-scale wave, the DVFBC should, by similar reasoning, enhance the baroclinic component of the planetary-scale wave.

$$J(\Psi_{syn}, \nabla^2\theta_{syn}) + J(\theta_{syn}, \nabla^2\Psi_{syn}) \qquad (3.93)$$
$$= \frac{1}{2} J(\Psi_{syn,1}, \nabla^2\Psi_{syn,1}) - \frac{1}{2} J(\Psi_{syn,3}, \nabla^2\Psi_{syn,3})$$
$$= -2\, ki \cdot l \cdot kr^2 \cdot cor \cdot A(x)^2 \sin(2ly)$$

Linearizing the above equation gives

$$J(\Psi_{syn}, \nabla^2\theta_{syn}) + J(\theta_{syn}, \nabla^2\Psi_{syn}) = -2ki \cdot l \cdot \langle k\rangle^2 \langle cor\rangle \cdot A_o^2 \sin(2ly) \qquad (3.94)$$

The DVFBC tends to increase the baroclinic energy of the long wave, whereas the DHF decreases the energy. We calculate the net effect below.

$\frac{d}{dt}$ (Baroclinic energy in the planetary-scale waves) due to syn. eddies

$$\simeq \langle \theta' \mid \{J(\Psi_{syn}, \nabla^2\theta_{syn})' + J(\theta_{syn}, \nabla^2\Psi_{syn})' - 2F \cdot J(\Psi_{syn}, \theta_{syn})'\} \rangle$$

Where $\langle A \mid B\rangle = \frac{1}{X \cdot Y} \iint A \cdot B \cdot dx \cdot dy$

Using (3.66), (3.89), and (3.94) gives:

$$= \langle \theta' \mid (A_o^2 / \langle Ut\rangle) \{ -2\beta \cdot l \cdot \frac{F}{M} \langle k\rangle^2 ki + l \cdot F \cdot (\frac{real(w)}{\langle k\rangle}$$
$$+ 2\beta \langle k\rangle^2 / K^4) ki + l \cdot F \cdot \langle coi\rangle \cdot \langle k\rangle \cdot Ut'\} \rangle + \text{smaller terms}$$

The above result assumes $\langle \theta' \mid \int^x ki(x)\, dx\rangle = 0$. This is true when θ' is sinusoidal and $ki \propto -\theta'$.

Using (3.52), (3.67), and (3.73)

$$= \langle \theta' \mid 1 \cdot F \cdot ki\, A_o^2 \{ 4\beta \langle k \rangle^2 F / K^2 M + real(w) / \langle k \rangle$$
$$- imag(w)^2 \cdot c_g \cdot M / [\langle k \rangle^2 \langle Ut \rangle^2 K^2 (2F - K^2)] \} / \langle Ut \rangle \rangle$$

The synoptic-scale wave drains baroclinic energy from the basic-state wave when the last term of this equation is small (i.e. for small imag(w)/<Ut>). These results, however, are different for the Eady model. When beta is zero, imag(w) is proportional to <Ut>, and the last term can dominate. (See chapter 4.)

Potential-Vorticity Flux

The quasi-geostrophic equations were written using the baroclinic and barotropic streamfunctions. In this formulation, the heat and (various) vorticity fluxes of the synoptic eddies appear in the equations for the large-scale flow. If the quasi-geostrophic equations were written with the upper and lower potential vorticity, the potential vorticity flux is then a natural way to describe the synoptic eddies' fluxes.

$$\frac{dq}{dt} + J(\Psi, q) + \beta \frac{\partial \Psi}{\partial x} = -J(\Psi_{syn}, q_{syn}) + \text{Dissipation}$$
$$\text{where } q_i = \nabla^2 \Psi_i \pm F (\Psi_3 - \Psi_1) \quad \text{for levels 1 and 3}$$
$$J(\Psi_{1,syn}, q_{1,syn}) = J(\Psi_{1,syn}, \nabla^2 \Psi_{1,syn} - F \cdot (\Psi_{1,syn} - \Psi_{3,syn}))$$
$$J(\Psi_{3,syn}, q_{3,syn}) = J(\Psi_{3,syn}, \nabla^2 \Psi_{3,syn} + F \cdot (\Psi_{1,syn} - \Psi_{3,syn}))$$

The divergence of the potential vorticity flux (DPVF) can be rewritten using the heat and vorticity fluxes (3.95 and 3.96). The zonal-mean DPVF (3.97) is determined by the heat flux, and it is down gradient, consistent with baroclinic instability theory.

$$J(\Psi_{1,syn},\ q_{1,syn}) = J(\Psi_{1,syn},\ \nabla^2\Psi_{1,syn}) - 2F\cdot J(\Psi_{syn},\ \theta_{syn}) \qquad (3.95)$$

$$J(\Psi_{3,syn},\ q_{3,syn}) = J(\Psi_{3,syn},\ \nabla^2\Psi_{3,syn}) + 2F\cdot J(\Psi_{syn},\ \theta_{syn}) \qquad (3.96)$$

$$\langle J(\Psi_{syn},\ q_{syn})\rangle = \mp\ 1\cdot F\cdot \sin(2ly)\ \langle k\rangle\ \langle coi\rangle\ A_o^{\,2} \quad \text{for level 1/3} \qquad (3.97)$$

When the effects of DUt' and DU' are smaller than those of U' and Ut', the wavy part of the DVPF is given by (3.98) and (3.99). (Using equations 3.89, 3.92, 3.95, 3.96.)

$$J(\Psi_{1,syn},\ q_{1,syn}) = J(\Psi_{1,syn},\ \nabla^2\Psi_{1,syn}) - 2F\cdot J(\Psi_{syn},\ \theta_{syn}) \qquad (3.98)$$

$$= -\,1\cdot ki\cdot \langle k\rangle^2\ |1 + \langle co\rangle|^2\ \sin(2ly)\ A_o^{\,2} - 1\cdot F\cdot \sin(2ly)\ A_o^{\,2}\ \{$$

$$\int^{x} -2\langle coi\rangle\ \langle k\rangle\ ki(x)\,dx - \left(\frac{real(w)}{\langle k\rangle} + \frac{2\beta\ \langle k\rangle^2}{K^4}\right)\frac{ki}{\langle Ut\rangle} - \frac{\langle coi\rangle\ \langle k\rangle\ Ut'}{\langle Ut\rangle}\ \}$$

$$J(\Psi_{3,syn},\ q_{3,syn}) = J(\Psi_{3,syn},\ \nabla^2\Psi_{3,syn}) + 2F\cdot J(\Psi_{syn},\ \theta_{syn}) \qquad (3.99)$$

$$= -\,1\cdot ki\cdot \langle k\rangle^2\ |1 - \langle co\rangle|^2\ \sin(2ly)\ A_o^{\,2} + 1\cdot F\cdot \sin(2ly)\ A_o^{\,2}\ \{$$

$$\int^{x} -2\langle coi\rangle\ \langle k\rangle\ ki(x)\,dx - \left(\frac{real(w)}{\langle k\rangle} + \frac{2\beta\ \langle k\rangle^2}{K^4}\right)\frac{ki}{\langle Ut\rangle} - \frac{\langle coi\rangle\ \langle k\rangle\ Ut'}{\langle Ut\rangle}\ \}$$

The DPVF can either enhance or lessen the potential vorticity in the long wave; no general rule exists because the DPVF is primarily controlled by Ut' whereas the potential vorticity is determined by U' and Ut'. (If U' were arbitrary, the eddy fluxes could be up or down gradient.) Long waves, however, do not have an arbitrary structure. We will consider a simple case where the inviscid growth rate is small, and where the long wave is equivalent barotropic with no surface winds (i.e. $\Psi = \theta$).

In this special case, the integrals in (3.98) and (3.99) are 90° out

of phase with the long wave, and <coi> Ut' is smaller than ki. Therefore, the in-phase DPVF is:

$$J(\Psi_{1,syn}, q_{1,syn}) \text{ (in phase)} =$$

$$= - 1 \cdot ki \langle k \rangle^2 |1 + \langle co \rangle|^2 \sin(2ly) A_o^2$$

$$+ 1 \cdot F \cdot \sin(2ly) A_o^2 \left(\frac{\text{real}(w)}{\langle k \rangle} + 2\beta \langle k \rangle^2 / K^4\right) \frac{ki}{\langle Ut \rangle}$$

$$= 1 \cdot ki \cdot \sin(2ly) A_o^2$$

$$\left[- \langle k \rangle^2 |1 + \langle co \rangle|^2 + \frac{F}{\langle Ut \rangle} \left(\frac{\text{real}(w)}{\langle k \rangle} + 2\beta \langle k \rangle^2 / K^4\right) \right]$$

Now if $\langle U \rangle \approx \langle Ut \rangle$, then $\frac{F}{\langle Ut \rangle} \left(\frac{\text{real}(w)}{\langle k \rangle} + 2\beta \langle k \rangle^2 / K^4\right) \approx F$

$$J(\Psi_{1,syn}, q_{1,syn}) \approx 1 \cdot ki \sin(2ly) A_o^2 \left(- \langle k \rangle^2 |1 + \langle co \rangle|^2 + F \right)$$

If $\langle k \rangle^2 |1 + \langle co \rangle|^2 > F$, and since $ki \propto -Ut'$ then

$$J(\Psi_{1,syn}, q_{1,syn}) \propto Ut'(x) \sin(2ly)$$

Since $q_1' = \nabla^2 \psi_1 - F (\Psi_1 - \Psi_2) = \nabla^2 (\Psi + \theta) - 2F \cdot \theta$

and $\Psi' \approx \theta'$,

Therefore, $q_1' = \nabla^2 (\Psi + \theta) - 2F \cdot \theta$

$$\propto - Ut(x) \cdot \sin(2ly)$$

$$\propto - J(\Psi_{1,syn}, q_{1,syn})$$

Here, the DPVF increased the potential vorticity of the long wave in the upper layer. On the other hand, the longer synoptic-scale waves (i.e. $\langle k \rangle^2 |1 + \langle co \rangle|^2 < F$) decrease the potential vorticity in the upper layer.

The in-phase DPVF for the lower layer is

$$J(\Psi_{3,syn}, q_{3,syn}) \text{ (in phase)} =$$

$$= -1 \cdot ki \langle k \rangle^2 |1 - \langle co \rangle|^2 \sin(2ly) A_o^2$$

$$- 1 \cdot F \cdot \sin(2ly) A_o^2 \left(\frac{real(w)}{\langle k \rangle} + 2\beta \langle k \rangle^2 / K^4 \right) \frac{ki}{\langle Ut \rangle}$$

$$= 1 \cdot ki \cdot \sin(2ly) A_o^2$$

$$\left[- \langle k \rangle^2 |1 - \langle co \rangle|^2 - \frac{F}{\langle Ut \rangle} \left(\frac{real(w)}{\langle k \rangle} + \frac{2\beta \langle k \rangle^2}{K^4} \right) \right]$$

Now if $\langle U \rangle \approx \langle Ut \rangle$, then $\frac{F}{\langle Ut \rangle} \left(\frac{real(w)}{\langle k \rangle} + 2\beta \langle k \rangle^2 / K^4 \right] \approx F$

Therefore, $J(\Psi_{3,syn}, q_{3,syn}) \approx 1 \cdot ki \cdot \sin(2ly) A_o^2 \{ - \langle k \rangle^2 |1 - \langle co \rangle|^2 - F \}$

$$J(\Psi_{3,syn}, q_{3,syn}) \propto Ut'(x) \sin(2ly)$$

If $\theta \approx \Psi$, then $q_3 = \nabla^2 \psi_3 + F (\Psi_1 - \Psi_2)$

or $q_3 \propto 2F \cdot \theta$

$$\propto Ut'(x) \sin(2ly)$$

$$\propto J(\Psi_{3,syn}, q_{3,syn})$$

The DPVF decreased the potential vorticity of the long wave in the lower layer.

In summary, the zonal-mean potential vorticity flux is down gradient. The wavy part of the DPVF can, in general, either increase or decrease the potential vorticity in the long wave. However in the simple situation, the DPVF decreased the long waves' potential vorticity in the lower layer. The synoptic-scale wave also enhanced the upper layer's potential vorticity when $\langle k \rangle^2 |1 + \langle co \rangle|^2$ was larger then F.

Discussion

According to our analysis, the zonal-mean heat flux is poleward, proportional to the square of the synoptic-eddy amplitude, and proportional to the inviscid growth rate. If the inviscid growth rate is balanced by dissipation, then the dissipation determines the amplitude of the synoptic

eddies, and consequently the degree of nonlinearity. Therefore, dissipation is a critical factor.

The synoptic-eddy heat flux has large-scale variations which are controlled by the spatial growth and the local eddy amplitude. Regions of spatial growth, show strong poleward heat fluxes; regions of large eddy amplitudes also show strong poleward heat fluxes. The two factors combine to produce the strongest heat fluxes downstream of the peak spatial growth and upstream of the largest synoptic-eddy amplitudes.

The various (relative) vorticity fluxes are controlled by the spatial growth. Typically, the barotropic component of the long wave is in-phase with the baroclinic component. The vorticity fluxes will then add baroclinic and barotropic energy to the long wave. This flux would look like a convergence of zonal momentum into the regions of spatial growth.

The potential vorticity flux reduced the zonal-mean potential vorticity, as one would expect from baroclinic instability theory. The flux, however, could either strengthen, or weaken the potential vorticity in a long wave. But for the case of an equivalent barotropic wave with small surface winds, the fluxes decreased the potential vorticity in the lower layer. (A decrease occurred in the upper layer when $\langle k \rangle^2 \, |1 + \langle co \rangle|^2$ was less than F.)

Chapter 4

4.0 Growth rate of Long Waves

In the previous chapter, we looked at a synoptic-scale wave growing on a fixed large-scale flow. In this chapter, we use this analysis to examine the temporal evolution of a small-amplitude long wave in the presence of synoptic-scale waves. Our analysis is restricted to small amplitudes so that the dynamics are linear, the eddy parameterization can be used, and finally, so that the long wave does not alter the mean flow.

If atmospheric observations can be used as guide, Lau (1979b) found that the transient-eddy heat flux extracted energy from the stationary-wave APE, with a time scale of 1.5 to 4.5 days. The vorticity fluxes appeared to be less important than the heat flux (Holopainen et al., 1982). We might then expect that the synoptic-scale waves stabilize the long waves since the eddy heat flux reduces the baroclinic energy in the long wave.

An Upper Bound on the Growth Rate

Before discussing potentially destabilizing mechanisms, we will find an upper bound on the growth rate. Consider a flow with no zonal curvature and with no dissipation. The change of the eddies' energy is approximately given by (4.1). This energy change only comes from the ZAPE, and not from the zonal barotropic energy (ZBT). Since the zonal flow has no curvature, and zonal momentum is conserved, d(ZBT)/dt is zero.

The eddy baroclinic energy (EBC) = $\frac{1}{2}(K^2 + 2F)\,|\theta'|^2$

The eddy barotropic energy (EBT) = $\frac{1}{2}K^2\,|\psi'|^2$

The total energy change is $\frac{d}{dt}(EBC + EBT) \approx -2F \frac{\partial}{\partial y}\langle\theta\rangle \langle v'\theta'\rangle$ (4.1)

Now v' and θ' can be written with the EBC and EBT.

$|v'|^2 = 2k^2 EBT / K^2$ (4.2)

$|\theta'|^2 = 2 EBC / (K^2 + 2F)$ (4.3)

Defining a growth rate as:

growth rate $= \frac{1}{2}\frac{d}{dt} \log(EBC + EBT)$

Then using (4.1), the growth rate $= -F \frac{\partial}{\partial y}\langle\theta\rangle \langle v'\theta'\rangle / (EBC + EBT)$

Equations 4.2 and 4.3, gives an upper bound for the growth rate.

$$\text{growth rate} < - \frac{2 \frac{\partial}{\partial y}\langle\theta\rangle \cdot k \cdot F \cdot (EBC \cdot EBT)^{1/2}}{K \cdot (EBC + EBT) \cdot (K^2 + 2F)^{1/2}}$$

Defining $R = \frac{EBT}{EBC}$

$$\text{growth rate} < \frac{-2F \frac{\partial}{\partial y}\langle\theta\rangle \cdot k \cdot R^{1/2}}{K (1 + R) (K^2 + 2F)^{1/2}} \quad (4.4)$$

Energy is not conserved in this linear system; however, energy is conserved if we include a source of energy (GE). Similarly, potential-enstrophy is conserved if we have a source of potential enstrophy (GPE). Since GE and GPE are related, GE and GPE can be eliminated by using the conservation of energy and potential-enstrophy, and we can find a better upper bound for the growth rate.

ZBC = energy in the zonal baroclinic flow (constant)

Conservation of energy implies: $GE + \frac{d}{dt} EBC + \frac{d}{dt} EBT = 0$ (4.5)

where GE = generation of ZBC

Now $K^2 \cdot EBT$ is eddy potential enstrophy in the barotropic eddies, $(K^2 + 2F) \cdot EBC$ is the eddy potential enstrophy in the baroclinic eddies, and $GPE = 2F \cdot GE$ is the generation of zonal potential enstrophy.

Conservation of potential enstrophy implies

$$2F \cdot GE + (K^2 + 2F) \frac{d}{dt} EBC + K^2 \frac{d}{dt} EBT = 0 \qquad (4.6)$$

Combining (4.5) and (4.6) to eliminate GE gives:

$$K^2 \frac{d}{dt} EBC + (K^2 - 2F) \frac{d}{dt} EBT = 0 \qquad (4.7)$$

The amplitude of a normal mode varies with time, but its structure is fixed. Therefore, EBC/EBT must be independent of time for a normal mode.

$$R = \frac{EBT}{EBC} = \frac{K^2}{2F - K^2} \qquad (4.8)$$

The short-wave cutoff ($K^2 > 2F$ implies stability) is a consequence of energy and potential-enstrophy conservation. If $K^2 > 2F$, then (4.8) implies the instability has negative energies which are physically impossible (unless your name is Dirac).

The short-wave cutoff can also be viewed as a triad interaction. We can define a total wavenumber as K^2 and K^2+2F for barotropic and baroclinic waves, respectively. Then the source of energy must have the middle wavenumber. If $K^2 > 2F$, then the zonal baroclinic flow has the smallest total wavenumber, and it cannot be the source of the instability.

Once EBT/EBC is found, the estimate of the growth rate can be refined. (Equations 4.4 and 4.8 are combined to eliminate EBC, and EBT.)

$$\text{growth rate} < -\frac{\partial}{\partial y}\langle\theta\rangle\, k\, [(2F - K^2) / (K^2 + 2F)]^{1/2} \qquad (4.9)$$

The above expression is an upper bound on the growth rate, and it is largest when $K^2 = 2^{1/2}F$, and $l = 0$. This happens to be the critical wavenumber. [Only the critical wavenumber is unstable when $Ut = \beta / 2F$ in the Phillips model (Pedlosky, 1979).] The upper bound is approximately $-k\, \partial\langle\theta\rangle/\partial y$, for long waves ($K^2 << 2F$). Thus, the long waves are only weakly unstable, if at all. The long waves are weakly unstable at best because most of the energy from the ZBC goes into the EBC, whereas baroclinic instability requires both EBC and EBT.

A Non-energetic Factor

The synoptic-scale wave drains energy from the long wave through its heat flux. Energy changes, however, are not the only stability criterion. For example, consider a hypothetical process which conserves energy but converts the long wave's baroclinic energy into barotropic energy. (This process conserves the total energy but reduces the potential enstrophy.) This hypothetical process increases R (i.e. EBT/EBC). By (4.4), this process increases the upper bound of the long wave's growth.

According to the theory, the synoptic eddies reduce the long wave's EBC and increase the EBT (when the barotropic and baroclinic components are nearly in phase). Like our hypothetical process, the synoptic eddies are transferring EBC to EBT. (Unlike the hypothetical process, the net long-wave energy can change.) Perhaps, the synoptic eddies are destabilizing the long waves by converting the long wave's EBC into EBT.

Another Non-Energetic Factor

The phase of the eddy fluxes is also important. If the eddy flux is 90° out-of-phase with the long wave, then the long wave's energy doesn't change. However, if the out-of-phase fluxes alter the long wave's vertical tilt, the modified long wave can be potentially more unstable.

The heat flux has a component out of phase with Ut'. The (wavy) out-of-phase heat flux reduces the thermal wind east of the largest thermal wind, and increases it to the west. This flux attempts to shift the thermal wave westward. If the baroclinic component is moved towards the ideal position, 90° west of the barotropic component, the poleward heat flux and conversion of ZAPE to EAPE are maximized. The stronger conversion could increase the growth rate of the long wave.

Three mechanisms were discussed in the preceding paragraphs. The synoptic eddies can stabilize the flow by draining energy from the long waves. The conversion of baroclinic to barotropic energy increases the upper bound of the growth rate, so the synoptic eddies might be destabilizing. The third mechanism, the out-of-phase heat flux, alters the structure of the planetary-scale wave which could make the wave more unstable. To find the quantitative changes in the growth rate, a set of equations is developed below.

Equations for Planetary-Scale Motions

The time evolution of the large-scale flow is found by assuming that the large-scale flow varies on a slow time scale, and by using a multiple-time-scale analysis. Basically, we use the equations for the long waves

with parameterized synoptic-scale waves. For a consistent analysis, the synoptic-scale waves can only grow on the slow time scale. This would occur if the largest growth rates are nearly zero (baroclinic adjustment).

The equations for the planetary-scale waves can be derived by splitting the flow into three components: synoptic scale, planetary scale, and zonal.

$$\Psi = \Psi_{syn}(t,T,x,X) + \Psi_{ps}(T,X) + \langle\Psi(t,T)\rangle \qquad (4.10)$$

$$\theta = \theta_{syn}(t,T,x,X) + \theta_{ps}(T,X) + \langle\theta(t,T)\rangle \qquad (4.11)$$

$T = \varepsilon \cdot t$ is the slow time scale

$X = \varepsilon \cdot x$ is the long length scale

$\varepsilon < O(1)$

Ψ_{syn}, θ_{syn} - synoptic-scale streamfunctions

Ψ_{ps}, θ_{ps} - planetary-scale streamfunctions

$\langle\Psi\rangle$, $\langle\theta\rangle$ - zonal flow

Ψ_{ps}, $\theta_{ps} = O(\delta) << 1$

Ψ_{syn}, $\theta_{syn} \leq O(\varepsilon^{1/2})$

i) The leading order equation for Ψ_{syn}, and θ_{syn} is the same as in Part A. Using that section, one finds $\Psi_{syn} = A(T)\Psi(t,x,X)$. As previously mentioned, the growth rates must be small (baroclinic adjustment hypothesis).

ii) The scaling for the leading order equation for Ψ_{ps} is:

$$J(\langle\Psi\rangle, \nabla^2\Psi_{ps}) = O(\varepsilon \cdot \Psi_{ps}) \qquad (U = O(1))$$

$$J(\Psi_{ps}, \nabla^2\Psi_{ps}) = O(\varepsilon \cdot \Psi_{ps}^{\,2})$$

$$J(\Psi_{syn}, \nabla^2\Psi_{syn}) = O(\Psi_{ps} \cdot \Psi_{syn}^2)$$

= effect of the synoptic-scale waves on the planetary scale

This last scaling is suggested by the WKB analysis.

Note that $l^2 = O(1)$.

This scaling suggests that the long wave cannot vary on the fast time scale. If it did, no term could balance the term $\frac{\partial}{\partial t}\nabla^2\Psi_{ps}$. Therefore, the long wave must vary on the slow time scale, which provides some justification for using two time scales.

The terms of the form $J(\Psi_{syn}, \nabla^2\Psi_{syn})$ are included in the equation for the long wave under the restriction that $|\Psi_{syn}|^2$ is $O(\varepsilon)$. In addition, terms like $J(\Psi_{ps}, \nabla^2\Psi_{ps})$ are small, and can be neglected.

iii) Consider the baroclinic equation for the zonal flow.

$$-(2F + l^2)\frac{\partial}{\partial t}\langle\theta\rangle = - J(\Psi, (\nabla^2 - 2F)\theta) - J(\theta, \nabla^2\Psi) + \text{Heating}$$

$$J(\Psi_{syn}, (\nabla^2 - 2F)\theta_{syn}) = O(\Psi_{syn}^2)$$

$$J(\theta_{syn}, \nabla^2\Psi_{syn}) = O(\Psi_{syn}^2)$$

$$J(\Psi_{ps}, (\nabla^2 - 2F)\theta_{ps}) = O(\varepsilon\cdot\Psi_{ps}^2)$$

$$J(\theta_{ps}, \nabla^2\Psi_{ps}) = O(\varepsilon\,\Psi_{ps}^2)$$

For the multiple-time scales to work, $\langle\theta\rangle$ must vary on the slow time scale. Either the heating is weak, $O(\varepsilon\cdot\langle\theta\rangle)$, or the heating is balanced by the eddy heat flux. In the latter case, heating cannot be too large or else the synoptic eddies would strong and nonlinear in the O(1) equation. Hence, the heating must be $O(\varepsilon\cdot\theta)$ or smaller.

By assumption, we are examining weak long waves, so we can use linear versions of the governing equations (4.12 and 4.13) and synoptic-eddy parameterization. The only difficulty is that the synoptic eddies' amplitude, A(T), is undetermined. We, however, circumvent this problem by considering the synoptic-eddy amplitude to be a free parameter.

$$\frac{\partial}{\partial t}\nabla^2\psi_{ps} = -\beta\frac{\partial}{\partial x}\psi_{ps} - J(\langle\psi\rangle, \nabla^2\psi_{ps}) - J(\langle\theta\rangle, \nabla^2\theta_{ps}) + \nu\nabla^4\psi_{ps} \qquad (4.12)$$
$$- do\,\nabla^2(\psi_{ps} - \theta_{ps}) - J_{ps}(\psi_{syn}, \nabla^2\psi_{syn}) - J_{ps}(\theta_{syn}, \nabla^2\theta_{syn})$$

$$\frac{\partial}{\partial t}(\nabla^2 - 2F)\,\theta_{ps} = -\beta\frac{\partial}{\partial x}\theta_{ps} - J(\langle\psi\rangle, (\nabla^2 - 2F)\,\theta_{ps}) \qquad (4.13)$$
$$- J(\langle\theta\rangle, (\nabla^2 + 2F)\,\psi_{ps}) + r\cdot\theta_{ps} - do\,\nabla^2(\theta_{ps} - \psi_{ps})$$
$$- J_{ps}(\psi_{syn}, (\nabla^2 - 2F)\,\psi_{syn}) - J_{ps}(\theta_{syn}, \nabla^2\theta_{syn})$$

$\psi_{ps}, \theta_{ps} \propto \sin(ly)\cdot\exp i(k_{ps}x - wt)$

J_{ps} is the projection of the jacobian onto the planetary-scale waves

do - Ekman pumping

v, r - damping due to unresolved motions, and Newtonian damping

The effects of the synoptic-scale wave (J_{ps}) on the planetary-scales are given below.

$$J_{ps}(\theta_{syn}, \nabla^2\theta_{syn}) + J_{ps}(\psi_{syn}, \nabla^2\psi_{syn}) \qquad (4.14)$$
$$= -\langle k\rangle^2\, m\cdot\sin(2my)\, A(T)^2\, (1 + \langle co\rangle)^2\, ki(X) \;+ \text{smaller terms}$$

$$J_{ps}(\theta_{syn}, \nabla^2\psi_{syn}) + J_{ps}(\psi_{syn}, \nabla^2\theta_{syn}) = \qquad (4.15)$$
$$= -2m\cdot\langle k\rangle^2\cdot\langle cor\rangle\, \sin(2my)\, A(T)^2\, ki(X)$$

$$2F\cdot J_{ps}(\psi_{syn}, \theta_{syn}) = m\cdot F\cdot\sin(2my)\{-\int^X 2\langle coi\rangle\cdot\langle k\rangle\cdot ki(x)\cdot dx \qquad (4.16)$$
$$+ \langle coi\rangle\, kr'(X) + \langle k\rangle\, coi'(X)\,\}\, A(T)^2 \;+\; \text{smaller terms}$$
$$= m\cdot F\cdot\sin(2my)\{-\int^X 2\langle coi\rangle\,\langle k\rangle\, ki\cdot dx$$

$$- \left(\frac{\text{real}(w)}{\langle k\rangle} + 2\beta \langle k\rangle^2 K^{-4}\right) \frac{ki}{\langle Ut\rangle}$$

$$- \langle k\rangle \frac{\langle coi\rangle}{\langle Ut\rangle} Ut' - \langle k\rangle \langle coi\rangle DUt / \langle Ut\rangle K^2 \} A(T)^2$$

+ smaller terms

A(T) is the average amplitude of the synoptic-scale wave.

k (m) is the zonal (meridional) wavenumber of the synoptic-scale wave.

Note that the terms in (4.14-4.16) are linear functions of the basic-state wave - a necessary condition to linearize (4.12) and (4.13).

Define

$$A = - \frac{\partial}{\partial \Psi_{ps}} [J_{ps}(\Psi_{syn}, \nabla^2\Psi_{syn}) + J_{ps}(\theta_{syn}, \nabla^2\theta_{syn})] \qquad (4.17)$$

$$C = - \frac{\partial}{\partial \theta_{ps}} [J_{ps}(\Psi_{syn}, \nabla^2\Psi_{syn}) + J_{ps}(\theta_{syn}, \nabla^2\theta_{syn})] \qquad (4.18)$$

$$B = - \frac{\partial}{\partial \Psi_{ps}} [J_{ps}(\theta_{syn}, \nabla^2\Psi_{syn}) + J_{ps}(\Psi_{syn}, (\nabla^2-2F)\theta_{syn})] \qquad (4.19)$$

$$D = - \frac{\partial}{\partial \theta_{ps}} [J_{ps}(\theta_{syn}, \nabla^2\Psi_{syn}) + J_{ps}(\Psi_{syn}, (\nabla^2-2F)\theta_{syn})] \qquad (4.20)$$

Now the fluxes can be written with A, B, C and D.

$$J_{ps}(\Psi_{syn}, \nabla^2\Psi_{syn}) + J_{ps}(\theta_{syn}, \nabla^2\theta_{syn}) = - A\cdot\Psi_{ps} - C\cdot\theta_{ps} \qquad (4.21)$$

$$J_{ps}(\theta_{syn}, \nabla^2\Psi_{syn}) + J_{ps}(\Psi_{syn}, (\nabla^2-2F)\theta_{syn}) = - B\cdot\Psi_{ps} - D\cdot\theta_{ps} \qquad (4.22)$$

Equations 4.12 and 4.13, can be rewritten into a linear system for any single planetary-scale wave.

$$iw\cdot\Psi_{ps} = a\cdot\Psi_{ps} + b\cdot\theta_{ps} \qquad \text{(from 4.11, 4.21, and 4.22)}$$

$$iw \cdot \theta_{ps} = c \cdot \Psi_{ps} + d \cdot \theta_{ps} \qquad \text{(from 4.12, 4.21, and 4.22)}$$

The frequency, w, is an eigenvalue of the matrix formed from the elements a, b, c, and d.

$$\text{(growth rate)} - i \cdot \text{real}(w) = \frac{1}{2}(a + d) \pm \left[\frac{1}{4}(a - d)^2 + b \cdot c\right]^{1/2} \qquad (4.23)$$

$$a = ik_{ps}\,\beta / K_{ps}^2 - ik_{ps} \cdot U - K_{ps}^2 \cdot v - do - A / K_{ps}^2 \qquad (4.24)$$

$$b = -ik_{ps}\,Ut + do - C / K_{ps}^2 \qquad (4.25)$$

$$c = \left[-ik_{ps}\,Ut\,(K_{ps}^2 - 2F) + do \cdot K_{ps}^2 - B\right] / (K_{ps}^2 + 2F) \qquad (4.26)$$

$$d = -ik_{ps}\,U + \left[ik_{ps}\,\beta - r - do \cdot K_{ps}^2 - D\right] / (K_{ps}^2 + 2F) \qquad (4.27)$$

Where $K_{ps}^2 = k_{ps}^2 + l^2$

$M_{ps} = K_{ps}^2 (K_{ps}^2 + 2F)$

Note: $K^2 = k^2 + m^2$ is the square of the synoptic wavenumber

Equation 4.23 determines the growth rate for small-amplitude long waves on a uniform zonal flow. Figure 7 shows the linear growth rate for some large-scale modes. (Parameter values correspond to those used in the numerical model.) As shown by figure 7, the $2k_o$, $2l_o$ mode was not destabilized by the parameterized eddies. The other three modes, however, grow faster with stronger synoptic eddies. It, therefore, appears that the parameterized eddies can increase the growth rate of long waves even though the eddy heat fluxes may reduce the energy of the long waves.

Figures 8-13 show how <Ut> and <U> affect the growth rate. Since the long wave is growing by a modified baroclinic instability, a stronger <Ut> always increases the growth rate. A smaller <U> decreases the 'group velocity' of the synoptic-scale waves, and consequently increases the effect of the synoptic eddies (3.73).

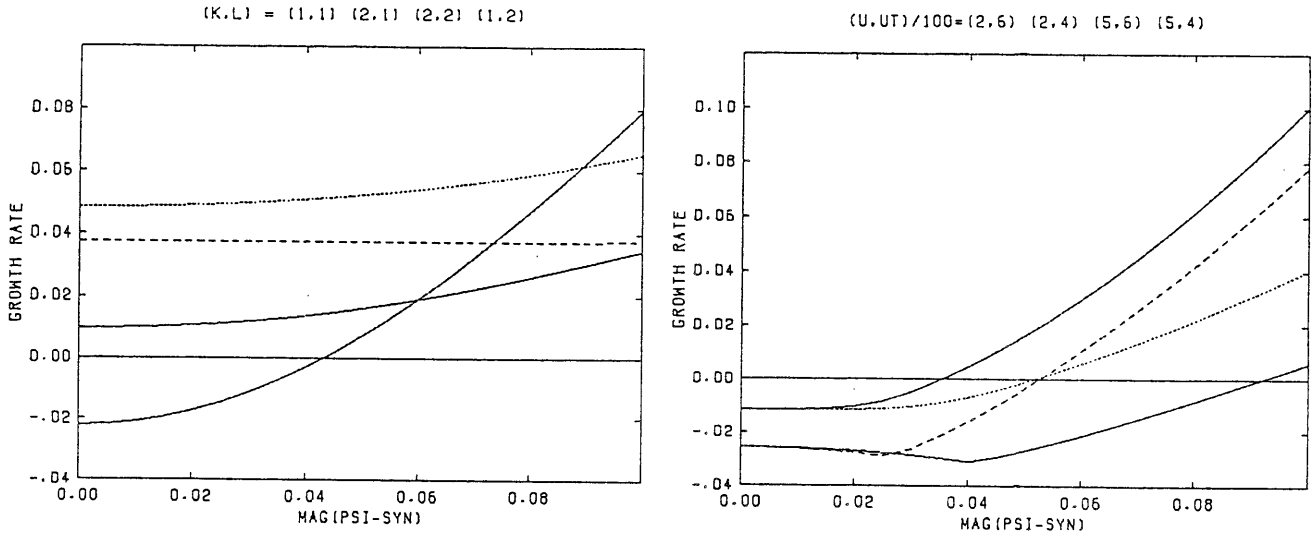

Fig. 7. Growth rate for different wavenumbers. <U> = <Ut> = 0.1
From right top to bottom (k,l)/0.67 = (1,1), (2,1), (2,2), (1,2)

Fig. 8. Growth rate for different <U>, <Ut>; (k,l) = (.67, .67)
From right top to bottom (U,Ut)/100 = (2,6), (2,4), (5,6), (5,4)

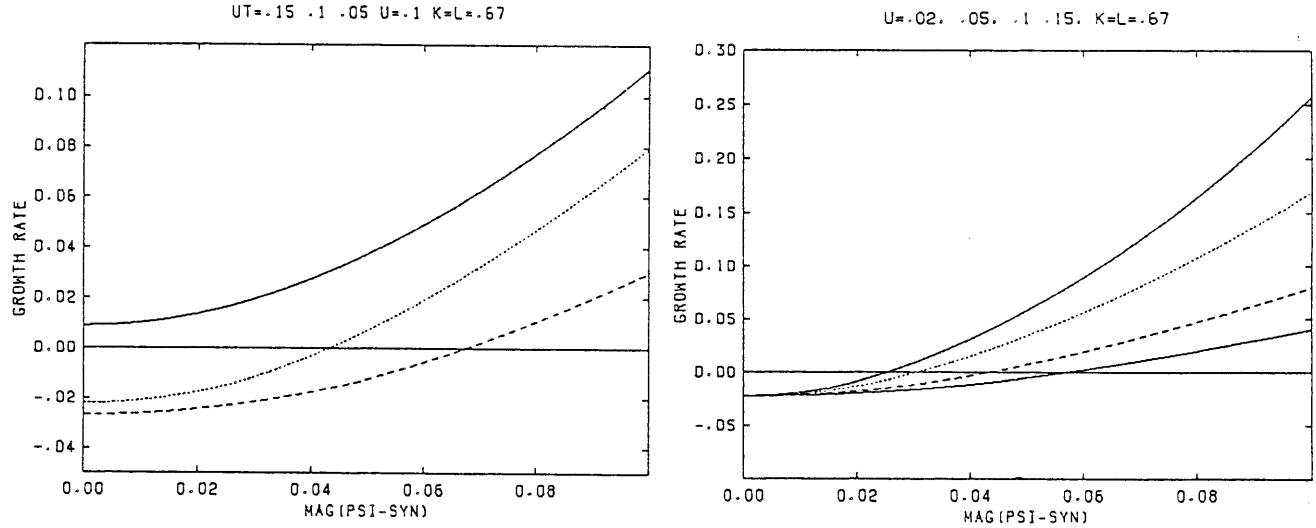

Fig. 9. Growth rate for different <Ut>; (k,l) = (.67, .67),
U = 0.1 From right top to bottom : <Ut> = .15, .1, .05

Fig. 10. Growth rate for different <U>; (k,l) = (.67, .67),
Ut = 0.1 From right top to bottom: <U> = .02, .1, .15

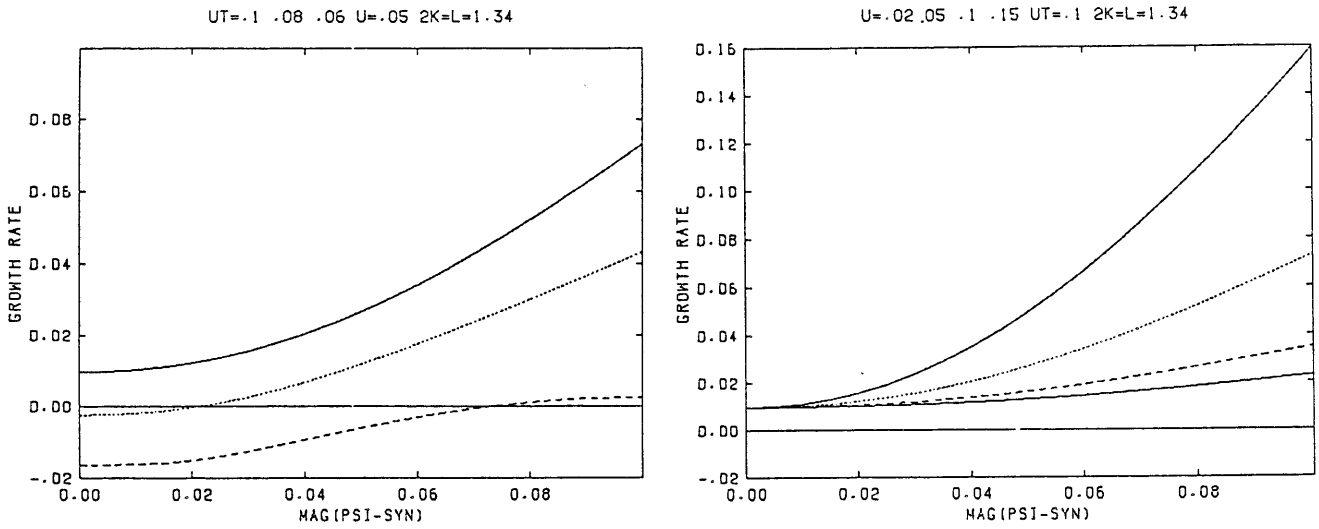

Fig. 11. Growth rate for different <Ut>; (k,l) = (.67, 1.34), Ut = 0.1 From right top to bottom: <Ut> = .1, .08, .06

Fig. 12. Growth rate for different <U>; (k,l) = (.67, 1.34), Ut = 0.1 From right top to bottom: <U> = .02, .05, .1

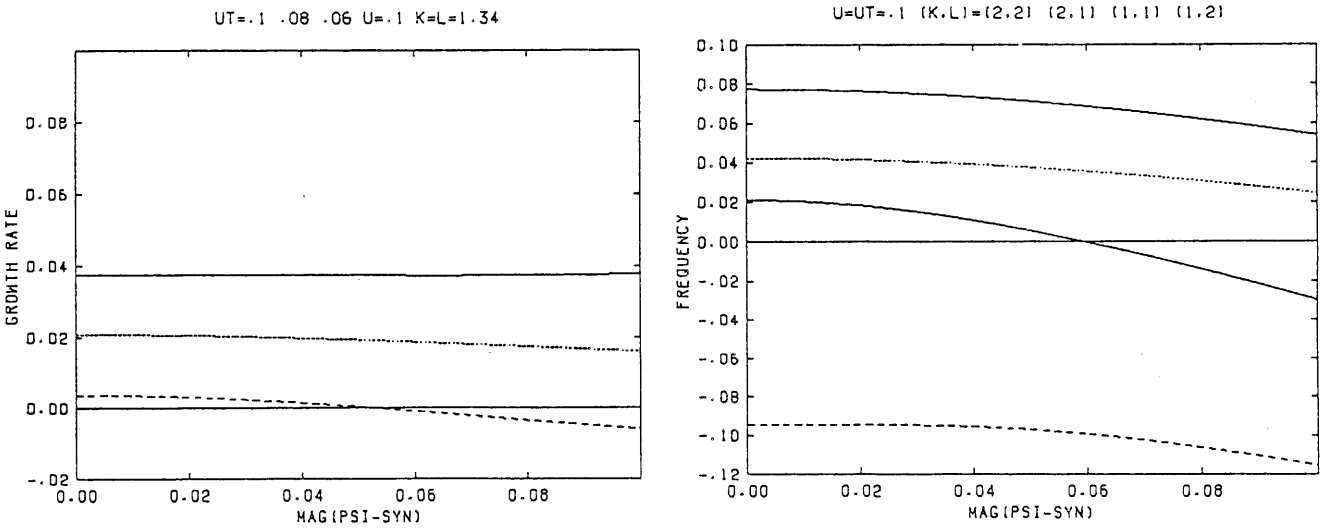

Fig. 13. Growth rate for different <Ut>; (k,l) = (1.34, 1.34), U = 0.1 From right top to bottom: <Ut> = .1, .08, .06

Fig. 14. Frequency for different wavenumbers, <U> = <Ut> = .1 From right top to bottom (k,l)/0.67 = (2,2), (2,1), (1,1), (1,2)

Equation 4.23 is still not illuminating, so we make a perturbation expansion in order to isolate the growth-rate factors. We assume the meridional velocity, dissipation and synoptic-eddy effects are small. Furthermore, the synoptic-scale wave will have the most unstable zonal wavelength. With these assumptions, we can reasonably approximate the spatial growth as a function of Ut'. (DUt' is simply $-(l^2+k_{ps}^2)Ut'$). One also finds that the heat flux (<coi>kr' + <k>coi') depends only on Ut'. (k' and coi' both depend on U', but their dependences cancel each other.) Therefore, the synoptic-eddy fluxes only depend on θ_{ps}, and terms A (4.17) and B (4.19) are both zero.

The growth rate depends on real part of the right-hand side of (4.23). The first term, real(a+d)/2, shows that the viscosity (v), Ekman pumping (do) and Newtonian cooling (r) reduce the growth rate (4.28).

$$\frac{1}{2}\,\mathrm{real}(a+d) = -\frac{1}{2}K_{ps}^2 v - r \,/\, 2(K_{ps}^2+2F) - do(K_{ps}^2+F)/(K_{ps}^2+2F) \qquad (4.28)$$
$$- \mathrm{real}(D) \,/\, 2(K_{ps}^2+2F)$$
$$\frac{1}{2}\,\mathrm{imag}(a+d) = -k_{ps}U + k_{ps}\,\beta(K_{ps}^2+F) \,/\, M_{ps} - \mathrm{imag}(D) \,/\, 2(K_{ps}^2+2F)$$
$$A = 0$$

Real(D) is the only synoptic-eddy term in $\frac{1}{2}$ real(a+d). This term has both negative and a positive contributions; however, the term d(ki)/dUt is positive, and dominates (see below).

Using $DUt = - K_{ps}^2 \cdot Ut'$, and (3.15), (3.16), and (3.20) gives

$$D = m \cdot A(T)^2 \{ 2\langle k\rangle^2 \langle cor\rangle \frac{dki}{dUt} - 2F \cdot \langle coi\rangle \langle k\rangle \frac{dki}{dUt} / i \cdot k_{ps} - \frac{F}{\langle Ut\rangle} [real(w_{syn}) / \langle k\rangle + 2\beta \langle k\rangle^2 / K^4] \frac{dki}{dUt} - F \langle k\rangle \frac{\langle coi\rangle}{\langle Ut\rangle} (1 - K_{ps}^2 / K^2) \} (dUt'/d\theta_{ps}) \quad (4.29)$$

Using $\langle cor\rangle = \frac{\beta \cdot F}{M \langle Ut\rangle}$ gives

$$D = m \cdot A(T)^2 \{ - 2F \langle coi\rangle \langle k\rangle \frac{dki}{dUt} / i \cdot k_{ps} - \frac{1}{\langle Ut\rangle} (\frac{F}{\langle k\rangle} real(w_{syn}) + 4 \frac{\beta}{M} F^2 \langle k\rangle^2) \frac{dki}{dUt} - F \cdot \langle k\rangle \frac{\langle coi\rangle}{\langle Ut\rangle} [1 - K_{ps}^2 / K_{syn}^2] \} (dUt'/d\theta_{ps}) \quad (4.30)$$

$$\frac{dki}{dDUt} = - \frac{\langle k\rangle^2 \langle Ut\rangle K^2 (2F - K^2)}{imag(w_{syn})\, c_g} < 0 \quad (4.31)$$

Since $\theta_{ps} \propto Ut'$, $dUt'/d\theta_{ps}$ is positive.

For example, if $\theta = c(x) \sin(2l_o y)$, then $Ut'(x) = c$. (See Appendix B.)

By (4.30), imag(D) < 0 and real(D) > 0 (when the last term is small compared with the penultimate term). This condition will occur when the inviscid growth rate is small.

Since real(D) is positive, it is a stabilizing factor (4.28). This stabilization can be identified with the synoptic eddies extracting baroclinic energy from the long wave.

The square-root term (4.23) also affects the long wave's growth rate.

Let $E = -(k_{ps} \beta F / M_{ps})^2 + (k_{ps} \cdot Ut)^2 (2F - K_{ps}^2) / (2F + K_{ps}^2)$ (4.32)

Then (growth rate) - i·real(w) = $\frac{1}{2}$ (a + d) $\pm$ { E (4.33)

+ $ik_{ps}\,\beta\,F\,[\,-v\cdot K_{ps}^{2} + r / (K_{ps}^{2} + 2F) - 2do\cdot F / (K_{ps}^{2} + 2F)$

$+ D / (K_{ps}^{2} + 2F)] / M_{ps}$

$- ik_{ps}\,Ut\,[(2F - K_{ps}^{2})\,C - 2do\cdot K_{ps}^{2}(F - K_{ps}^{2})] / M_{ps}\,\}^{1/2}$

+ smaller terms

Case 1: E is positive, Inviscidly Unstable Case

When E is positive, the planetary-scale wave is inviscidly unstable. Equation 4.33 can evaluated using a Taylor series about the point where the dissipation and synoptic-eddy effects vanish. Retaining only the linear terms gives (4.34).

growth rate = $\frac{1}{2}$ real(a + d) $\pm$ $E^{1/2}$ { 1 - (4.34)

$k_{ps}\,\beta\cdot F\cdot$Imag(D) / $2\cdot E\cdot(K_{ps}^{2} + 2F)\cdot M_{ps}$}

Note that imag(C) = 0, and imag(D) < 0.

The '+' root must be used since it corresponds to the more unstable mode. Here, only the synoptic-eddy term, D, affects the growth rate. Real(D) stabilizes the flow by reducing the energy in the long wave through the term $\frac{1}{2}$ real(a+d). Imag(D), the out-of-phase heat flux, increases the growth rate even though it does not affect the energy. The out-of-phase heat flux shifts the baroclinic component of the long wave westward which allows the long wave to extract more ZAPE which can be destabilizing.

Change in growth rate due to Imag(D), the out-of-phase heat flux,

$= E^{-1/2}\,k_{ps}\beta\cdot F\cdot$Imag(D) / $2(K_{ps}^{2}+2F)\,M_{ps}$

$\propto 1/k_{ps}$

Since $E \propto k_{ps}^2$ and $\text{Imag}(D) \propto 1/k_{ps}$

The out-of-phase heat flux favors long, narrow waves for the change in the growth rate goes as $1/k_{ps}$. The waves need be narrow for they must be inviscidly unstable. Of course, the waves cannot be too narrow else they will be stable due to the short-wave cutoff. More limiting, however, is that the long waves cannot be much narrower than the synoptic-scale waves, otherwise no interaction can occur.

The growth rate is a sum of the growth rate without synoptic eddies and the change caused by the synoptic eddies. The former does not encourage long wavelengths, while the latter does. Therefore, an intermediate wavelength is favored for instability.

Case 2: E is Negative, Inviscidly Stable Case

When E is negative (4.32), the long wave is inviscidly stable. Equation 4.33 can be expanded in a Taylor series about the point of vanishing dissipation and synoptic-eddy effects, giving equation 4.35 for the growth rate.

$$\begin{aligned} \text{growth rate} = \frac{1}{2}\,\text{real}(a + d) \pm (k_{ps} / 2M_{ps}) \{ & \\ + \beta F [-K_{ps}^2 \cdot v + r / (K_{ps}^2 + 2F) - 2do \cdot F / (K_{ps}^2 + 2F) & \\ + \text{real}(D) / (K_{ps}^2 + 2F)] & \\ - Ut \cdot [(2F - K_{ps}^2)\,\text{real}(C) - 2do \cdot K_{ps}^2 (F - K_{ps}^2)] \} & |E|^{-1/2} \end{aligned} \qquad (4.35)$$

Note that real(D) > 0.

C can be found using (4.14) and (4.18).

$$C = \langle k \rangle^2 \, m \cdot A(T)^2 \, |1 + \langle co \rangle|^2 \, \frac{\partial ki}{\partial Ut} \, \frac{\partial Ut}{\partial \theta_{ps}}$$

Therefore, real(C) < 0, and imag(C) = 0

Equation 4.35 has two possible normal modes which are artifacts of the two-level model. The positive root (4.35) will be called the 'external' mode, and the other will be called the 'internal' mode. The 'external' mode is barotropic (i.e. external) when <Ut> is zero.

Properties of the two modes:

1) $w_{ext} - U \cdot k_{ps} < w_{int} - U \cdot k_{ps} < 0$ (from 4.35)

2) For inviscidly stable waves, cor_{ps} is given by,

   $cor_{ps} = k_{ps} \, Ut \, (K_{ps}^2 - 2F) \, / \, [(w - U \cdot k_{ps})(K_{ps}^2 + 2F) + \beta \, k_{ps}]$

   Therefore $(EBC/EBT)_{ext} < (EBC/EBT)_{int}$ (assuming $K_{ps}^2 < 2F$)

4) The 'external' mode is real and the 'internal' mode is artificial when <Ut> is zero (Lindzen et al., 1968; Held, 1983).

The growth rate of the 'external' mode is given by the positive root of equation 4.35. The eddy fluxes, real(D), and real(C), increase the growth rate. The 'internal' mode, on the other hand, has a smaller growth rate.

This instability process prefers narrow waves because real(C), and real(D) are proportional to 'l'. However, it strongly prefers small values of |E| which correspond to stable waves near neutral (inviscid) stability.

Summary

In summary, our analysis provides a possible answer to the question raised in the introduction, "Why did the long waves grow faster in the GCM experiments than predicted by linear theory?" We find that synoptic-scale waves can destabilize the long waves by a symbiotic mechanism.

We identified three growth-rate factors. The in-phase transient-eddy heat flux reduced the long wave's baroclinic energy. This flux helped stabilize the long wave. The 90° out-of-phase heat flux destabilized the inviscidly unstable long wave by moving the long wave's baroclinic component westward. The out-of-phase flux changed the long waves' vertical tilt, allowing the long wave to extract more ZAPE which can destabilize the long wave.

The eddy vorticity fluxes were the other destabilizing factor. These fluxes added baroclinic energy to the long wave which helped counteract the stabilizing in-phase heat flux. Moreover, the vorticity fluxes could help destabilize the inviscidly stable 'external' waves. This mechanism works by increasing the barotropic energy which favors inviscidly stable waves.

All these synoptic-eddy effects have a preference for narrow long waves. The restriction, of course, is that the long waves cannot be too narrow else they would not interact with the synoptic eddies.

4.1 Frequency Changes

The synoptic-eddy fluxes can affect the long wave's frequency. Here, we examine these changes with assumptions similar to the preceding section.

Case 1: E is Positive, Inviscidly Unstable Case

When E is positive (4.32), the long wave is inviscidly unstable. For small dissipation, and eddy effects, (4.33) can be expanded in a Taylor series about the inviscid flow.

$$\begin{aligned} \text{real}(w) = {} & k_{ps}\, U - k_{ps}\, \beta(K_{ps}^2 + F) / M_{ps} + \text{imag}(D) / 2(K_{ps}^2 + 2F) \\ & \pm -k_{ps}\{\beta\, F[\, -K_{ps}^2\, v + r / (K_{ps}^2 + 2F) - 2do \cdot F / (K_{ps}^2 + 2F) \\ & \quad + \text{real}(D) / (K_{ps}^2 + 2F)] \\ & \quad - Ut\, [(2F - K_{ps}^2)\text{real}(C) - 2do \cdot K_{ps}^2 (F - K_{ps}^2)] \,\} / (2M_{ps}\, E^{1/2}) \end{aligned} \tag{4.36}$$

Note: The '+' root is important because it corresponds the unstable mode.

The change in real(w) due to synoptic eddies = (4.37)

$$= \frac{\text{imag}(D)}{2(K_{ps}^2+2F)} - \frac{k_{ps}}{M_{ps}\, E^{1/2}} \left\{ \frac{\beta \cdot F \cdot \text{real}(D)}{(K_{ps}^2 + 2F)} - Ut(2F - K_{ps}^2)\, \text{real}(C) \right\}$$

Note that real(C) < 0, real(D) > 0, and imag(D) < 0

The equation for the frequency (4.37) contains many terms. The effect of the synoptic eddies is to reduce the long wave's frequency.

Case 2: E is Negative, Inviscidly Stable

When E is negative, the long wave is inviscidly stable. The lowest order Taylor series for the frequency is given by (4.38).

$$\text{real}(w) = k_{ps} \cdot U - k_{ps}\,\beta(K_{ps}^2 + F) \,/\, M_{ps} + \text{imag}(D) \,/\, 2(K_{ps}^2 + 2F) \qquad (4.38)$$
$$\pm -|E|^{1/2} \{\, 1 + k_{ps}\,\beta\, F\, \text{imag}(D) \,/\, 2(K_{ps}^2 + 2F)\, M_{ps}\, |E|\}$$

Change in frequency due to D =

$$= \text{imag}(D) \,/\, 2(K_{ps}^2 + 2F)\, \{1 \pm - k_{ps}\,\beta\, F \,/\, M_{ps}\, |E|^{1/2}\}$$

Remember that imag(D) < 0

The frequency change depends on |E|. When |E| is large, the synoptic eddies decrease the frequency of the external mode ('+' root). (Note: equation 4.38 is not valid for small |E|.) The frequency of the internal mode is given by negative root of equation 4.38, and it is decreased by the synoptic eddies.

Summary

In summary, the parameterized synoptic eddies can alter the frequency of long waves (for example, figure 14). For the inviscidly unstable long wave and the internal modes, the synoptic eddies reduce the frequency of the long wave. For the external mode, the frequency change depends on the difference of terms, so we cannot make a general statement.

4.2 Atmospheric Observations

In the previous sections, we examined a synoptic-scale wave that was modulated by a long basic-state wave. The analysis, although for a simple situation, shows that the synoptic-scale wave can have planetary-scale modulations of its amplitude, heat and vorticity fluxes. In this section, we check whether our analysis is consistent with atmospheric observations and some instability calculations.

There are two problems with using atmospheric observations: the synoptic/transient-long wave interactions are poorly analyzed, and a beta-plane channel is unlike a sphere. In an attempt to overcome these problems, one can restrict observations to stationary planetary-scale waves in the latitude band between 30 N and 60 N, and process the synoptic-eddy data with a Blackmon band-pass filter (Blackmon, 1976). This filter retains frequencies characteristic of synoptic eddies (2.5 to 6 days).

The synoptic-scale wave, according to our theory, has only two spatial characteristics, k(x) and co(x). Both quantities are complex numbers and are difficult to measure. More easily measured are the vertical phase tilt and -ki, the spatial growth.

Spatial Growth

Many factors affect the spatial growth; however, here we will only consider Ut'. Ignoring the other factors is probably not too bad because (1) U' is not important at most unstable wavenumber, (2) effects of DU' and DUt' are smaller by scaling, and (3) U', DU', DUt' are probably strongly (anti-)correlated with Ut'. Therefore, for our purposes, we can consider the spatial growth to be proportional to Ut' (4.39).

$$\text{Theory:}\quad ki \approx -\frac{\langle k\rangle^2 \langle Ut\rangle K^2 (2F - K^2)}{M \cdot \text{imag}(w) \cdot c_g} \quad Ut' \qquad (4.39)$$

(from equation 3.73)

Note that $K^2 < 2F$, $\text{imag}(w) > 0$, and $c_g > 0$

$$\text{Observations:}\quad |\Psi_{syn}| = \Psi_{oo} e^{\int^{x} -ki(x)\cdot dx}$$

$$\text{Therefore,}\quad ki = -\frac{\partial}{\partial x} \log|\Psi_{syn}| \quad \text{where } |\Psi_{syn}| \text{ can be measured} \qquad (4.40)$$

The results of **Lau et al.** (1981) (figures 15-17) qualitatively show the expected theoretical result. The thermal wind peaks at 80 W and 130 E; the 500 mb geopotential variations peak at 55 W and 175 E. (The 850 mb temperature field was shown because it better represents the stability properties.) Like the theory, the spatial growth peaks downstream of the strongest thermal winds ($\propto$ -dT/dy).

Using the root-mean-square 500 mb height variations, the spatial growth was estimated by (4.40). This estimated -ki has a correlation of 0.70 with the 850 mb thermal wind at 45 N. With 18 points, this correlation is significant at the 0.9995 confidence level (figure 18). Thus, the observations are consistent with the spatial growth being proportional to the thermal wind (4.39).

Vertical Tilt

Synoptic-scale waves usually tilt westward with height. This tilt depends on many factors. Nevertheless, the situation is simple when the basic-state surface wind is zero, and the meridional winds are neglected. According to scaling theory, the tilt can only be a function of U F / β, and Ut'. Figure 19 shows that the westward tilt is stronger with Ut'.

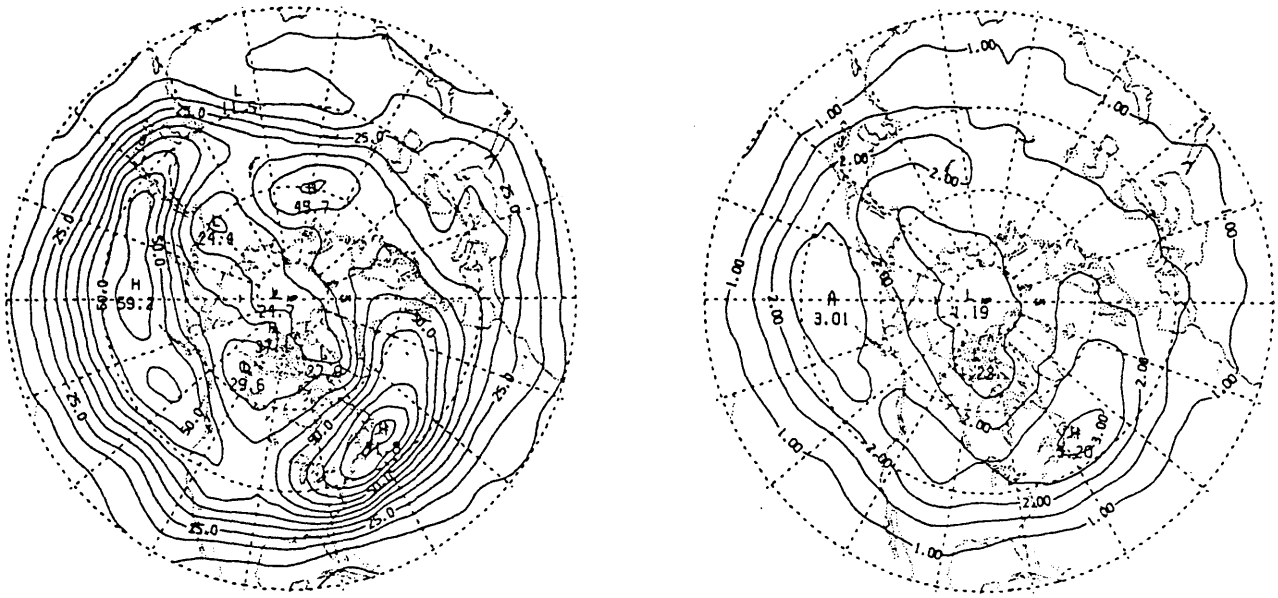

Fig. 15. Root-mean-square of 500 mb height variations in winter (Blackmon band-passed fields from Lau et al., 1981).

Fig. 16. Root-mean-square of 500 mb temperature variations in winter (Blackon band-passed fields from Lau et al., 1981).

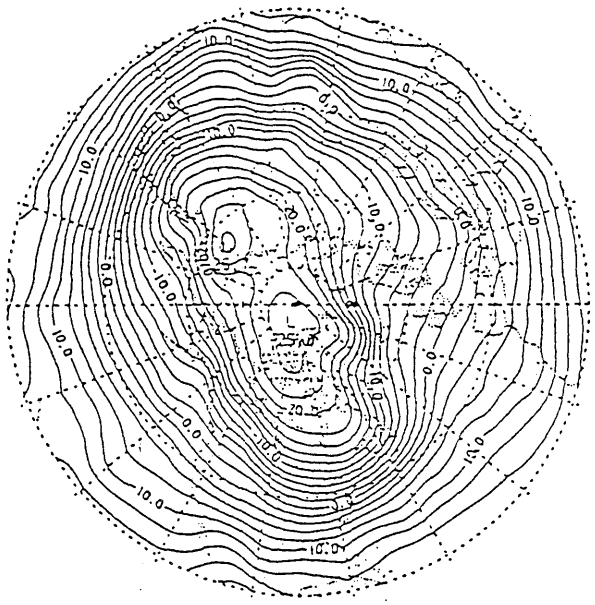

Fig. 17. 850 mb winter temperatures (Lau et al., 1981).

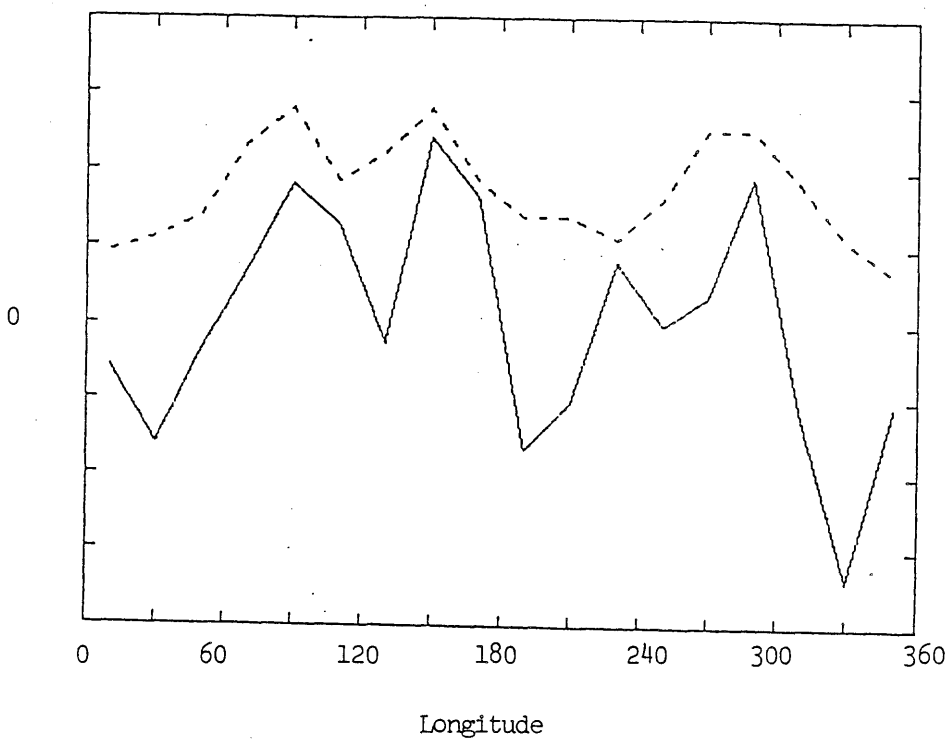

Fig. 18 Thermal wind versus spatial growth at 45 N during winter. (abscissa:longitude, ordinate: arbitary units)

Lau (1979a) calculated the phase lag between the 500 and 850 mb waves that had periods between 4 and 6.5 days (figure 20). In this figure, an arrow pointing north indicates no phase lag, and eastward pointing arrow indicates the 500mb wave lags the 850mb wave by 45 degrees. Thus, a clockwise rotation is rough measure of westward tilt with height. Lau's results are consistent with our theory; regions with the largest thermal winds have the largest vertical tilts.

Heat Flux

The zonal asymmetries of the heat flux are primarily determined by the local spatial growth, Ut', and DUt' (3.89). When imag(w)/<Ut> is small, the terms involving ki are largest and the heat flux should peak downstream of the strongest spatial growth and upstream of the largest synoptic-eddy amplitudes. Blackmon and White (1982) mentioned that they found the largest heat fluxes were west of the largest transient-eddy amplitudes.

Over the western Atlantic and western Pacific, the eddy heat flux converges in the north, and diverges in the south (figure 21; Holopainen, 1983). The sign of this 'dipole' is consistent with our theory. (These dipoles correspond to the left side of figure 4, where Ut' is large.)

Vorticity Flux

Lau (1979b) computed the 300 mb vorticity flux and he found a north-south dipole structure off the eastern coasts of Asia and the United States (figure 22). The northern pole is convergent, and the southern pole is divergent, consistent with our theory (left side of figure 5).

According to the theory, however, dipoles of one sign should exist in

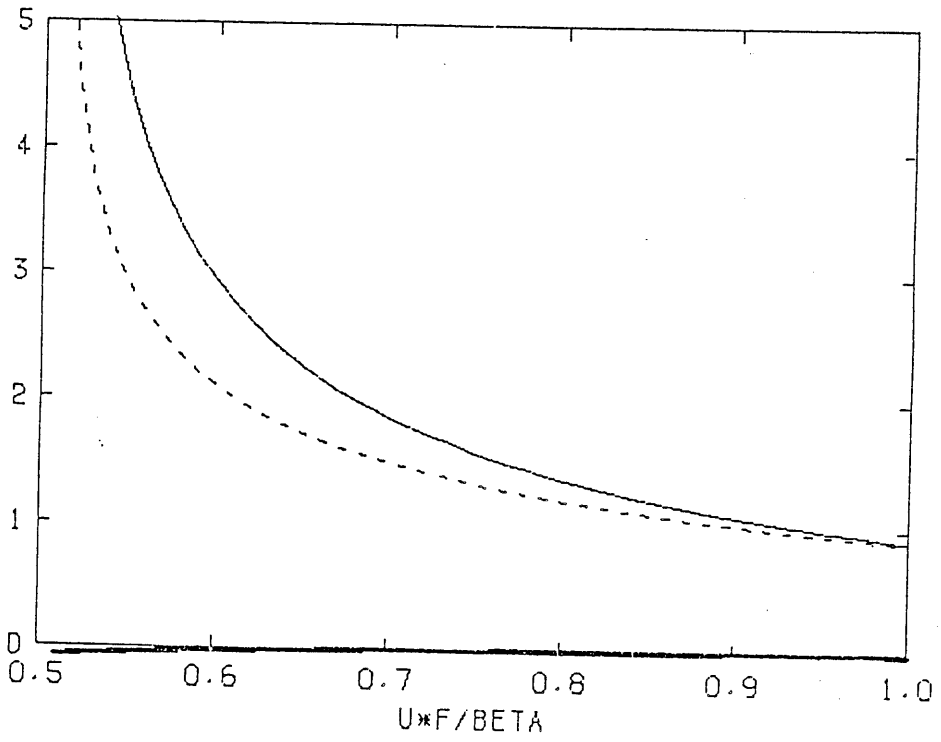

Fig 19. Vertical tilt as function of U F /β
Solid: d(vertical tilt)/DUt
Dashed: d(coi)/dUt
Dark Solid: d(cor)/dUt

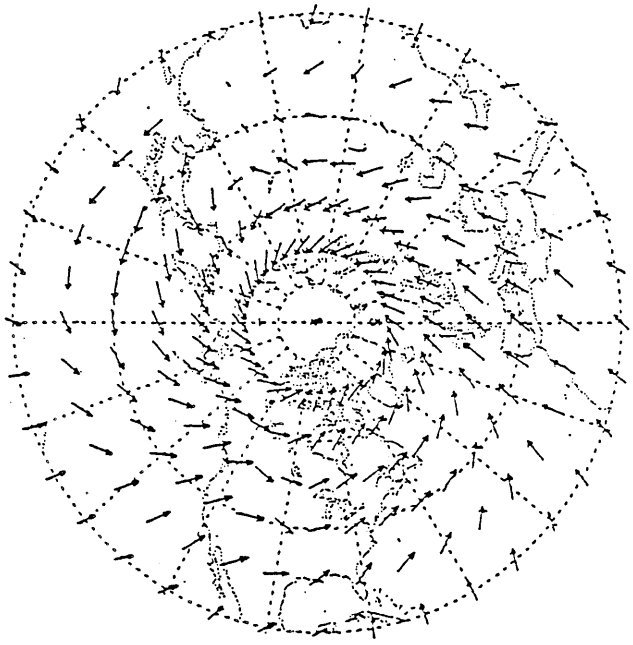

Fig. 20. Phase shifts from Lau (1979a). A clockwise rotation indicates a westward tilt with height

Fig. 21. Convergence of heat flux (winter, 500 mb, band passed) from Holopainen (1983)

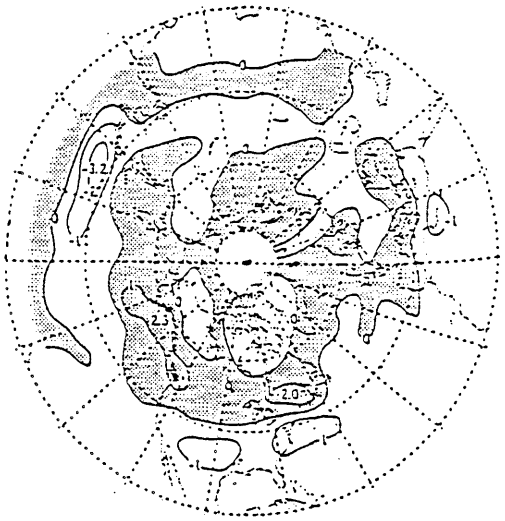

Fig 22. Convergence of 300 mb vorticity flux (winter, band passed) from Lau (1979b)

regions of spatial growth, and opposite-signed dipoles should exist in regions of spatial decay. Figure 22 does not show dipoles over regions of spatial decay. Perhaps, if the zonal mean were removed, other dipoles would appear.

Energy

The heat and vorticity fluxes can affect the long wave's energy. According to our theory, the heat flux reduces the baroclinic energy of the long wave, and the vorticity flux adds energy. Lau (1979b) and **Holopainen et al.** (1982) found that the transient-eddy heat flux drains APE from the stationary winter planetary-scale waves. **Holopainen et al.** (1982) found that the vorticity flux did add energy to the stationary planetary-scale waves, again consistent with our results.

In summary, the atmospheric observations show some features which are consistent with our analysis. For example, the correlation of the thermal wind and spatial growth (0.70 at 45N) is moderately strong. In addition, the observed heat and vorticity fluxes, and vertical tilt of the transient eddies qualitative agree with our theory.

4.3 Comparison with Niehaus

Our analysis is based on a WKB solution of the most unstable mode. It describes the spatial modulation of a synoptic-scale wave. Others [e.g. Frederiksen (see references); Niehaus, 1980] have used computers to solve the eigenvector problem to get precise answers for specific situations. This section will attempt to explain Niehaus' results (1980, 1981) using our analysis.

Model

Basic State: $\Psi(x,y,z) = - y\cdot(z + 0.5) + H(z)\cdot\cos(kx + ly)$ (4.41)

$0 < z < 1$

$H(z)\cdot\cos(kx + ly)$ is a basic-state wave forced by a surface vertical velocity. $H(z)$ is given by:

$$H(z) = a\cdot e^{Kz} + b\cdot e^{-Kz} \quad (4.42)$$

Where $K^2 = k^2 + l^2$

a and b are defined by

$$\frac{1}{2}\frac{dH}{dz}(0) - H(0) = g \quad (4.43)$$

$$\frac{3}{2}\frac{dH}{dz}(1) - H(1) = 0 \quad (4.44)$$

where g is the strength of the surface forcing

Some properties of the Eady model (with no basic-state wave):
(see Gill, 1982)

i. Waves longer than a critical value are unstable.

ii. The unstable waves have the same phase velocity, i.e. U(z=1/2).

iii. For unstable waves, real($\partial w/\partial k$) = U(z=1/2).

iv. Maximum growth rate = $0.3098 \frac{dU}{dz}$

v. $c^2 = (\frac{dU}{dz})^2 \ (\frac{1}{2} \tanh(\frac{K}{2}) - \frac{1}{K}) \ (\frac{1}{2} \coth(\frac{K}{2}) - \frac{1}{K})$

vi. Most unstable zonal wavenumber is k = 1.606 (l = 0)

When the basic-state meridional wavenumber was zero, Niehaus (1980) found the most unstable mode was unaffected by the basic-state wave. Her result is like our analysis since this particular state has a uniform zonal flow, and an unmodulated synoptic-scale wave.

In this section, the local eddy amplitude, and the local wavelength from Niehaus (1980) are compared with our analysis. The three cases, which we examine, are listed in table 1.

Table 1: Niehaus' Results

	Standard 1	Standard 2	Weak 2	Comments
k_{ps}	.2	.4	.4	basic-state wave-
l_{ps}	-.1	-.2	-.2	numbers
g	.25	.5	.2	surface forcing
growth rate	.2999	.3110	.3101	.3098 for zonal flow
a	-10.94	-2.677	-1.071	from (4.42-4.44)
b	8.515	1.290	.5161	"
U'(z=0)	.2425	.2774	.1110	* sin(kx + ly)
U'(z=1/2)	.4620	.4633	.1853	"
U'(z=1)	.6873	.6725	.2690	"
$\frac{dU'}{dz}$(z=0)	.4350	.3549	.1419	"
$\frac{dU'}{dz}$(z=1/2)	.4438	.3917	.1567	"
$\frac{dU'}{dz}$(z=1)	.4582	.4483	.1793	"

To compare Niehaus' results with the WKB results, we will use the zonal asymmetries at z = 1/2 as representative of the flow.

i.e. $U'(x) = U'(x)_{z=1/2}$ (for comparison)

$$\frac{d}{dz}U(x) = \frac{d}{dz}U(x)_{z=1/2}$$

The local wavelength (4.45) for the most unstable zonal wavenumber can be simplified by property 'iii' of the Eady model (i.e., c_g is one). In addition, the most unstable zonal wavenumber is 1.606 (property vi) which further simplifies to (4.46). Using U' from table 1, Standard 1's local wavelength is given by (4.47). This result compares nicely with figure 23 from Niehaus (1981).

$$kr'(x) = - \langle k \rangle \, U'(x) / c_g \qquad (4.45)$$

Since $c_g = 1$, $kr'(x) = - \langle k \rangle \cdot U'(x)$

Since the most unstable wavenumber is (k,l) = (1.606, 0)

$$\text{real } k(x) \approx 1.6 - 1.6 \cdot U'(x) \qquad (4.46)$$

For Standard 1, $U' = 0.46 \cdot \sin(kx)$

$$\text{real } k(x) = 1.6 - 0.7 \cdot \sin(kx) \quad \text{for Standard 1} \qquad (4.47)$$

The spatial growth at the most unstable zonal wavenumber is given by (4.48). This equation can be simplified by setting β to 0, c_g to 1, F to 4, and noting that the curvature terms are small compared with other terms.

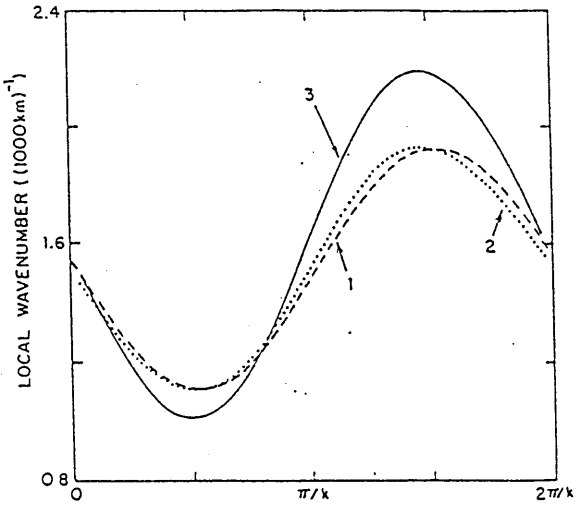

Fig. 23. Local wavenumber for Standard-1 at z=0 (Niehaus, 1981). 1)Phase function 2) Multiple-scales solution 3) Numerical solution

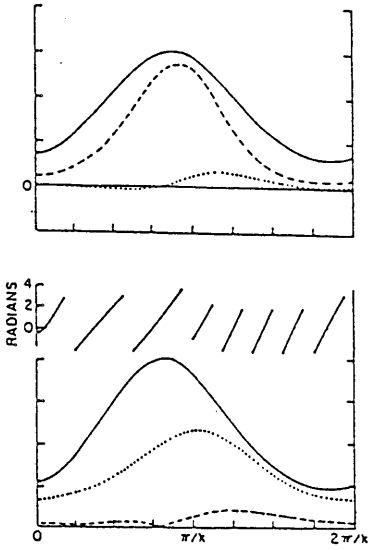

Fig. 24. Standard-1 (Niehaus, 1981) at z=0. a) solid line: $|T'|$, dashed: v'T', dotted: u'v' b) phase(Ψ'), c) solid: $|\Psi'|$, dashed: u', dotted: v'

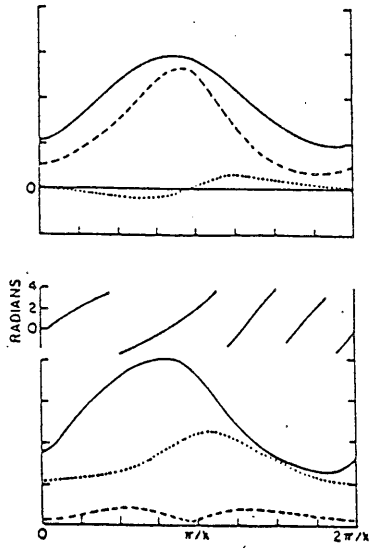

Fig. 25. Like Fig. 24 except for Standard-2.

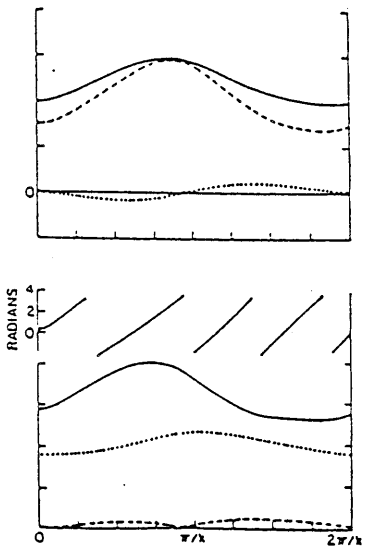

Fig. 26. Like Fig. 24 except for Weak-2.

$$ki(x) = -\frac{\frac{\partial}{\partial Ut}\,imag(w)\; Ut'(x)}{c_g} - \frac{\beta\, k^2\, F\, DU'(x)}{M^2 \cdot imag(w) \cdot c_g} + \frac{k^2\, Ut\, (K^2 - F)\, DUt'(x)}{M \cdot imag(w) \cdot c_g} \qquad (4.48)$$

$$ki(x) = -\frac{(\frac{\partial}{\partial Ut}\; imag(w))\; Ut'}{c_g}$$

$$\text{or } ki(x) = -\frac{\partial}{\partial U_z}\, imag(w)\, \frac{\partial U'}{\partial z}(x) \qquad (4.49)$$

The partial derivative in (4.49), can be evaluated in the two-level model; however, the exact result is used instead (k = most unstable, l= 0, property 'iv' of the Eady model).

$$\frac{\partial}{\partial U_z}\, imag(w) = 0.3098$$

$$\text{Therefore } ki(x) \approx -0.3098 \cdot \frac{\partial U'}{\partial z}(x)$$

$$\text{and } |\Psi| = \Psi_{oo}\, e^{\int^x -ki \cdot dx} = \Psi_{oo} \exp \int^x 0.3098 \cdot \frac{dU'}{dz} \cdot dx \qquad (4.50)$$

$$\text{Since } \frac{dU'}{dz} \approx \sin(kx + ly)$$

$$ki \approx -ki_o \sin(kx + ly)$$

$$\text{which implies } \frac{|\Psi|_{max}}{|\Psi|_{min}} = \frac{\exp(ki_o / k_{ps})}{\exp(-ki_o / k_{ps})} = \exp(2ki_o / k_{ps})$$

The (relative) eddy-amplitude is easily determined from the spatial growth by (4.50). The predicted amplitude is a deformed sinusoid with a peak at 180°. The distortion flattens the troughs and sharpens the peaks. Niehaus' results (figures 24c, 25c, and 26c) are roughly like the WKB solution. However, the WKB solution under predicts the peak amplitude and shifts the peaks eastward.

Table 2: WKB Predictions

	Standard 1	Standard 2	Weak 2	Comments
$\frac{dU'}{dz}$	.4438	.3917	.1567	Niehaus (z=1/2)
ki_o	.14	.12	.049	.3098 dU'/dz
$\|\Psi\|_{max}/\|\Psi\|_{min}$	4.0	1.8	1.3	WKB at z=1/2
$\|\Psi\|_{max}/\|\Psi\|_{min}$	4.3	3.2	1.5	Niehaus (z=0)
$\|\Psi\|_{max}/\|\Psi\|_{min}$		2.6		Niehaus (z=1/2)
$\|\Psi\|_{max}/\|\Psi\|_{min}$		2.4		Niehaus (z=1)
angle of $\|\Psi\|_{max}$	150^o	145^o	130^o	Niehaus (z=0)

The perturbation zonal winds are large according to Table 1. For example, U'(1) is 69% of the steering-level winds in "Standard 1." Clearly, the basic-state wave is not weak, and parameter δ is not small. We can improve our results by including the $O(\delta)$ correction described in Appendix A.

$$|\Psi| \approx e^{-\int^x ki(x)\cdot dx + g1(x)} \quad \text{(includes } \delta \text{ correction)}$$

Where $g1(x) = -\frac{1}{2} \log \frac{dH}{dk}$ from (A.5)

At the most unstable zonal wavenumber, real $\frac{dH}{dk} = 0$

and $\frac{dH}{dk} \approx -2i\cdot imag(w)\ U(x)\ M(x)$ from (3.60)

Where $M(x) = (k^2(x) + l^2)\ (k^2(x) + l^2 + 2F)$

For Niehaus' model $F = 4$

Therefore $|\Psi| \approx \dfrac{e^{-\int^x ki(x)dx}}{\left|\frac{dH}{dk}\right|^{1/2}}$ with $O(\delta)$ correction

For the purposes of the calculations, we let $\langle k \rangle = 1.6$ and $l = 0$

The O(δ) correction improved our results. (Compare figures 27, 28, and 29 with 24c, 25c, and 26c.) The eddy's amplitudes and phases are better predicted (table 3). The barotropic winds, which strongly control the O(δ) correction, shifted the strongest eddy amplitudes westward and increased the spatial modulation.

Table 3: WKB Predictions with the O(δ) Correction

	Standard 1	Standard 2	Weak 2	Comments
$\|\Psi\|_{max}/\|\Psi\|_{min}$	4.7	2.7	1.5	WKB
$\|\Psi\|_{max}/\|\Psi\|_{min}$	4.3	3.2	1.5	Niehaus (z=0)
angle of $\|\Psi\|_{max}$	140°	115°	125°	WKB
angle of $\|\Psi\|_{max}$	150°	145°	130°	Niehaus (z=0)
angle of $\|\Psi\|_{min}$	340°	330°	320°	WKB
angle of $\|\Psi\|_{min}$	330°	330°	320°	Niehaus (z=0)

Discussion

Our analysis reproduces Niehaus' results fairly well, even though the models differ significantly, and basic-state waves are strong. Ut strongly controlled the instability's amplitude, while U influenced the amplitude by an O(δ) correction. The curvature of the zonal flow had almost no effect on the instability, unlike Niehaus' conjecture (1981).

Some of our results were not apparent in Niehaus' work. For example, the local instability properties were important in determining the spatial modulation; the local instability and the local group velocity do not

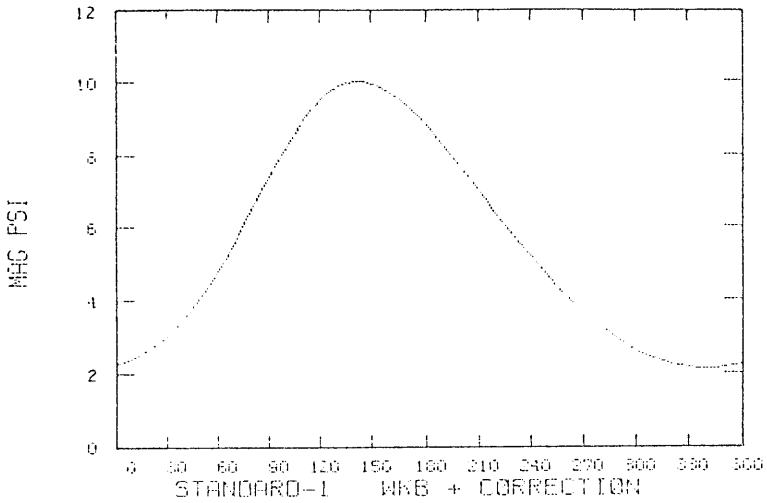

Fig. 27. Standard-1 Ψ' from WKB analysis with the $O(\delta)$ correction (compare with fig. 24c)

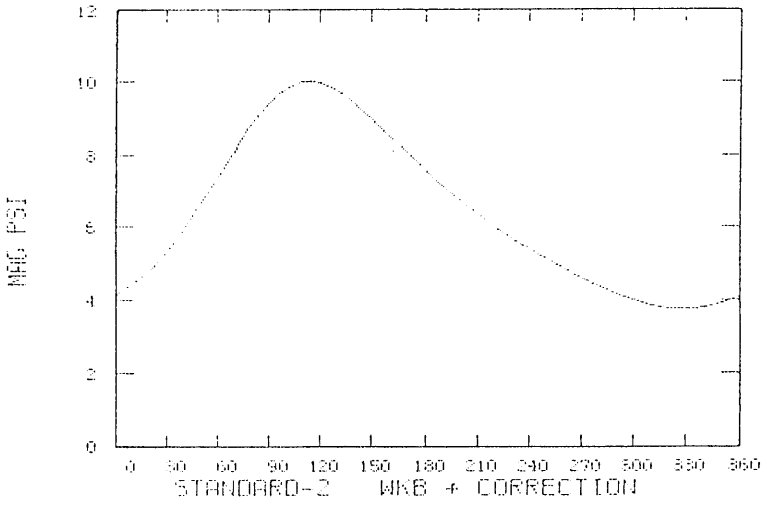

Fig. 28. Like fig. 27 except for Standard-2 (compare with fig. 25c).

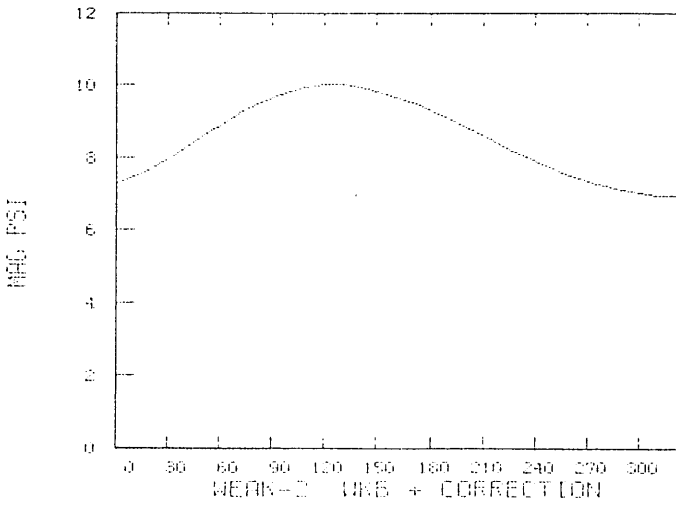

Fig. 29. Like fig. 27 except for Weak-2 (compare with fig. 26c).

cancel each other as suspected by Niehaus (1981). In addition, the curvature of the basic-state flow was not significant as Niehaus (1981) speculated.

The surface wind, which was arbitrarily set to 0.5, was important. It controls the group velocity which helps determine the spatial modulation. Decreasing the surface wind by 10% should produce a 5% increase in spatial modulation (i.e. k'). The factor of 1/2 comes from the 'group velocity' being twice as fast as the surface wind speed.

Beta, which is missing in the Eady model, was also important. It controls ∂(imag(w))/∂Ut, an important factor in the spatial growth. It also controls the group velocity, another important factor. For example in the Eady model, the phase speed and real(∂w/∂k) are equal for synoptic-scale and transient long waves. Therefore, the (relative) group velocity is zero, suggesting extremely large interactions.

4.4 Comparison With Frederiksen

Frederiksen (see references) has computed the instability of many non-zonal flows using a multi-level spherical model. He was attempting to explain the locations of storm tracks and cyclogenesis. Since he was looking for the most unstable normal modes, one may expect that the local wavenumbers are given by the following relationships.

For the most unstable wavenumber and ignoring the curvature terms,

$$\text{real}(k') \approx - \langle k \rangle \cdot U' / c_g$$

$$ki \approx - \frac{\partial}{\partial Ut} \text{imag}(w) \cdot Ut' / c_g$$

These equations are consistent with some of Frederiksen's results. The instabilities are strongest downstream of the strongest thermal winds, and long wavelengths occur in regions of strong barotropic winds. There are, however, significant differences. For instance, when the basic-state wave was purely barotropic, we may expect that the instability's wavelength changes, not its amplitude. However, Frederiksen (1978, 1979b, and 1980) found substantial amplitude variations. Perhaps the basic-state wave is so strong that changes of the local wavelength alter the local instability. [In Frederiksen (1978), the local wavelength varies by a factor of two. Here, regions of average wavelength should show spatial growth.] Another explanation is that the barotropic basic-state wave changes the wavetrain's latitude. In many of Frederiksen's basic states, the local instability is a strong function of latitude. This latitude factor could explain some of Frederiksen's calculations (1979b and 1980).

In summary, Frederiksen has calculated the normal modes of many non-zonal flows. The instabilities' amplitude and heat fluxes appear to be qualitatively explained by the local instability properties. The thermal wind has a direct effect on the local instability. The barotropic wind may indirectly alter the local instability by changing the local wavelength, and by making the wavetrain meander through regions of differing local instability.

Chapter 5

5.0 Description of the Numerical Model

We developed a numerical model to test our analytical theory. In the model, we do not use a separation of time and length scales, so the model can be used to test the accuracy and sensitivity of our theory. In particular, we calculate the energetics of the synoptic/planetary-scale interactions, examine the sensitivity to radiative forcing and dissipation, and test the baroclinic-adjustment hypothesis.

The numerical model simulates a two-level quasi-geostrophic flow on a periodic beta-plane channel. The model is based on equations that are identical to the theory's except the theory used a simpler dissipation.

Model Equations

$$\frac{\partial}{\partial t}\nabla^2\psi = -\beta\frac{\partial\psi}{\partial x} - J(\psi, \nabla^2\psi) - J(\theta, \nabla^2\theta) + \nu\nabla^4\psi \qquad (5.1)$$
$$- do\,\nabla^2(\psi - \theta) + \omega_{org}$$

$$\frac{\partial}{\partial t}(\nabla^2 - 2F)\theta = -\beta\frac{\partial\theta}{\partial x} - J(\psi, (\nabla^2 - 2F)\theta) - J(\theta, \nabla^2\psi) \qquad (5.2)$$
$$- do\,\nabla^2(\theta - \psi) + r\,(\theta - \theta_e) - Q_f - \omega_{org}$$

$$\frac{\partial}{\partial x}\theta(x,y,t) = 0 \qquad \text{for } y = 0,\ Y \qquad (5.3)$$

$$\frac{\partial}{\partial x}\psi(x,y,t) = 0 \qquad \text{for } y = 0,\ Y \qquad (5.4)$$

$$\theta(x, y, t) = \theta(x + X, y, t);\quad \psi(x, y, t) = \psi(x + X, y, t) \qquad (5.5)$$

β = scaled beta parameter = 0.25 for calculations

F = scaled Froude number = 3.7415 for calculations

ν = scaled eddy diffusion coefficient = $\frac{1}{125}$

do = scaled Ekman parameter = 0.025 for most calculations

$\theta_e(y)$ = radiative equilibrium temperature

$= -0.3 \left(\frac{y}{Y} - \frac{1}{2} \right)$ for most calculations

r = Newtonian cooling, $2F/r = 40$ inertial time periods for most calculations

$\omega_{org}(x,y)$ is a surface vertical velocity due to orography

$Q_f(x,y)$ is the diabatic heating (excluding Newtonian cooling)

Q_f and ω_{org} are zero except in the section on forced waves.

The model equations (5.1 and 5.2) have been scaled. Time was scaled by 1/f ($\approx$ 6 hours), distance was scaled by the internal Rossby radius of deformation ($\approx$ 1000 km), and pressure was scaled by the average surface pressure (1000 mb). The top and bottom of the model are at 200 and 900 mb respectively, approximately at the tropopause and top of the planetary boundary layer. [If the vertical boundaries were at 0 and 1000 mb, F would decrease (3.11). Decreasing F would increase the critical shear (β/Ut) and lengthen the critical wavelength ($K_c^2 = 2^{1/2} F$).]

Numerics

We used a spectral model for it requires fewer degrees of freedom to accurately determine the group velocities which control the spatial modulation of the synoptic eddies. As an alternative, a grid-point method is less accurate. For example, fourteen grid points per wavelength are needed to model the group velocity to within 10%. [This is for a second-order centered space differencing and a linear advection equation (Mesinger and Arakawa, 1976).]

By design, our model conserves energy and enstrophy in the inviscid

system for small time steps (i.e. no aliasing). Conservation prevents non-linear computational instabilities as discussed by Phillips (1959). We avoided aliasing by using 50% more collocation points in each direction than degrees of freedom. For example, the model had 10 degrees of freedom in the zonal direction, so a 16-point fast Fourier transform was used.

The model's spectral modes (5.6-5.7) satisfy the boundary conditions (5.3-5.5), and are eigenvectors of the operator ∇^2. The latter property makes the operator ∇^2 easy to invert. The former is necessary for the Galerkin approximation (Gottlieb and Orszag, 1977). The zonal-mean field was expanded in cosines instead of sines because cosines reduce the Gibbs phenomena when trying to describe the field 'U = constant'. Cosines, however, make the jacobian more difficult to evaluate using the fast, pseudo-spectral method. (See Appendix E.)

$$\Psi = \sum_{n=1}^{5} a_{n0} \cos(n\, l_o y) + \sum_{n,m=1}^{5} \text{Real } a_{nm} \sin(n\, l_o y) \exp(im\, k_o x) \qquad (5.6)$$

$$0 = \sum_{n=1}^{5} b_{n0} \cos(n\, l_o y) + \sum_{n,m=1}^{5} \text{Real } b_{nm} \sin(n\, l_o y) \exp(im\, k_o x) \qquad (5.7)$$

$0 < y < Y = \pi / l_o$

For the numerical model, $n = 0,\ldots,5 \quad m = 1,\ldots,5$

The numerical model has 110 degrees of freedom.

Alternate Equations

The numerical model can use (5.1) and (5.2). However, an alternative set of equations (5.8-5.10) was used because it is faster to solve. Three jacobians are evaluated per time step instead of four.

$$\frac{1}{dp}(2F - \nabla^2)\omega_2 = 2F\cdot\beta\frac{\partial\theta}{\partial x} + F\cdot J(\Psi_1, \nabla^2\Psi_1) - F\cdot J(\Psi_3, \nabla^2\Psi_3) \qquad (5.8)$$
$$- 2F\,\nabla^2 J(\Psi, \theta) + \frac{F}{dp}\omega_4 + \nabla^2(Q + r(\theta - \theta_e))$$

$$\frac{\partial}{\partial t}\nabla^2\Psi_3 = -\beta\frac{\partial}{\partial x}\Psi_3 - J(\Psi_3, \nabla^2\Psi_3) - \frac{1}{dp}(\omega_4 - \omega_2) + \frac{\nu}{2}\nabla^4\Psi \qquad (5.9)$$

$$\frac{\partial\theta}{\partial t} = - J(\Psi, \theta) + \frac{1}{2F\cdot dp}\omega_2 - \frac{r}{2F}(\theta - \theta_e) - \frac{Q}{2F} \qquad (5.10)$$

Where $\Psi_1 = 2\theta + \Psi_3$

Equation 5.8 determines the vertical velocity at the middle level, and it includes dissipation. Equation 5.9 is the vorticity equation for the lowest layer, while equation 5.10 is the thermo-dynamic equation.

Time Stepping

We used the Lorenz-n-cycle scheme (Lorenz, 1971) to integrate (5.8-5.10) forward in time. Using four substeps per time step, this scheme is second order (i.e., the error is $O(dt^3)$). To the scheme's advantage, it needs initial conditions at only one time, and it is very accurate for the linear advection problem, dh/dt = U·dh/dx. The latter property may be good for modeling group and phase velocities.

The model used a time step of 5 inertial periods except for one simulation. The exception, the low-friction/strong-radiative-forcing case, used a time step was 2.5 inertial periods. In this case, the nonlinearities and waves were very large.

Domain size

The domain size is dynamically important, especially for a limited-

resolution model. The domain size determines whether the synoptic- and planetary-scale waves are resolved, and whether the baroclinic adjustment hypothesis holds. Given the constraints, the length scale was chosen (k_o, l_o = .67) so that the most unstable mode had $k \approx 3k_o$. With this choice, the model can resolve some long waves ($k = k_o, 2k_o$) and some shorter waves ($k = 4k_o, 5k_o$). The width of the beta-plane is π/l_o, or roughly 4700 km. Thus, the model can be viewed as a beta-plane channel with terrestrial length scales but with a wavenumber 3 symmetry.

5.1 Cases

The numerical model was run with several different parameters. The different cases were used to test the sensitivity of the system.

Control run

Strong forcing

Thermal equilibrium temperature gradient was increased by 4/3.

Weak friction

Ekman pumping, and Newtonian cooling were reduced by 1/2

Weak friction/Strong forcing

Ekman pumping, and Newtonian cooling were reduced by 1/2. The thermal-equilibrium temperature gradient was doubled to approximate the control run's radiative forcing.

Quasi-linear

Only wave-mean flow interactions were allowed.

Wide basin

Meridional width of the domain was doubled. This case shows the dependence of baroclinic adjustment on the domain width.

Gross Features of the Numerical Simulations

The numerical model had some features common to more complicated models. The zonal flow was driven by radiation, and the eddies converted ZAPE into EAPE. In the control run, most of the conversion of ZAPE into EAPE was done by the synoptic-scale modes ($k=3k_o$). Some other cases showed significant conversions by longer waves.

Common Features

1. The surface zonal flow is small.
2. The upper-layer flow is westerly (thermal wind balance).
3. The flow has a westerly jet except in the wide-basin case.
4. The zonal flow was linearly unstable, and strongly unstable in the wide-basin and weak-friction/strong-forcing cases.

In the model, only the surface drag (Ekman pumping) can change the mean zonal momentum. If the zonal flow reaches a steady state, the surface drag cannot add zonal momentum. Thus, the mean surface wind must be small, and the upper-level flow must be westerly by thermal wind balance.

The flow didn't reach a steady state in the model (the model had not obvious stable equilibrium state). The amplitudes of the synoptic eddies changed continuously, and the zonal flow changed in response to the eddies. The oscillations were caused by a coupling of the synoptic-scale waves, the zonal flow and the radiative forcing. When the zonal flow was unstable, the synoptic eddies grew, and made the zonal flow neutral by reducing the temperature gradient and ZAPE. Even though the flow became neutral, the eddies continued to extract ZAPE. However, the eddies were too strong, and they continued to extract more ZAPE than supplied by radiative forcing.

Consequently, the flow became stable, and the eddies began to decay. The heating eventually made the flow unstable, repeating the process. The oscillation's period should be determined by the radiative time scale.

The model had multiple time-mean states, which should not be confused with multiple equilibria. The off-center westerly jet can appear in the either side of the channel because of a symmetry property (figure 30). These states are curious but are not important in this thesis because they don't change the energetics or conclusions. (See Appendix F.)

The zonal flow was sensitive to the dissipation and the forcing. The westerly jet was stronger in the strong-forcing cases (figures 31, and 32), and the weak secondary jet disappeared in the weak-friction cases.

5.2 Energetics I

The more-or-less traditional energy cycle (figure 33) is similar to the atmosphere's. Radiation heats the southern regions and cools the northern regions, creating zonal baroclinic energy. Fluid motions then transform this energy into eddy baroclinic and eddy barotropic energies. The energy that has not been lost to dissipation is then converted from eddy barotropic energy into zonal barotropic energy. (Unlike the energy cycle that is divided into APE and KE, there is no direct conversion between the zonal baroclinic and zonal barotropic energies.)

The zonal baroclinic $\cos(l_o y)$ mode had the most energy, and it was strongly forced by radiation. The zonal barotropic mode $\cos(l_o y)$ had the second most energy. This mode was not forced by solar radiation, but by the requirement that the surface wind be small (at equilibruim, the mean surface drag cannot remove zonal momentum). Unexpectedly, the barotropic

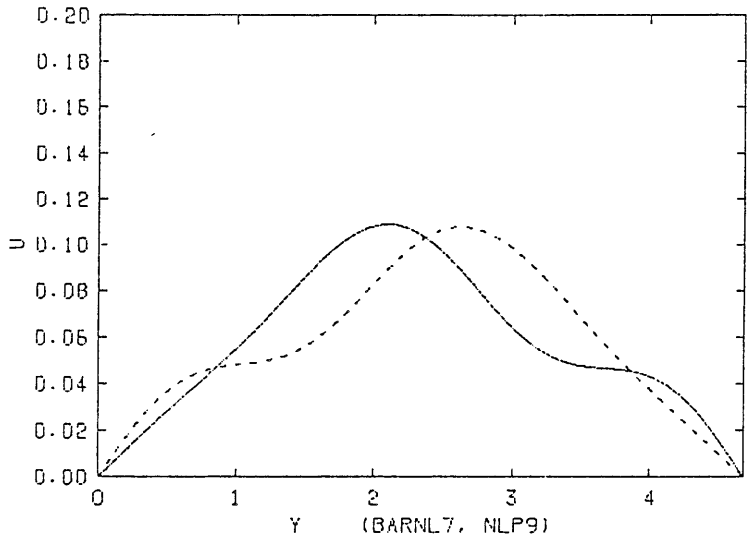

Fig. 30. The time- and zonal-mean U for two different initial conditions. (Shows multiple time-mean states.)

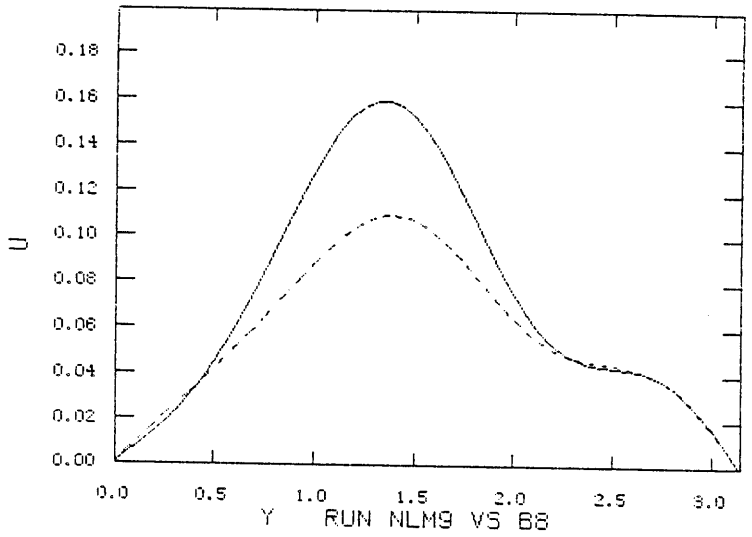

Fig. 31. Zonal-mean U for control (B8, dashed) and strong-forcing case (M9, solid).

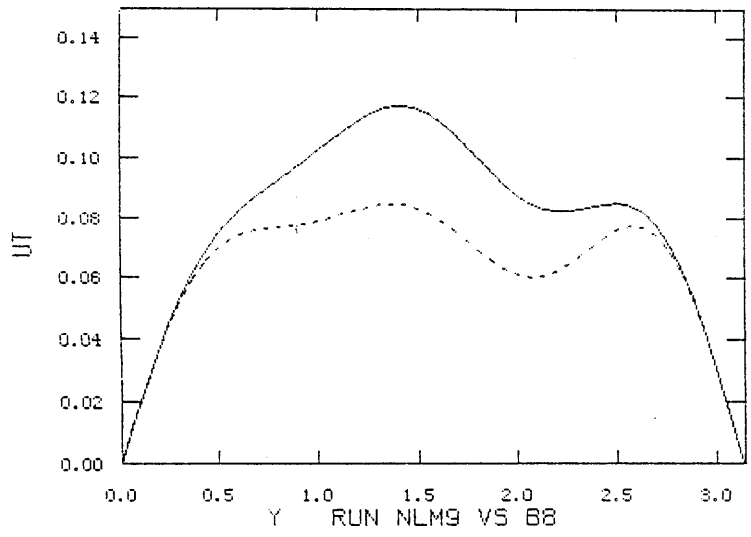

Fig. 32. Zonal-mean Ut for control (B8, dashed) and strong-forcing case (M9, solid).

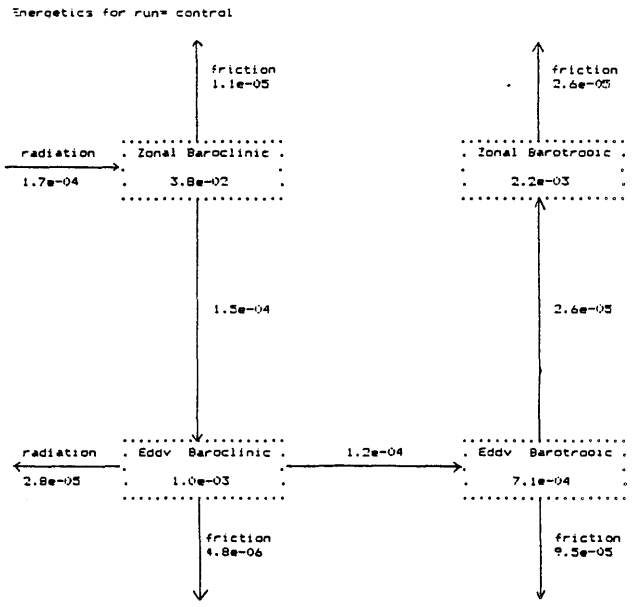

Fig. 33. Energetics for the control run.

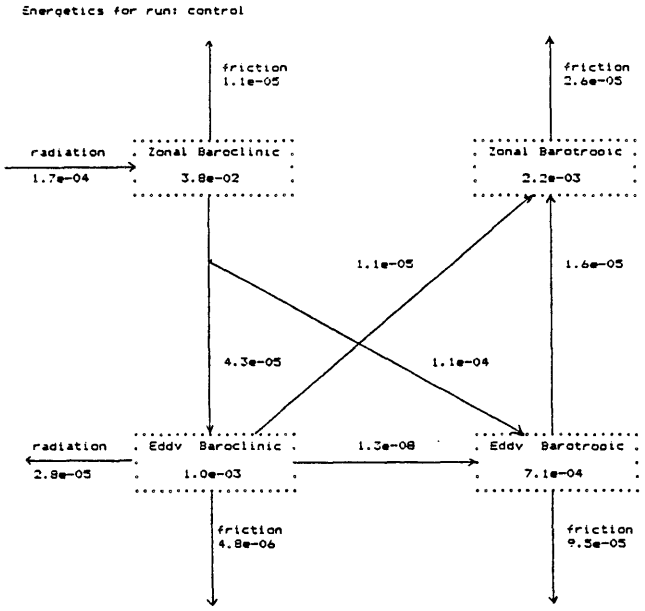

Fig. 34. Energetics for the control run divided by triad group.

energy in the zonal $\cos(l_o y)$ mode did not come from the Ekman pumping even though the pumping 'forces' the barotropic mode. Instead, the energy came from the btw-btw-btz and bcw-bcw-btz triads.

In the control run and low-friction cases, the synoptic-scale waves ($k=3k_o$) had the most wave energy, and dominated the energy conversions. In the other cases, (strong radiative forcing, weak-friction/strong-radiative forcing), the large-scale waves ($k=k_o$, $2k_o$) were much stronger, and were comparable to the synoptic-scale waves. Increasing the radiative forcing by one-third (strong-radiative forcing) increased the amplitude of the long ($2k_o$, l_o) modes by two orders of magnitude. Thus, the model was very sensitive to the radiative forcing.

The modes in the model fall into one of four groups; they are either baroclinic (BC) or barotropic (BT), and either zonal (Z) or wavy (W). Among the four groups, there are only 5 triad interactions (see below). Figure 34 shows the energy flow calculated by triad type.

Fundamental Triad Types

Baroclinic zonal-Barotropic wave-Baroclinic wave (BCZ-BTW-BCW)

Barotropic zonal-Barotropic wave-Barotropic wave (BTZ-BTW-BTW)

Barotropic zonal-Baroclinic wave-Baroclinic wave (BTZ-BCW-BCW)

Baroclinic wave -Baroclinic wave-Barotropic wave (BCW-BCW-BTW)

Barotropic wave -Barotropic wave-Barotropic wave (BTW-BTW-BTW)

The prominent feature in figure 34 was the large BCZ-BCW-BTW triad. This triad is a conversion of ZAPE into EKE and EAPE, and the large values implies that baroclinic-instability-type processes dominate the energetics.

The BTZ-BTW-BTW triad moved energy from the barotropic waves to the

barotropic zonal flow. This energy flux is consistent with a barotropic energy cascade as predicted by geostrophic turbulence theory.

The BTZ-BCW-BCW triad moved energy from the baroclinic waves to the barotropic zonal flow. This energy flux is approximately equal to that of the BTZ-BTW-BTW triad, suggesting that the barotropic zonal flow is maintained by both baroclinic and barotropic processes.

The BTW-BTW-BTW triad shifted energy between the barotropic modes. This triad moved energy from the synoptic scale ($k=3k_o$) to other length scales (table 4). The simulations showed a cascade of barotropic energy into the longer waves.

Table 4: Barotropic Energy Changes by Zonal Wavenumber Caused by BTW-BTW-BTW Triads.

k	Control	Weak-fr.	Strong rad.	Strong rad/ weak fr.
k_o	1.46×10^{-8}	1.87×10^{-8}	3.10×10^{-6}	4.45×10^{-5}
$2k_o$	2.33×10^{-9}	1.52×10^{-8}	1.94×10^{-6}	-1.49×10^{-6}
$3k_o$	-2.48×10^{-8}	-6.21×10^{-8}	-7.58×10^{-6}	-2.74×10^{-5}
$4k_o$	4.65×10^{-9}	1.87×10^{-8}	5.00×10^{-7}	-1.28×10^{-5}
$5k_o$	3.31×10^{-9}	9.44×10^{-9}	2.04×10^{-6}	-3.82×10^{-6}

The BCW-BCW-BTW triads converted eddy baroclinic energy into eddy barotropic energy. This triad is, in some sense, a measure of the wave-wave interactions. It was stronger when the radiative forcing was strong (strong radiative forcing, and weak-friction/strong-forcing cases). Tables 5 and 6 show the energy changes caused by the BCW-BCW-BTW triads. The common features are that the $2k_o$ and $3k_o$ modes lost while the shorter modes

($4k_o$, $5k_o$) gained baroclinic energy. In addition, the long waves gained, while the short waves lost barotropic energy.

Table 5: Barotropic Energy Changes by Zonal Wavenumber Caused by BCW-BCW-BTW Triads.

k	Control	Weak-fr.	Strong rad.	Strong rad/ weak fr.
k_o	1.60×10^{-8}	2.72×10^{-8}	4.94×10^{-6}	4.90×10^{-5}
$2k_o$	6.79×10^{-9}	2.43×10^{-8}	1.43×10^{-6}	4.06×10^{-5}
$3k_o$	-1.50×10^{-9}	-2.15×10^{-8}	8.15×10^{-8}	1.88×10^{-5}
$4k_o$	-4.43×10^{-9}	-1.35×10^{-9}	-8.02×10^{-7}	3.75×10^{-6}
$5k_o$	-3.86×10^{-9}	-9.92×10^{-9}	-4.63×10^{-7}	-5.25×10^{-6}

The BTW-BTW-BTW triads and BCW-BCW-BTW triads had similar effects on the barotropic energy of the long modes. This is like our analysis where modulated synoptic-scale waves convert similar amounts of baroclinic and barotropic energy into long-wave barotropic energy. (The case of strong-forcing/weak-friction was the exception. However, the theory's assumptions were poor in that case.)

Table 6: Baroclinic energy changes by zonal wavenumber caused by BCW-BCW-BTW triads.

k	Control	Weak-fr.	Strong rad.	Strong rad/ weak fr.
k_o	1.79×10^{-8}	1.73×10^{-8}	2.18×10^{-6}	-1.74×10^{-5}
$2k_o$	-1.60×10^{-8}	-1.64×10^{-8}	-9.82×10^{-6}	-1.02×10^{-4}
$3k_o$	-4.29×10^{-8}	-9.63×10^{-8}	-3.75×10^{-6}	-7.16×10^{-5}
$4k_o$	1.73×10^{-8}	2.81×10^{-8}	2.77×10^{-6}	3.66×10^{-5}
$5k_o$	1.06×10^{-8}	4.86×10^{-8}	3.44×10^{-6}	4.74×10^{-5}

Geostrophic Turbulence

Salmon (1982) presented an idealized picture of two-layer geostrophic turbulence (figure 1). Solar radiation adds baroclinic energy to the very large scales; turbulence moves baroclinic energy to smaller scales; baroclinic instability, a process with length scales of the Rossby radius of deformation, converts baroclinic energy into barotropic energy; a barotropic energy cascade then moves barotropic energy to the large scales.

Salmon's idealized picture and our numerical results differ. The barotropic zonal flow in the model gained like amounts of energy from the barotropic and baroclinic waves. Similarly, the energy cascade among the barotropic waves was comparable with the energy flux from the BTW-BCW-BCW triads. These differences were due to the scale of the models. In Salmon's work, the Rossby radius of deformation is assumed to be many scales shorter than the very large-scale flow, so that active triads tend to be 'local.' Our model, on the other hand, only has a restricted range of scales, so all triads can be active.

In the context of two-layer turbulence, the atmosphere has a larger range of scales than our numerical model; however, it is still not large. The zonal wavenumber of the most unstable mode is approximately 10, and the distance from 30 N to 60 N is about 3 Rossby deformation radii. Our numerical model, therefore, suggests that the atmosphere may not have the necessary range of scales for two-layer geostrophic turbulence.

5.3 Linear Stability

The linear growth rate is a useful diagnostic quantity for it determines whether linear waves grow or decay. A difference from the model's results must be caused by nonlinearites or temporal variations of the zonal flow. We also calculate the growth rates to check the baroclinic adjustment hypothesis which is used by our analysis (i.e., linear modes can only grow on the slow time scale).

The growth rates were calculated by the procedure documented in Appendix G. The calculated growth rate includes the effects of dissipation and limited spatial resolution.

A normal mode of the zonal flow has the form:

$$\{\Psi, \theta\} = \sum_n \{g_n, h_n\} \sin(n \cdot l_o y)\, e^{ikx - iwt}$$

Where $k = k_o, 2k_o, \ldots, 5k_o$

The model has 50 different normal modes for a zonal basic state.

Table 7: E-folding time:most unstable mode (in days)
(negative numbers imply decay)

k	Cntl	Weak-fr	Strong rad	Strong rad/ weak fr.	q-lin
k_o	-14	-32	-18	-104	-14
$2k_o$	-76	-179	43	35	-66
$3k_o$	125	132	50	15	192
$4k_o$	-13	-14	-12	-11	-13
$5k_o$	-5	-6	-5	-5	-5

The longest waves, k_o, were always stable, while the $2k_o$ waves were stable except when the radiative forcing was strong. If linear dynamics holds, the 'stable' long waves should decay with time. A non-vanishing long wave implies that wave-wave interactions may be important for maintaining that long wave.

The length of the $3k_o$ wave was set near the critical wavenumber by design. Not unexpectedly, a $3k_o$ mode was the most unstable in all but the strong-forcing case. Since the growth rate was always positive for this mode, some mechanism prevented these modes from growing indefinitely. Probably, wave-wave interactions are stabilizing these modes, although we can not rule out temporal variations of the zonal flow.

Baroclinic Adjustment

Stone (1978) found that a two-level model with atmospheric-like parameters was close to neutral stability. This lead him to the baroclinic adjustment hypothesis. He suggested that if the mid-latitude flow were baroclinically unstable, synoptic eddies would grow, transport heat northward (and upward), and stabilize the flow. If the flow were stable, the synoptic eddies would decay, and solar radiation would eventually make the flow baroclinically unstable. As a result, the zonal flow should be near baroclinic neutrality.

Baroclinic adjustment assumes that the eddies stabilize the zonal flow by their fluxes. A poleward heat flux reduces the meridional temperature gradient which stabilizes the flow. Baroclinic instability also forces an upward heat flux which can alter the static stability, and again stabilize the zonal flow (Gutowski, 1983). Lastly, westerly jets can also stabilize the zonal flow. This last mechanism and the meridional heat fluxes were

important in our numerical simulations.

Baroclinic adjustment held in the control run; the largest growth rate was only 1/125 day^{-1}. However, baroclinic adjustment did not hold in other models (Vallis and Road, 1984; Haidvogel and Held, 1980). Is the control run unusual, or is there some parameter range where baroclinic adjustment holds? To investigate this question, we ran the model with different parameters.

Range of Validity

The baroclinic adjustment hypothesis is, in some sense, a statement of two conditions: a statistically steady-state exists, and the wave-wave interactions can be ignored when compared with the wave-mean flow interactions. (If wave-wave interactions were more important, linear stability would then be meaningless.) With a steady zonal mean, and small wave-wave interactions, waves behave linearly. Under these conditions, and non-growing amplitudes, the linear growth rates must be small or negative.

Baroclinic adjustment implies the zonal flow is near neutral stability, and baroclinic adjustment may fail if either the zonal flow were unsteady, or if wave-wave interactions were important. While the first condition is not strictly true in our simulations (the zonal mean oscillates), the last condition appears to determine the validity of the baroclinic adjustment hypothesis.

Simple Estimate of the Eddy Amplitudes

$0 < y < Y$ (size of domain is Y)

$Q = (\theta_e - \theta) / t_{rad}$ (Newtonian heating)

$\theta_e = - a (y - \frac{Y}{2})$ = radiative equilibrium temperature field

t_{rad} = radiative damping time

Suppose the zonal flow is baroclinically neutral and uniform.

i.e., $\theta = - b (y - \frac{Y}{2})$

b = critical meridional temperature gradient

Now suppose the heating is balanced by the eddy heat flux divergence.

Therefore, $\frac{\partial}{\partial y} \langle v' \theta' \rangle = -(a - b)(y - \frac{Y}{2}) / t_{rad}$

where $\langle .. \rangle$ is the zonal average

then $\langle v'\theta' \rangle = \frac{1}{2} (a - b) y (Y - y) t_{rad}$

and the peak heat flux is $\langle v'\theta' \rangle_{max} = Y^2 \cdot (a - b) / 8 \cdot t_{rad}$

implying $|v|^2 = O(Y^2 \cdot (a - b) / 8 \cdot t_{rad})$

One expects baroclinic adjustment to fail when the wave-wave interactions are sufficiently strong. Since the eddy amplitude crudely measures these interactions, baroclinic adjustment should, by the above equation, fail when the domain is too wide or when the forcing is too strong.

Wide Domain

The Earth's atmosphere must be considered narrow for the distance from 30 N to 60 N is only about three Rossby deformation radii. The numerical model had a width of roughly 4700 km, so it was not unrealistic for a mid-latitude beta-plane. To test the effects of the domain width, the domain was made twice as wide.

Wide Domain Case

$l_o = .335$ (one-half of other runs)

$\theta_e = -0.3 \left(\frac{y}{Y} - 1\right)$ $0 < y < 2Y$

$Y = \pi / l_o$

The growth rate of the synoptic mode ($3k_o$) went from 1/125 to 1/9.7 days^{-1}. The new growth rate was much larger, so baroclinic adjustment did not hold in the wide-domain run. Haidvogel and Held (1980), and Vallis and Roads (1984) used widths of 10 and 14 Rossby radii respectively, and they obtained similar results. Hence, baroclinic adjustment appears to fail when the domain is too wide.

Strong Forcing

The previous, simple analysis suggested that strong radiative forcing can prevent baroclinic adjustment. The strong-radiative-forcing case supports this view. When the radiative-equilibrium temperature gradient was increased by one-third, the largest growth rates went from 1/125 to 1/43 day^{-1}. The flow was not as close to neutrality, and the eddy amplitudes were larger.

A more extreme response to radiative forcing was shown by the weak-friction, and weak-friction/strong-forcing cases. The difference between the two cases was that the strength of the solar forcing was doubled. The weak-friction case had weak long waves, and a near neutral zonal flow (largest growth rate was 1/132 day^{-1}). When the forcing was doubled, the flow became strongly nonlinear, the long waves were stronger, and the largest growth rate was 1/15 day^{-1}.

Dissipation

At first glance, dissipation is not related to baroclinic adjustment. It is, however, important. The weak-friction and the weak-friction/strong-forcing cases test the effects of a weaker friction.

Weak Friction

do = .0125	(one-half of control run)
t_{rad} = 80	(one-half of control run)
$v = \frac{1}{125}$	(same as control run)
$\theta_e = -0.3\ (\frac{y}{Y} - \frac{1}{2})$	(same as control run)
Solar forcing = θ_e / t_{rad}	(one-half of control run)

Weak friction/strong radiative forcing

do, t_{rad}, v	(same as in weak-friction case)
$\theta_e = -0.6\ (\frac{y}{Y} - \frac{1}{2})$	(twice as strong as control run)
Solar forcing = θ_e / t_{rad}	(same as control run)

Table 8: E-folding time:most unstable mode

k	Cntl.	Weak-fr	Strong rad/weak fr.
k_o	-14	-32	-104
$2k_o$	-76	-179	35
$3k_o$	125	132	15
$4k_o$	-13	-14	-11
$5k_o$	-5	-6	-5

In the weak friction case, the dissipation and solar forcing were reduced by 50%. (The radiative-equilibrium temperature did not change.) Even though the forcing was much weaker, the largest growth rate was like the control run's. Here, the weaker forcing did not bring the flow closer to neutral stability.

In the weak-friction/strong-forcing case, the dissipation was one-half of the control run's value; however, the strength of the solar forcing remained the same. The largest growth rate was 1/15 day^{-1}, so baroclinic adjustment was a poor hypothesis in this case.

Discussion

We examined the baroclinic adjustment hypothesis since we assumed that the synoptic-scale wave grew on a slow time scale. Baroclinic adjustment is also interesting since it limits the range of climatic and atmospheric variability.

Our simple analysis suggested that a wider channel or a stronger solar forcing could make baroclinic adjustment a poor approximation. Our numerical simulations support this conclusion. Our analysis, however, overlooked the role of dissipation. In the weak-friction/strong-forcing case, halving the dissipation, while keeping the solar forcing constant, changed the baroclinic adjustment hypothesis from excellent to poor.

Another Eddy Amplitude Estimate:

$0 < y < Y$ (size of domain is Y)

$Q = (\theta_e - \theta) / t_{rad}$ (Newtonian heating)

$\theta_e = -a\,(y - \frac{Y}{2})$

a = temperature gradient of the radiative equilibrium temperature

Suppose the zonal flow is baroclinically neutral, and uniform.

$\theta = -b\ (y - \frac{Y}{2})$

b = thermal shear for neutral stability

Now consider the neutral mode which is governed by linear dynamics.

It has a heat flux related to its inviscid growth rate.

Using (3.48) gives

$\langle v'\theta' \rangle = \langle -i \cdot k \cdot co \cdot \psi^{*} \cdot \psi \rangle$

or $\langle v'\theta' \rangle = \langle k \rangle \langle coi \rangle |\psi|^2$

but $\langle coi \rangle = \frac{imag(w)}{\langle k \rangle \langle Ut \rangle}$

Therefore, $\langle v'\theta' \rangle = \frac{imag(w)}{\langle Ut \rangle} |\psi|^2$

Imag(w), the inviscid growth rate, is equal to $1/t_d$ by the baroclinic adjustment hypothesis. (Growth rate is balanced by the dissipation in our model.)

Since $Ut = -\frac{\partial \theta}{\partial y} = -\frac{\partial}{\partial y} [-b\ (y - \frac{Y}{2})] = b$

and $imag(w) = 1/t_d$

Therefore, $\langle v'\theta' \rangle = |\psi|^2 / b\ t_d$

Suppose the heating is balanced by the eddy heat flux divergence.

Therefore, $\frac{\partial}{\partial y} \langle v'\ \theta' \rangle = -(a - b)\ (y - \frac{Y}{2}) / t_{rad}$

or $\langle v'\theta' \rangle = (a - b)\ y\ (Y - y) / 2 \cdot t_{rad}$

but $\langle v'\theta' \rangle = |\psi|^2 / b \cdot t_d$

Therefore, $|\psi|^2 = O(Y^2 \cdot b \cdot (a - b) \cdot t_d / t_{rad})$

When the above quantity is large, we expect that the wave-wave interactions are strong, and baroclinic adjustment is hard to achieve. Hence, weak dissipation (large t_d) may ruin the baroclinic adjustment hypothesis.

In the weak-friction case, 'a' was unchanged, the dissipation and the radiative-damping time scales were doubled, and 'b' is slightly smaller (weaker friction). Since b > (a-b) in the control run, the weak-friction case should have a slightly larger synoptic-eddy amplitude and a slightly larger growth rate. These predictions were consistent with our simulations. The eddy amplitudes were slightly stronger in the weak-friction case than in the control run. The baroclinic eddy energy went from 0.00100 to 0.00120, and the barotropic eddy energy went from 0.000712 to 0.000735. The growth rate was not smaller in the control run; however, the difference in the growth rates (1/125 vs. 1/132 $days^{-1}$) is not likely to be significant given a sampling period of only 50 model days.

Summary

In summary, we examined the baroclinic adjustment hypothesis because it was used by our theory. It also has applications for understanding the general circulation for it restricts the possible time-mean flows. Our numerical simulations show that baroclinic adjustment was a good hypothesis for many model runs. The zonal flow was stabilized by the poleward heat flux and the formation of a westerly jet. However, we found that the hypothesis broke down when the basin was too wide, the forcing was too strong, or the friction was too weak.

$$G = Y^2 \cdot b \cdot (a - b) \cdot t_d \; / \; t_{rad} \qquad (5.11)$$

where Y = domain width

t_d = (effective) eddy dissipation time scale

t_{rad} = radiative damping time scale

a = radiative-equilibrium temperature gradient

b = temperature gradient for neutral stability

According to our simple analysis, baroclinic adjustment should be worse when 'G' (5.11) is larger. The various cases agree with this analysis. When the width was changed from 4700 km to 9400 km, baroclinic adjustment failed. (This may explain why the models of Vallis and Road (1984), and Haidvogel and Held (1980) did not show baroclinic adjustment.) When 'a' was increased by one-third (strong-forcing case), baroclinic adjustment was a poorer assumption. When t_d and t_{rad} were both halved, the largest growth rate was only slightly changed.

These results have implications for numerical models for they suggest that these models can be sensitive to the dissipation of the synoptic eddies, a quantity dependent on the model's parameterizations. A strong dissipation (small t_d) may put the flow into a 'baroclinic adjustment regime', whereas a weak dissipation may increase the eddy amplitudes and make the flow highly nonlinear. In addition, the results indicate that the flow is sensitive to the width of the beta-plane channel.

The applicability of baroclinic adjustment to the atmosphere was initially examined by Stone (1978). He found that a two-level model with atmopheric-like parameters was close to neutral stability. Lindzen et al. (1980) and Gutowski (1985b) pointed out that inviscid neutrality can also be achieved by changing the vertical profile. The degree to which baroclinic adjustment holds in the atmosphere still needs further study.

5.4 Eddy Energetics

In this thesis, we are concerned with the energetics of two classes of waves: the synoptic-scale ($k = 3k_o$) and the long ($k = k_o, 2k_o$) waves.

(1) $k = 3k_o$	synoptic waves
(2) $k = k_o, l = l_o$	long-waves
(3) $k = k_o, l = 2l_o$	of the
(4) $k = 2k_o, l = l_o$	numerical
(5) $k = 2k_o, l = 2l_o$	model

The energy cycle of the synoptic-scale waves had features like in the atmosphere. The synoptic-scale waves gained most of their energy from the zonal thermal wind by BCW-BTW-BCZ triads. In the control run, much of the energy in the synoptic scales was lost to friction, with less lost to radiative damping, conversion into zonal barotropic energy, and to other wavenumbers.

The long waves gained most of their energy from the zonal thermal wind like in winter observations (Saltzman, 1970). Our long waves lost most of their energy to dissipation and usually to the zonal barotropic flow. The wave-wave interactions generally increased the barotropic energy of the long waves in agreement with theory.

Parameterization versus Numerical Results

The synoptic-eddy parameterization determines how the synoptic eddies should, on average, affect the long waves. We can use it to predict the energetics of this interaction (Appendix D). These predicted energy fluxes were compared with those determined by the numerical model which is the main test of our parameterization.

For the long waves as a group, the synoptic-eddy parameterization reasonably estimated the energy that the long waves gained from the 'other waves' (figure 35). The 'other' waves removed baroclinic energy [9.5×10^{-9} (actual) vs. 4.5×10^{-9} (est.)] and added barotropic energy [1.3×10^{-8} (actual) vs. 5.9×10^{-9} (est.)] to the long waves. Here, our analysis gave good estimates. The net effect of the 'other' waves was to add energy to the long waves. By itself, this energy flux is destabilizing, but it is much smaller than the conversion of ZBC into EBC and EBT.

The parameterization also gave a fair estimate for the strongest long wave (figure 39). The vorticity fluxes added barotropic and baroclinic energy, while the heat flux reduced the baroclinic energy of this long wave. The 'other' waves reduced the net energy in this mode.

The energy fluxes for the weaker modes, on the other hand, were not well predicted (figures 36-38). Generally, the weaker modes gained more baroclinic energy than predicted; however, the energy in these weaker modes was at least an order of magnitude smaller than the strongest long mode, so they are unimportant.

The prediction of weak long waves is subject to many errors. For example, a spatially modulated synoptic-scale wave has many Fourier modes, including long modes. The signature of this spectral contamination is a

Key for figures 35-54.

See figure 35 (left to right)

9.8e-8: long-wave EBC gain due to BCW-BCZ-BTW triads
9.5e-9: long-wave EBC loss due to BCW-BCW-BTW triads
[4.5e-9]: result from the synoptic-eddy parameterization to be compared with 9.5e-9
2.5e-8: long-wave EBC loss due to BCW-BCW-BTZ triads
4.1e-8: long-wave EBT gain due to BCW-BCZ-BTW triads
1.2e-8: long-wave EBT loss due to BTW-BTW-BTZ triads
1.3e-8: long-wave EBT loss due to BTW-BTW-BTW triads
[5.9e-9]: result from the synoptic-eddy parameterization to be compared with 1.3e-8

Note: figures 35-54 only show the energetics of the long-wave mode(s). Many energy fluxes involving the zonal and 'other modes' are not shown.

Fig. 35-39. Long-wave energetics for the control run

Fig. 40-44. Long-wave energetics for the weak-friction case

Fig. 45-49. Long-wave energetics for the weak-friction/ strong-forcing case

Fig. 50-54. Long-wave energetics for the strong forcing case

Fig. 35, 40, 45, 50: Energetics for the long waves as a group

Fig. 36, 41, 46, 51: Energetics for k_o, l_o long modes

Fig. 37, 42, 47, 52: Energetics for k_o, $2l_o$ long modes

Fig. 38, 43, 48, 53: Energetics for $2k_o$, l_o long modes

Fig. 39, 44, 49, 54: Energetics for $2k_o$, $2l_o$ long modes

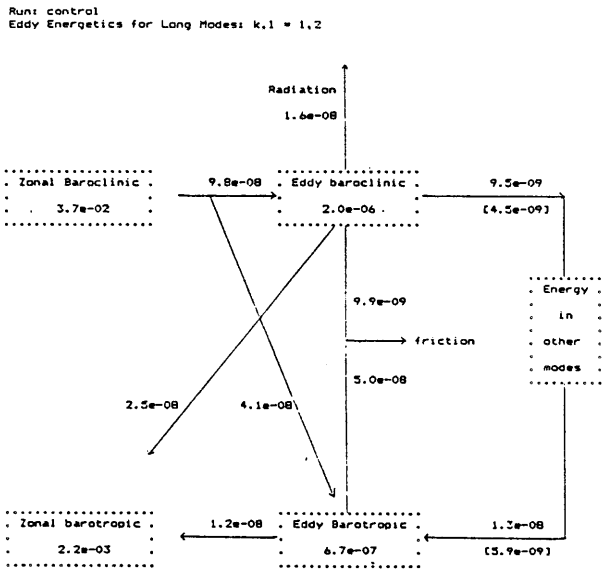

Fig. 35. (see key)

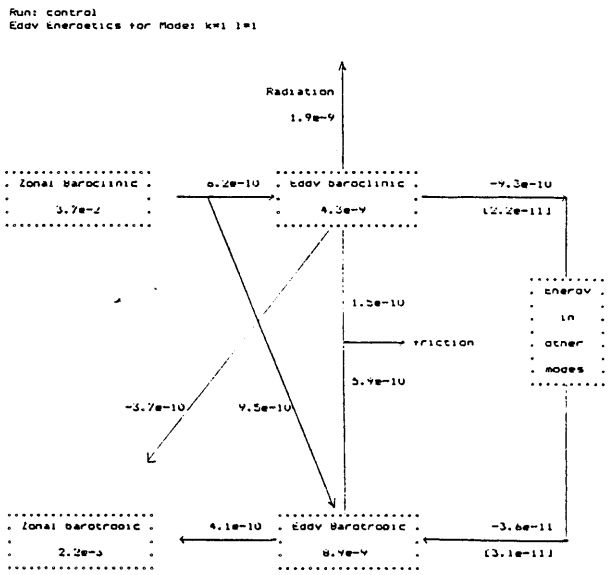

Fig. 36. (see key)

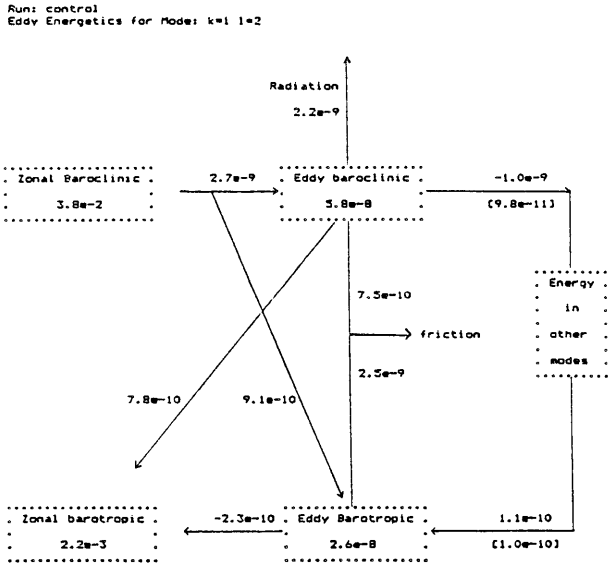

Fig. 37. (see key)

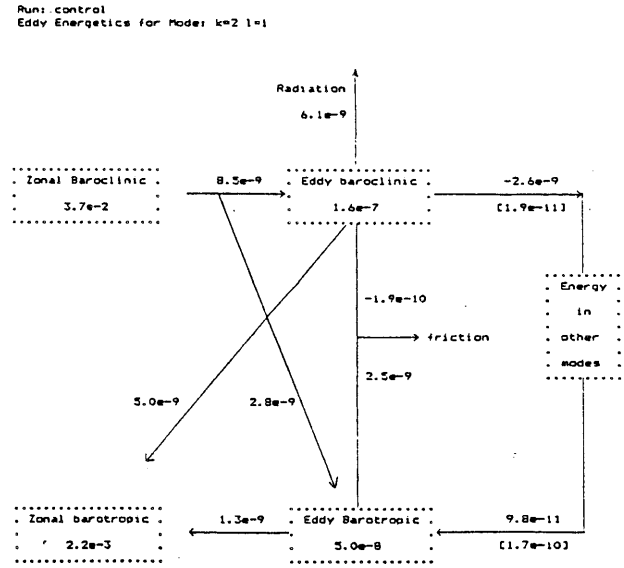

Fig. 38. (see key)

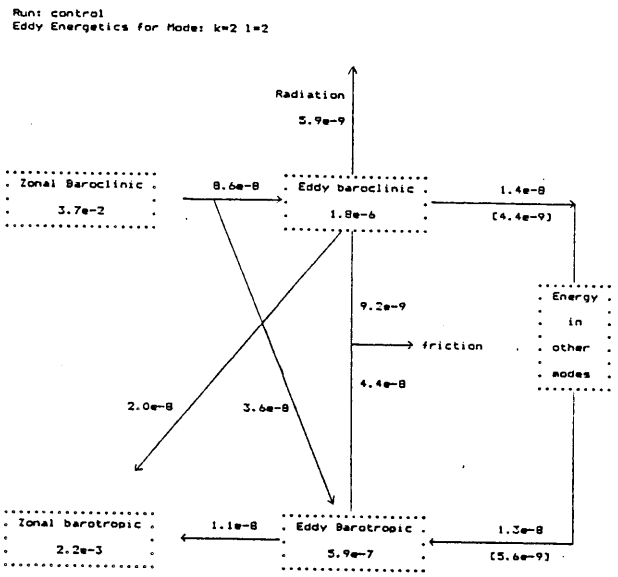

Fig. 39. (see key)

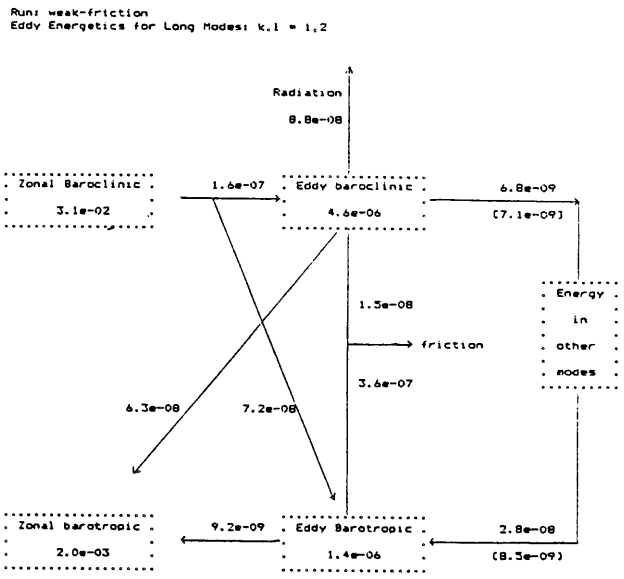

Fig. 40. (see key)

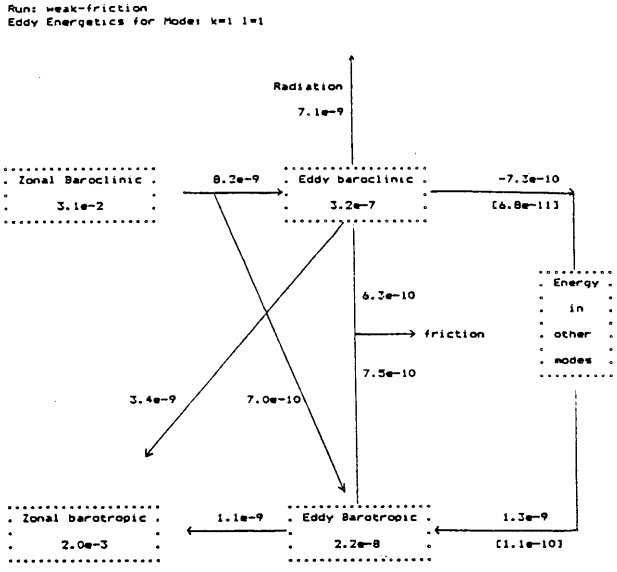

Fig. 41. (see key)

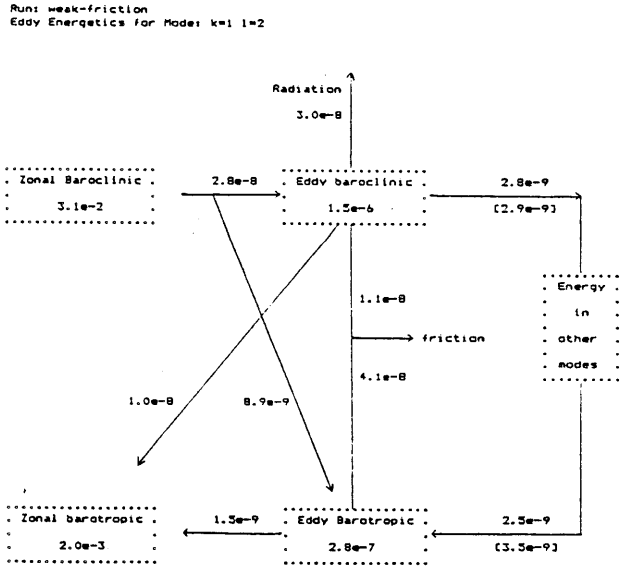

Fig. 42. (see key)

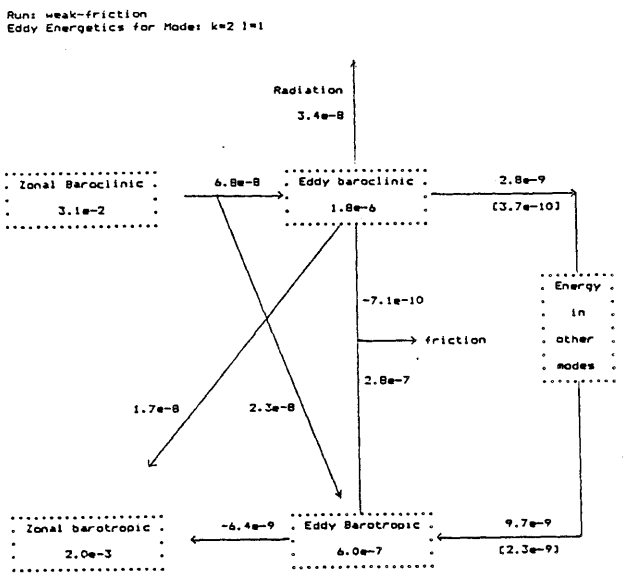

Fig. 43. (see key)

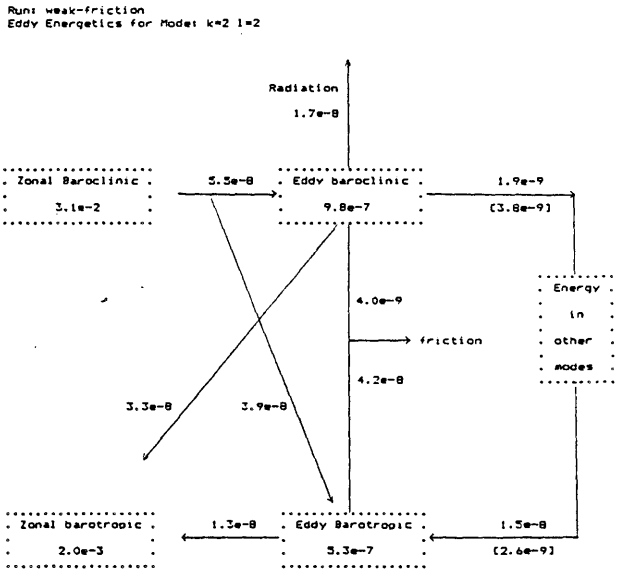

Fig. 44. (see key)

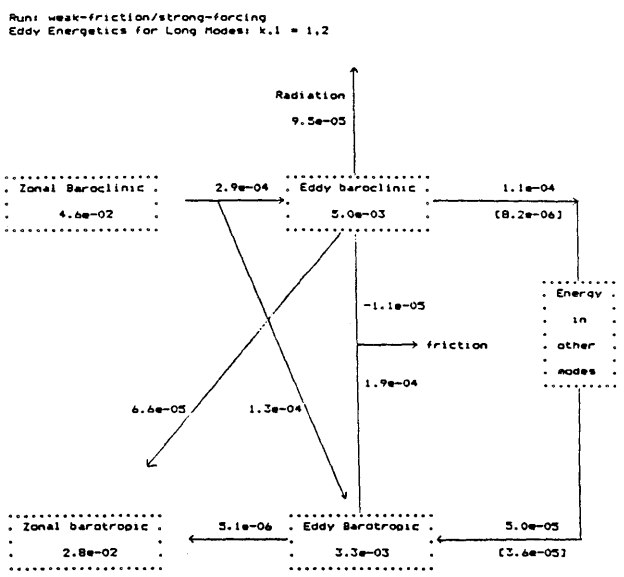

Fig. 45. (see key)

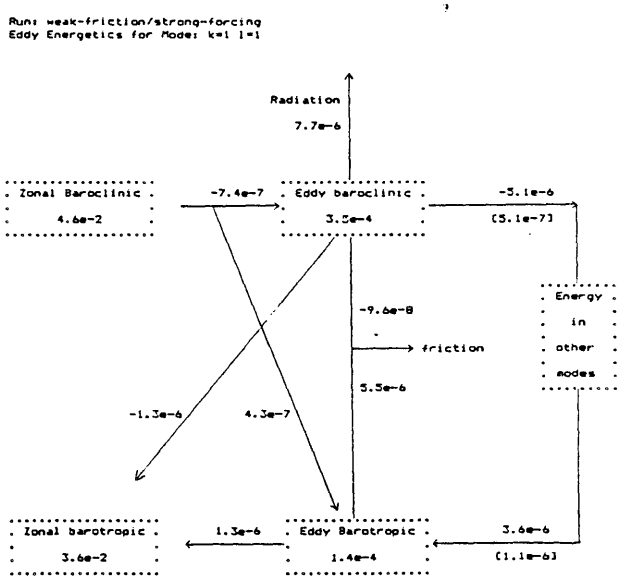

Fig. 46. (see key)

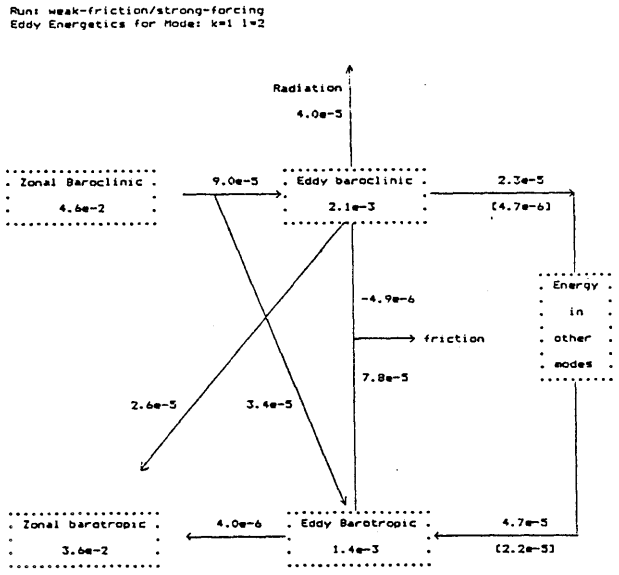

Fig. 47. (see key)

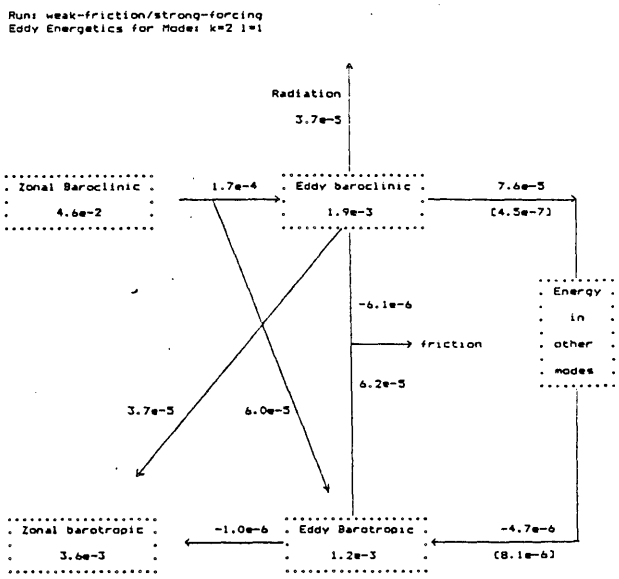

Fig. 48. (see key)

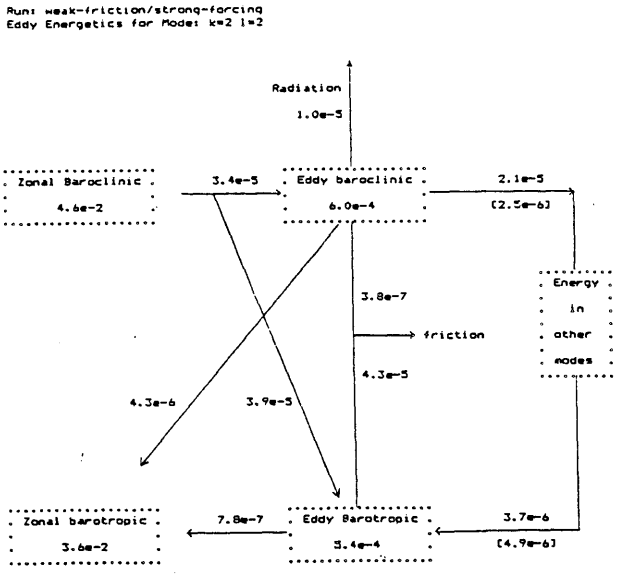

Fig. 49. (see key)

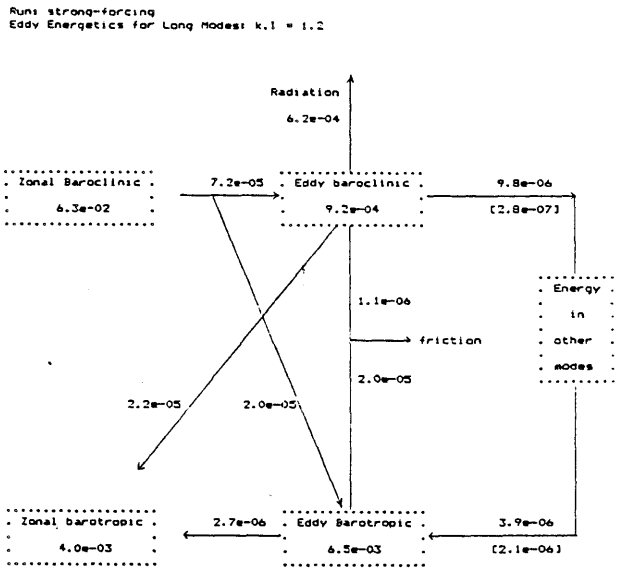

Fig. 50. (see key)

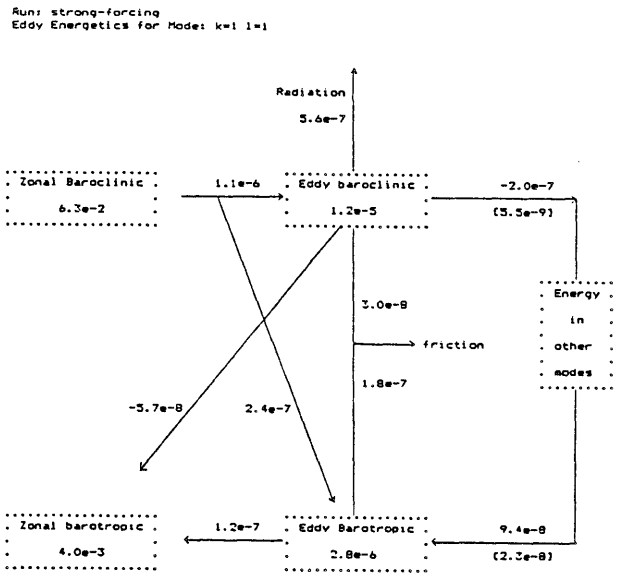

Fig. 51. (see key)

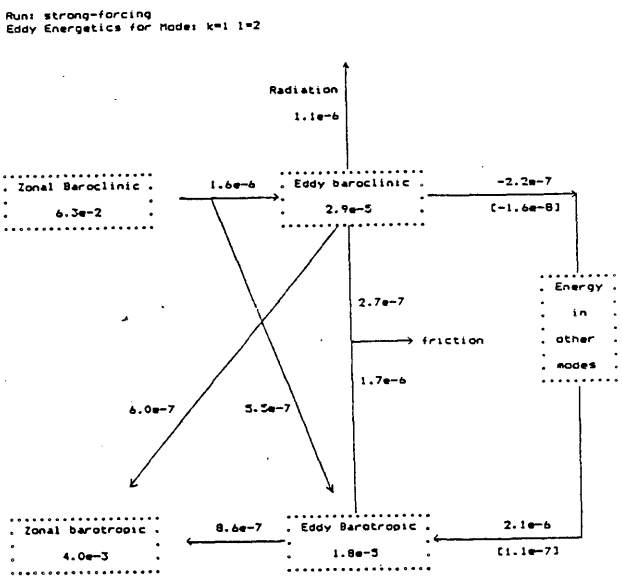

Fig. 52. (see key)

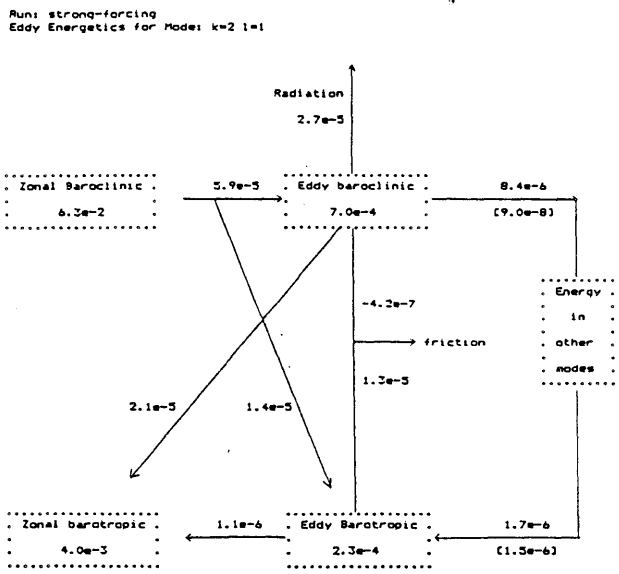

Fig. 53. (see key)

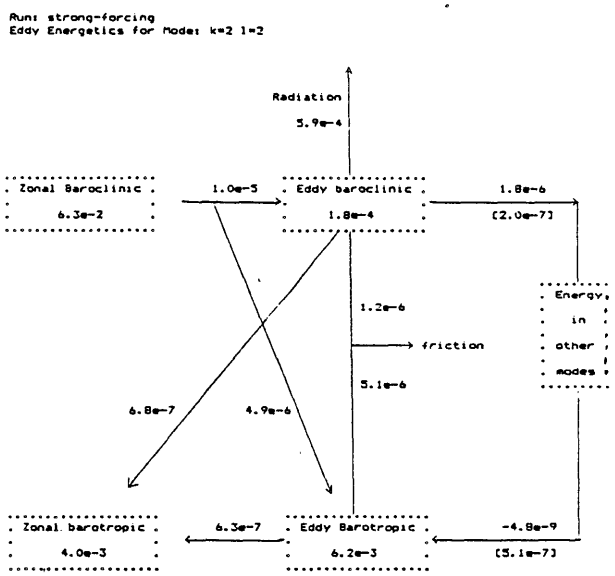

Fig. 54. (see key)

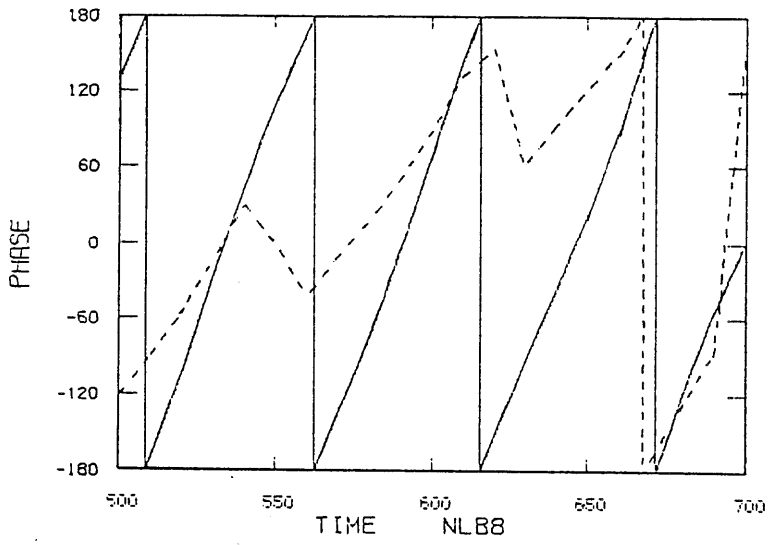

Fig 55. Phase of the barotropic component of the $3k_o$ [1_o, $2l_o$] modes (i.e synoptic scale)
Solid: $l=l_o$
Dashed: $l=2l_o$

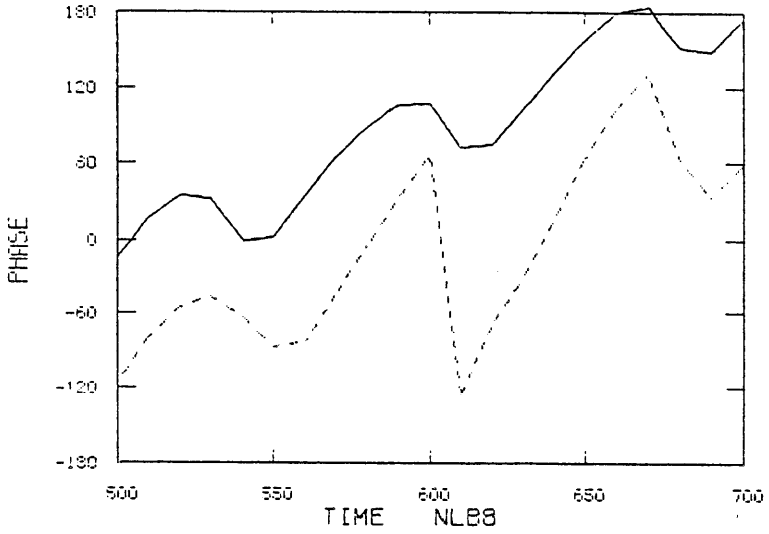

Fig. 56. Phase of the barotropic component of the k_o [l_o, $2l_o$] modes (i.e. long wave)
Solid: $l=l_o$
Dashed: $l=2l_o$

phase speed and frequency which are unlike those predicted by linear theory. The correlation between the phase angles of the $3k_o$ and k_o modes (figures 55 and 56) could indicate such spectral contamination. Spectral contamination, however, can only produce a small 'error', but it may appear since the weak modes had small amplitudes.

The flow is not nearly uniform in 'y' as we assumed. Therefore, the normal modes (of the zonal-mean flow) are combinations of $\sin(n \cdot l_o y)$ modes. The energetics of the weakest modes are bound to differ from the strongest, so we have another potential 'error'.

The third source of error comes from only considering one type of nonlinearity, the interaction between a slowly varying long wave and a inviscidly unstable synoptic-scale wave. Other nonlinearites, regardless of size, can be important for small-amplitude modes.

Other Cases

In the weak-friction case, the parameterization gave good estimates for wave-wave interactions of the long waves as a group, and for the three strongest long-wave modes (figures 40-44). The wave-wave energy fluxes added barotropic and removed baroclinic energy from the long waves. Generally, the net effect was to add a small amount of energy into the long waves. The prediction for the weakest long mode, like in the control run, had the most error.

In the weak-friction/strong-forcing case, the parameterization gave a correct sign on how the 'other waves' affected the long waves as a group (figures 45-49). The parameterization gave a reasonable estimate for the strongest long-wave mode (figure 47). This accuracy was unexpected since

baroclinic adjustment doesn't hold. In addition, the long waves were very strong (table 9) which could imply that other nonlinear processes may now be important.

The prediction for the strong-forcing case (figures 50-54) showed the most error. The signs of the predicted energy fluxes were correct for the long waves as a group and for the strongest mode. Like in the weak-friction/strong-forcing case, the long waves were stronger than the synoptic-scale modes (table 9).

Table 9: Ratio of Energy in the Long and Synoptic-scale Modes

Most unstable Growth Rate

Run	**Cntl.**	**Weak-fr.**	**Strong-forcing**	**Weak-fr./strong-forcing**
E_{ps}/E_{syn}	1.6×10^{-3}	3.1×10^{-3}	3.8	2.4
max. growth rate (days^{-1})	1/125	1/132	1/43	1/15

E_{ps} = energy in the ($k=k_o$, $2k_o$; $l=l_o$, $2l_o$) modes

E_{syn} = energy in the ($k=3k_o$) modes

The errors in the predicted energy fluxes appear to be more related to the E_{ps}/E_{syn} than to the linear instability of the zonal flow. One may suspect that when E_{ps}/E_{syn} is O(1), interactions among the long waves are now important. Our theory should begin breaking down for it only considers a subset of all nonlinear interactions.

Summary

In summary, the parameterization reasonably estimated how the 'other waves' affected the energy of the strongest long-wave modes and the long waves as a group. The vorticity flux of the synoptic-scale waves added, while the heat fluxes reduced the energy in the transient long waves. The net result was more barotropic and less baroclinic energy in the long waves. Hence, our analysis and modeling results are consistent.

The modeling results showed that the parameterization had limitations; the long modes that were weak compared with others in that simulation were poorly handled. Explanations include spectral contamination, eigenmodes not of the form sin(ly), and nonlinear interactions among the long-wave modes. In addition, when the long waves were stronger than the synoptic-scale waves, the parameterization gave poor estimates as expected. Despite these limitations, these results support our analysis and the idea that the synoptic-scale waves may destabilize the long waves.

5.5 Discussion: Planetary-Scale Waves

In review, we numerically and theoretically examined the interactions between synoptic-scale and transient planetary-scale waves. Our results differ from those for wave propagation through a barotropic, inhomogeneous medium. We used a fundamentally different assumption -- the synoptic-scale wave is inviscidly unstable, but neutrally stable when dissipation is included. As a result, a 'local growth rate', rather than conservation of wave action, determines the amplitude of the synoptic-scale wave.

Our analysis suggests that the synoptic-scale waves are spatially modulated by the long wave which changes the 'local growth rate.' Regions with larger than average 'local growth rates' show spatial growth downstream. The synoptic-scale wave, of course, has only one growth rate; the 'local growth rate' just measures the local instability properties.

The thermal-wind anomalies modulate the synoptic-scale wave in a simple manner. Regions of larger thermal winds have positive 'local growth rates', and show spatial growth downstream. At the most unstable wavelength, the spatial growth (1/e-folding distance) is the 'local growth rate' divided by the group velocity (relative to the thermal wind anomaly).

The zonal barotropic wind can also modulate the synoptic-scale waves. It changes the local wavelength which will change the 'local growth rate' for the growth rate is dependent on the wavelength. Like the asymmetries in the thermal field, this effect is inversely proportional to the 'group velocity' (real $\partial w/\partial k$) relative to the asymmetries in the large-scale flow.

The curvature of the zonal baroclinic and barotropic flows can also modulate the synoptic-scale wave. The curvature, in some sense, acts like an effective beta which will change the 'local growth rate'. However, this

is a simplification, and the curvature effects are more complicated.

According to our theory, the heat flux of the synoptic eddies tends to drain energy from the long wave, while the (relative) vorticity fluxes add energy. According to atmospheric observations (Holopainen et al., 1982), the heat flux dominates, which suggests that the synoptic eddies are stabilizing. However, in our numerical model, neither flux is consistently larger.

Under close examination, the synoptic-scale waves can destabilize a long wave by changing long wave's structure. This allows the long wave to extract more ZAPE than would be normally possible. Basically, the spatially modulated synoptic-scale wave acts like a catalyst. Hence, we have a possible explanation to the question behind this thesis, "Why do the long waves in the GCM experiments grow faster than predicted by linear theory?"

We developed a numerical model to help verify the theory. This model identified conditions when the theory's assumptions were poor. For example, the assumption of baroclinic adjustment broke down when the channel width was too large, the radiative forcing was too strong, or when the dissipation was too weak. We also found that the energy fluxes due to the 'other waves' were only reasonably predicted for the long waves as a group, and for the strongest modes.

We found that the energy fluxes were well predicted when the total energy in the long waves was less than the energy in the synoptic scales. Our theory probably failed because it only considered one type of nonlinearity. When the long waves were strong, other nonlinearites are expected

to be stronger. This energetic restriction was satisfied when the long waves grew faster than predicted by linear theory (e.g. the GCM simulation by Gall et al., 1979b). In the atmosphere, however, the situation is more unclear. The transient kinetic energy peaks at total wavenumber 8 (Boer and Shepherd, 1983), but the stationary kinetic energy shows no decrease in the lowest wavenumbers.

The numerical simulations have some implications for GCMs. For instance, the zonal flow is sensitive to the dissipation time-scale of the synoptic eddies and to the large-scale radiative forcing. Under some conditions, this dissipation could make the difference between having or not having baroclinic adjustment. Since this dissipation is highly parameterized, the parameterizations should be carefully examined.

Another implication is that the synoptic-eddy fluxes are sensitive to the group velocity of the synoptic-scale waves. Since the group velocity can be difficult to model well, GCMs should use numerical schemes that model the group velocities accurately. Inaccurate group velocities can drastically change the effect of synoptic eddies on the long waves.

Chapter 6

Stationary Planetary-Scale Waves

So far, we have only considered the interactions between synoptic-scale and transient planetary-scale waves. In this chapter, we examine the effect of synoptic-scale waves on stationary long waves. While this problem has no direct connection with the GCM experiments (e.g. Gall et al., 1979b), it is interesting, for the standing waves contain much of the observed spatial variability.

Opsteegh and Vernekar (1982), Nigam (1983), and Nigam et al. (1986) have studied the effect of the synoptic eddies on the stationary long waves. They solved for the stationary waves using linear models which could optionally include an externally determined transient-eddy flux. They found that these fluxes must be included to accurately model the standing waves. Accurate modeling is necessary, even for short-term weather prediction. If a GCM poorly models the standing waves, then the errors will be considered a transient wave in an initial-value problem.

Our theory for stationary waves is linear and straightforward. When the transient eddies and dissipation are ignored, the linear stationary wave is given by (6.1).

For a single wave, the linear equation in a uniform zonal flow is

$$\frac{d}{dt} W = ik\,[A]\,W - F = 0 \qquad (6.1)$$

Where $W = (\Psi, \theta)^T$ is the stationary solution

$F = (\Psi\text{-forcing}, \theta\text{-forcing})^T$ is the forcing

$$[A] = \begin{pmatrix} -\beta / K^2 + U & -Ut \\ -Ut\,(K^2 - 2F) / (K^2 + 2F) & -\beta / (K^2+2F) + U \end{pmatrix}$$

The stationary solution is $W = [A^{-1}]\, F / ik$

The transient-eddy fluxes can be modeled with a synoptic-eddy parameterization. With our parameterization, we can find the effect of the eddy fluxes on the standing waves. The eddy parameterization just changes matrix [A], giving a new equation for the stationary waves, $[A']W' = F/ik$. We are most interested in when the parameterization strongly changes the stationary wave; i.e., the sensitivity of W to perturbations in [A]. [Goulub and Van Loan (1983) discuss the general problem.]

Let $[A'] = [A] + \varepsilon [G]$ $\qquad \varepsilon \ll 1$

[G] is the effect of the (eddy) parameterization

$[A']\, W' = F / ik$ implies $([A] + \varepsilon [G])\, W' = F / ik$ $(= [A]\, W)$

Collecting the $O(\varepsilon)$ terms gives $W' - W = - \varepsilon [A^{-1}]\, [G]\, W$

Thus $|W' - W| / |W| \leq \varepsilon\, ||A^{-1}||\, ||G|| + O(\varepsilon^2)$

Where $|W|$ is the norm of the vector W

$$|W| = |\Psi|^2 + |\theta|^2$$

and where $||A||$ is the L-2 norm of the matrix [A]

$$||A|| = \sup |[A]\, U| / |U|$$

where U is any non-zero vector

$$\text{Thus } |W' - W| / |W| \leq K(A)\, \varepsilon\, \frac{||G||}{||A||} + O(\varepsilon^2) \qquad (6.2)$$

Where $K(A) = ||A|| \cdot ||A^{-1}||$ = the condition number of matrix [A]

and $\varepsilon \frac{||G||}{||A||}$ is the strength of the parameterization

When the matrix A is diagonalizable, $||A|| = |\text{eigenvalue}_j|_{max}$

Then $K(A) = |\text{eigenvalue}_j|_{max} / |\text{eigenvalue}_j|_{min}$

or simply $K(A) = \frac{|w_j|_{max}}{|w_j|_{min}}$ (6.3)

Where w_j is simply the frequency of the j-th free wave. (The frequencies should be restricted to waves that are excited by the forcing.)

For a uniform zonal flow,

$$w = Uk - \beta \frac{k}{M} (K^2 + F) \pm \frac{k}{M} [(\beta F)^2 - Ut^2K^4 (4F^2 - K^4)]^{1/2}$$

Note that the above ideas are not restricted to a uniform basic state. They also hold for numerical models, where matrix A has finite dimension; however, this complication adds little to our discussion.

When the condition number is large, the stationary wave is sensitive to the parameterization (6.2). This only occurs when a free-wave frequency is near zero. (The numerator of 6.3 is bounded.) Therefore, the stationary wave is sensitive to small perturbations in [A] whenever the system is near resonance. (Resonant, in this context, implies a free mode with zero phase speed.)

Stationary waves are also sensitive to large deviations of [A]. Large deviations will occur if either the amplitude of the synoptic eddies is large or if the 'group velocity' of the synoptic eddies is close to zero.

A small group velocity, however, needs an easterly wind because the most unstable synoptic modes have an eastward group velocity. Hence, the latter condition is unlikely to occur.

In conclusion, the stationary wave will be strongly altered by the (parameterized) transient eddies when the magnitude of the forcing is not small ($\varepsilon\,||G||/||A|| = O(1)$) or when a free mode's frequency is near zero. The latter occurs when the forcing has the same wavenumber as a resonant wave. Therefore, a small-magnitude eddy parameterization should only make small changes to stationary waves in the non-resonant case.

The previous discussion suggested that a stationary wave should be sensitive when waves with near zero phase speeds are forced. However, the argument did not specify the parameterization; therefore, the stationary wave should be sensitive to all factors including dissipation, asymmetries in the flow, stationary nonlinearities, and temporal changes. Therefore, linear theory should show large errors even with the eddy parameterization.

6.1 Numerical Results

We used a time-dependent numerical model to calculate the time-mean states for two types of stationary forcings. The first was a diabatic heating; the second was a specified vertical velocity at the surface. This orographic-like forcing was used instead of the usual '$U\cdot h_x + V\cdot h_y$' because the model had a small surface wind which would make the forcing extremely sensitive to the zonal state.

The linear solutions were calculated using the time-mean zonal state determined by the numerical model. The linear solution takes into account the dissipation, and the curvature of the zonal flow.

Cases:

k=1 l=1 $\omega_4 = 0.0003 \cos(k_o x)\sin(l_o y)$ + Ekman pumping

k=1 l=2 $\omega_4 = 0.0003 \cos(k_o x)\sin(2l_o y)$ + Ekman pumping

k=1 l=1 $\omega_4 = 0.0003 \cos(2k_o x)\sin(l_o y)$ + Ekman pumping

k=1 l=1 $\omega_4 = 0.0003 \cos(2k_o x)\sin(2l_o y)$ + Ekman pumping

k=1 l=1 $q = 0.05 \cos(k_o x)\sin(l_o y)$ + radiative damping

k=1 l=2 $q = 0.05 \cos(k_o x)\sin(2l_o y)$ + radiative damping

k=2 l=1 $q = 0.05 \cos(2k_o x)\sin(l_o y)$ + radiative damping

k=2 l=2 $q = 0.05 \cos(2k_o x)\sin(2l_o y)$ + radiative damping

Linear versus Time-mean Solutions

The time-mean solutions were compared with the linear solutions by using a simple spatial correlation, and by finding variance unexplained by the linear solution. For these calculations, the time-mean solutions were restricted to the zonal wavenumber of the forcing. For example, if the forcing was at $k=k_o$ and $l=l_o$, the linear wave was compared with the time-mean solution restricted to zonal wavenumber k_o. The time-mean field was so restricted because most of the other waves were not statistically significant.

Table 10: Correlation of the linear and time-mean waves
(20 degrees of freedom)

$$c = \frac{|\Psi^*_{\text{time-mean}}\,\Psi_{\text{lin}}|}{2\,[|\Psi_{\text{time-mean}}|^2\,|\Psi_{\text{lin}}|^2\,]^{1/2}} + \frac{|\theta^*_{\text{time-mean}}\,\theta_{\text{lin}}|}{2\,[|\theta_{\text{time-mean}}|^2\,|\theta_{\text{lin}}|^2\,]^{1/2}}$$

k_o	l_o	forcing	linear	linear with param.
1	1	ω	.99	.99
1	1	q	1.00	1.00
1	2	ω	.97	.98
1	2	q	.95	.96
2	1	ω	.91	.92
2	1	q	.97	.98
2	2	ω	.92	.94
2	2	q	.91	.95

The correlations between the time-mean and linear solutions were strong, greater than 0.90. The synoptic-eddy parameterization improved the correlations, but not to an important degree for they were already large.

Table 11: % Unexplained Variance

$$\text{unexplained\_variance} = |\Psi_{\text{time-mean}} - \Psi_{\text{lin}}|^2 + |\theta_{\text{time-mean}} - \theta_{\text{lin}}|^2$$

$$\text{total\_variance} = |\Psi_{\text{time-mean}}|^2 + |\theta_{\text{time-mean}}|^2$$

$$\%\ \text{unexplained\_variance} = 100 \cdot \text{unexplained\_variance} / \text{total\_variance}$$

k_o	l_o	forcing	linear	linear with param.
1	1	ω	3%	2%
1	1	q	1	1
1	2	ω	6	3
1	2	q	11	9
2	1	ω	17	15
2	1	q	5	4
2	2	ω	17	24
2	2	q	37%	37%

The unexplained variance is the square of the difference of the time-mean and linear solutions. The eddy parameterization improved the unexplained variance; however, the improvement was not large for the unexplained variance was quite low except in the $2k_o$ $2l_o$ cases, which are discussed in the next section.

Resonance Response

The cases with $2k_o$, $2l_o$ forcing were poorly predicted by linear theory. Resonance is an explanation. Resonance is shown by strong responses to 'ω' or 'q' forcing, and the stronger responses differed more from linear theory (table 12). The $2k_o$, $2l_o$ cases had the poorest accuracy and the largest stationary-wave amplitudes.

Table 12: Variance versus % Unexplained Variance

k_o	l_o	forcing	Variance(lin. param.)	% unexplained variance
1	1	ω	3.0×10^{-5}	2%
1	2	ω	2.3×10^{-5}	3
2	1	ω	1.0×10^{-4}	15
2	2	ω	1.1×10^{-4}	24
1	1	q	2.5×10^{-4}	1
1	2	q	4.3×10^{-4}	9
2	1	q	5.3×10^{-4}	4
2	2	q	1.9×10^{-3}	37%

Variance is of the linear solution with the eddy parameterization

Resonance complicates the theoretical explanation of stationary waves. Some theories, for example Charney and DeVore (1979), assume that the main effect of resonance is to produce large-amplitude stationary waves which, in turn, produce important nonlinearities. This hypothesis was tested by reducing the forcing by 80% in the $2k_o$, $2l_o$, q case. This should **a priori** reduce the stationary wave's amplitude by 80%, and the 'stationary' nonlinear terms by 96%.

The correlations were not improved by the weaker forcing. They remained roughly the same for the phase errors did not improve (table 13). The high percentage of unexplained variance improved somewhat because the amplitudes were not as badly over estimated. Overall, linear theory only showed a minor improvement with the much weaker forcing.

Table 13: Weak versus Strong, Near-Resonant Forcing

	Regular Forcing			Weak Forcing		
	linear	lin./param.		linear	lin./param.	
Correlation	.91	.95		.89	.95	
% Unexplained Var.	.37	.37		.22	.25	
Variance	1.56	1.88	$\times 10^{-3}$	1.34	2.39	$\times 10^{-4}$
T.-M. Var.	0.9		$\times 10^{-3}$	1.3		$\times 10^{-4}$
Phase Error of: Ψ	17	8	$\pm 3^{o}$	18	8	$\pm 1^{o}$
forced mode 0	20	13	$\pm 2^{o}$	22	14	$\pm 1^{o}$

The amplitude of the weakly forced solution was comparable to the nonresonant solutions; therefore, the large errors cannot be attributed to the amplitude of the forced wave. Factors other than the 'stationary' nonlinear terms are the likely cause.

Unexpectedly, the zonal flow was sensitive to the forcing. The 80% weaker forcing reduced the amplitude of the time-mean wave by 60% rather than 80%. With the regular forcing, the large-amplitude stationary wave altered the zonal flow and made the forced wave less resonant (figure 57).

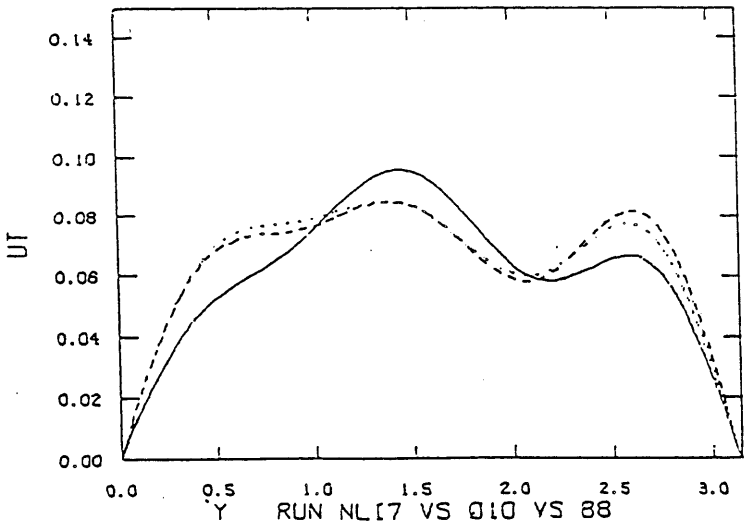

Fig. 57. Zonal-mean thermal wind Ut for three runs.
Solid: strong diabatic heating at $2k_o$, $2l_o$
Long dashes: weak forcing 20% of above
Short dashes: control run no stationary forcing

Phase Angle

Previously, we showed correlations between the linear and time-mean solutions. Correlations, however, can hide systematic differences. The phase angle is an example. In the 'orography' cases, the linear solution without the parameterized eddies had troughs east of the time-mean solution. The parameterized eddies moved the forced waves to the west, and eliminated the eastward bias. (Positive angles in the table 14 implies the linear solution is too far to the east)

Table 14: Phase Error of Forced Mode (in degrees)
Linear Solution (with param. eddies) vs. Time-Mean Solution

k_o	l_o	forcing	Ψ lin.	Ψ (param.)		θ lin.	θ (param.)	
1	1	ω	3^o	0^o	$\pm 1^o$	3^o	1^o	$\pm 1^o$
1	2	ω	1^o	-9^o	$\pm 3^o$	11^o	-3^o	$\pm 1^o$
2	1	ω	0^o	6^o	$\pm 1^o$	0^o	-1^o	$\pm 1^o$
2	2	ω	5^o	-1^o	$\pm 2^o$	10^o	3^o	$\pm 1^o$
average value (bias)			3^o	-1^o		6^o	0^o	

Consider the equation for a stationary wave

$$\frac{d}{dt} W = ik \cdot [A] \cdot W - F = 0$$

The stationary solution for a normal-mode structure is

$$W = i \frac{F}{w}$$

Where w is the complex frequency of the normal mode.

The phase of the complex number $(\frac{i}{w})$ is

arctan(imag(w) / real(w)) = arctan(frequency/growth_rate)

Therefore, the phase of the troughs is -arctan(frequency/growth_rate)

Previous calculations showed that, for the model's parameters, the eddy parameterization altered the dispersion relationship by:

1. Making the frequency more negative.
2. Tending to make the growth rate larger.

If the growth rate remains negative, then points (1) and (2) increase the positive argument of arctan(frequency/growth_rate). Thus, the wave should be shifted westward by the eddies.

A systematic phase error was not apparent for waves forced by the diabatic heating. This heating may force stronger 'internal' modes which may have argument-voiding positive frequencies.

Discussion

Away from resonance (small free-wave frequency), we expect that stationary waves are not sensitive to the synoptic eddies. This is not to say that these eddies have no effect, but rather that small factors will only produce small changes. Near resonance, however, theory suggests that the stationary waves are sensitive to the synoptic eddies and other neglected factors. Consequently, linear theory should do poorly for near-resonant forcings.

The comparison of linear theory with the time-mean solutions showed that linear theory well estimated the streamfunctions, at least for non-resonant forcing. The eddy parameterization improved the linear theory but the theory was generally insensitive to all parameterizations.

Linear theory poorly estimated the time-mean solution near resonance. This expected result was not caused by the amplitude of the stationary wave

being large, but by other neglected factors. Thus, near-resonant waves cannot be accurately modeled by simply including the 'stationary' nonlinear terms. The phase errors were roughly halved by the parameterized eddies but the amplitude of the stationary waves was consistently over-predicted. This may not be serious for a small 'effective friction' (eddy viscosity) would reduce those amplitudes.

Other researchers have examined the effect of transient eddies on stationary waves. They used eddy fluxes from observations (Opsteegh and Vernekar, 1982), and from a GCM climatology (Nigam, 1983; Nigam et al, 1986). They found that the transient-eddy fluxes made the linear solutions more realistic. They didn't decompose the solutions by wavenumber, so they couldn't find a near-resonant sensitivity. Such sensitivity was noted by Roads (1980) who compared the results from a GCM and a linear stationary wave model.

Chapter 7

Summary

We examined the interactions between synoptic- and planetary-scale waves in a simple baroclinic model. Such interactions provide a mechanism for the unexpected rapid growth of long waves in GCM experiments (e.g. MacVean, 1985). As a preliminary study, we examined the largest order interactions in a simple situation, in an attempt to gain a fundamental understanding.

Our analysis was broken into three sections: how the planetary-scale wave spatially modulated the synoptic-scale wave, how the fluxes of the synoptic-scale waves varied on the planetary-scale, and lastly how those fluxes altered the temporal evolution of a transient planetary-scale wave.

In the first part, the spatial modulation of the synoptic-scale wave was studied analytically. The approach assumes that the waves had a simple meridional structure, and it concentrates on describing the zonal structure. At this stage, the zonal and vertical structure of the planetary-scale wave is arbitrary. Our analysis shows that the modulation of the synoptic-scale wave is crucially dependent on whether or not the wave is inviscidly neutral or unstable. The latter case is considered in the belief that the zonal flow will equilibrate, by baroclinic adjustment, to a state where the most unstable modes will have small real growth rates (i.e., the flow is inviscidly unstable). One pleasing feature of our analysis is that the synoptic-eddy modulation occurs at a low order, and only the geometrical optics approximation is needed (Appendix A). This suggests a certain robustness of the basic results.

We found the spatially modulated synoptic-scale wave could be

described by a complex local wavenumber. The imaginary part determined the amplitude variations, while the real part determined the local wavelength. A major modulating factor was Ut'(x), variations of the planetary-scale thermal wind. Regions of positive Ut' showed spatial growth downstream. For the most unstable zonal wavenumber, the results had a particle interpretation; the spatial growth downstream was equal to the 'local growth rate' divided by its speed (group velocity).

The term U' also modulated the synoptic-scale waves. It produced significant changes in the local wavelength and could produce an important amplitude modulation. However, this modulation was sensitive to the synoptic wavelength, and it disappeared for the most unstable wavelength. For this reason, Ut' is probably more important on average. Results for a sphere, on the other hand, show a strong U' effect (e.g., Frederiksen, 1980). Perhaps the U' (and V') changed the latitude of the wavetrain which brought it into regions of differing local instability.

In the second part, we used the WKB solution to find the synoptic-eddy fluxes. The heat flux peaked downstream of the largest spatial growth (usually the strongest thermal winds) and peaked upstream of the largest eddy amplitudes. With this structure, the heat flux removed baroclinic energy from the planetary-scale mode. The divergence of the vorticity fluxes, on the other hand, was in phase with the long wave, and tended to add baroclinic and barotropic energy to the planetary-scales, consistent with observations (Holopainen et al. 1982).

Using the WKB solution, we parameterized the eddy fluxes in terms of the large-scale flow. The energy fluxes due to the synoptic-scale waves were not the only stability criterion. The out-of-phase heat flux could alter the structure of the long waves, and allow the long waves to convert

more ZAPE into EAPE. Altering the long wave requires no energy when the fluxes are 90^{o} out of phase, so the energy fluxes gave an incomplete description of the effect of synoptic eddies (i.e., the synoptic eddies can also play a catalytic role). For the constants of the numerical model, the parameterized eddies usually increased the growth rate of the long wave. This result could explain why the long waves grew faster than predicted by linear theory in the GCM experiments.

The numerical model supported our analysis. First, the model showed that baroclinic adjustment can occur. In addition, the energetics of the long-modes/synoptic interactions were comparable with predictions based on our synoptic-eddy parameterization. The numerical model also showed some conditions where baroclinic adjustment failed and where the parameterization failed to describe the energy fluxes.

The interaction of the synoptic-scale waves and the stationary long waves was studied by a hierarchy of models: linear, linear with parameterized eddies, and a time-dependent nonlinear model. Away from resonance, the results were not sensitive to the transient eddies. Correlations of the linear and time-mean solutions were above 0.90. The eddy parameterization improved the results slightly.

When the forcing was near resonance, the linear solutions showed large errors, as expected by theory. The parameterized eddies reduced the phase errors. But near resonance, the linear solutions were sensitive to all factors.

Conclusions

The baroclinic adjustment hypothesis can be a good approximation although it breaks down if the factor 'G' is too large (5.11). 'G' is large if the channel width is large, the radiative forcing is strong, or if the friction is small. Whether baroclinic adjustment applies to the atmosphere should be examined in more detail.

The net effect of the synoptic eddies cannot be determined by the energy fluxes due to the synoptic-scale eddies. These eddies can play catalytic role, and help destabilize the long waves.

The non-resonant stationary waves were not sensitive to the transient waves, and linear theory accurately described the stationary waves. Near resonance, however, linear theory gave poorer results.

All the previous results are dependent on having inviscidly unstable synoptic-scale waves. The results for inviscidly stable synoptic-scale waves would be much smaller and different. Therefore, one must be careful in applying results from inviscidly stable flows to inviscidly unstable flows. For example, applying barotropic ray-tracing theory in the mid-latitudes is suspect, if the wave is inviscidly unstable.

Appendix A: WKB Invalidity

The geometrical-optics approximation of the WKB technique (Bender and Orszag, 1979) was used to find the spatial modulation of the synoptic-scale waves. Here, we show that the next higher order approximation, physical optics, is not necessary. The validity of the WKB technique is harder to determine without having specific numbers; however, conditions for definite WKB breakdown are shown to be equivalent to a necessary condition for local instability (Pierrehumbert, 1984).

One does not expect the WKB solution to breakdown for the most unstable modes. The reasoning is outlined below.

1. For a definite WKB breakdown (T -> 0, see A.1, A.4, and A.5), the instability must satisfy some constraints which are necessary conditions for local instability. See Pierrehumbert (1984), and the following section 'WKB Breakdown for Small T.'

2. The most unstable modes are global rather than local unless they satisfy additional constraints. For reasonable flows, the most unstable modes are global.

3. Since our analysis is restricted to the most unstable modes, and local instabilities are associated with lower growth rates, we do not expect the 'T -> 0' WKB breakdown to be important.

The WKB expansion is given by (A.1). We will now justify neglecting

the term g_1 (geometrical-optics approximation).

$$\Psi = \exp\left(\int^{x} i \cdot k(x) \cdot dx + g_1(X) - i \cdot w \cdot t \right) \qquad (A.1)$$

The O(1) equation is $H(k) = \sum_{o}^{6} a_j k^j = 0$ from (3.51) (A.2)

Since there is separation of length scales ($\varepsilon << 1$) and the basic-state wave is weak ($\delta << 1$), terms involving dU/dx, dUt/dx, dV/dx, and dVt/dx are $O(\varepsilon \cdot \delta)$. Therefore, the terms can be neglected to $O(\varepsilon)$.

The $O(\varepsilon)$ equations involve the same terms as the O(1) equations because terms like dU/dx can be neglected. Therefore, the $O(\varepsilon)$ equation is given by (A.3).

$$\sum_{j=o}^{6} j \cdot a_j k^{j-1} \frac{d}{dX} g_1(X) + \frac{1}{2} j \cdot (j-1) a_j k^{j-2} \frac{dk}{dX} = 0 \qquad (A.3)$$

Note that $\frac{d}{dX} a_j$ is $O(\varepsilon \cdot \delta)$, so it can be ignored.

Define $T = \frac{dH}{dk} = \sum_{j=o}^{6} j\, a_j k^{j-1}$ (A.4)

Therefore, $g_1(X) = -\frac{1}{2} \log T$ (A.5)

WKB Breakdown for Small T

The WKB approximation will breakdown when T is zero (A.6). But when T is zero, the local group velocity is also zero and the wave has an extremum in its growth rate. These are conditions for local instability, as shown by Pierrehumbert (1984).

Equation A.5 implies $\exp g_1(X) = \text{constant}\ T^{-1/2}$ (A.6)

'Showing the group velocity is zero'

$H(w, k, X) = 0$ is a sixth order polynomial for 'k' (A.2)

When $T(w,k) = \frac{\partial}{\partial k} H(w,k) = 0$, then k must be a multiple root of H.

Proof:

$H(k) = a \cdot (r_1 - k) \ldots (r_6 - k)$

r_i is the i-th root of H

Since $H(k) = 0$, k must be equal to r_1, r_2, ... or r_6.

suppose $T(r_1) = 0$

then $\frac{\partial}{\partial k} H(r_1) = - a \cdot (r_2 - r_1) \ldots (r_6 - r_1)$

but $\frac{\partial}{\partial k} H(r_1) = T = 0$

Therefore, r_1 is equal to r_2, r_3, ... or r_6

Hence, k must be a multiple root when $T = 0$.

However, the group velocity, c_g, is given by $\text{real}(\frac{\partial w}{\partial k})$.

But $$\frac{\partial w}{\partial k} = - \frac{\partial H}{\partial k} \Big/ \frac{\partial H}{\partial w}$$
$$= - T \Big/ \frac{\partial H}{\partial w} = 0$$

Therefore, if $T \to 0$ (a definite WKB breakdown), one has the necessary conditions for local instability (Pierrehumbert, 1984).

Errors from $g_1(X)$

Our WKB expansion suggests that the error in neglecting g_1 is $e^{g_1(X)}$. However, $e^{g_1(X)}$ is not the real error. For example, if $g_1(X)$ were

constant, then the error just changes the amplitude of the solution which is not determined by our WKB analysis. Therefore, changes in g_1 are the important error.

From (A.5), $\exp g_1(X) = \text{constant } T^{-1/2}$

Therefore, variations of $\exp g_1 \approx -\frac{1}{2} \text{ constant } dT\ T^{-3/2}$

Where dT is the size of the variation of T

Therefore, the relative error = |variation of $\exp g_1$| / |$\exp g_1$|

$$= dT / T$$

Since $H = \sum_0^6 a_j k^j = 0$

then $T \cdot dk = \sum_{j=0}^{6} -k^j da_j$ using (A.4)

where da_j is the perturbation of a_j due to U', Ut', etc.

By the scaling, the large-scale flow has on $O(\delta)$ wave (i.e., $U'/U = O(\delta)$).

Since da_j depends on the large-scale wave, therefore $da_j = O(\delta \cdot a_j)$

Similarly, $dk = O(\delta \cdot k) = O(\delta)$ (since $k = O(1)$)

and $dT = O(\delta \cdot T)$

Therefore, the error from not using physical optics is $O(dT/T) = O(\delta)$.

The imaginary part of k also changes the amplitude of the solution. It alters the amplitude by $e^{\int^x ki \cdot dx} \approx O(dk \cdot X/x) \approx O(dk/\varepsilon)$, or more simply $O(\delta/\varepsilon)$. This is much larger than the change introduced by neglecting g_1. Therefore, the geometrical-optics approximation can be justified since the physical-optics approximation introduces a small change.

Appendix B: Parameterization

Introduction

We have three reasons for trying to parameterize the synoptic-scale (transient) eddies. First, the parameterization is used to find the growth rate of long waves in the presence of synoptic-scale waves. Of less direct relevance, transient-eddy parameterizations are used to save computer costs in climate models. Last, the existence of a parameterization is theoretically useful for it extends the range of linear theory when certain nonlinear processes behave in a linear manner.

The mixing-length theory is the basis for most eddy parameterizations. It views the eddies as turbulent, random-like motions that move conserved quantities in all directions. The net effect of these motions is to act like a strong molecular diffusion. The strength of mixing depends on the eddies' length and internal velocities, where large velocities and lengths favor mixing over small, weak eddies.

For a conserved quantity A, mixing-length theory suggests:

$$\langle u'A' \rangle = K^{xx} \frac{dA}{dx} + K^{xy} \frac{dA}{dy} + K^{xz} \frac{dA}{dz}$$

$$\langle v'A' \rangle = K^{yx} \frac{dA}{dx} + K^{yy} \frac{dA}{dy} + K^{yz} \frac{dA}{dz}$$

$$\langle w'A' \rangle = K^{zx} \frac{dA}{dx} + K^{zy} \frac{dA}{dy} + K^{zz} \frac{dA}{dz}$$

K^{ij} is the eddy diffusion coefficient

Mixing-length theory was initially applied to the eddy fluxes of heat, zonal momentum, and vorticity. Observed transient eddies, however, can transport the latter two quantities upgradient. [Held (1975) gave a simple explanation for the upgradient fluxes of zonal momentum.] This failure was blamed on the non-conservation of zonal momentum and vorticity. On the

other hand, potential temperature and potential vorticity are conserved, and their fluxes tend to be downgradient in the troposphere, consistent with the mixing-length hypothesis. As a result, more recent papers have applied mixing-length theory to the potential vorticity and potential temperature. (See the review by Shutts, 1983a.) One should remember that these theories only apply to the troposphere since the potential-vorticity flux can be upgradient in the stratosphere (Lau et al., 1981).

Originally, eddy parameterizations were applied to the zonal-mean flow. They were used in simple models such as the energy-balance models (North et al., 1981) and the statistical-dynamical models (Saltzman, 1978). These models became an important tool for climate studies. More recently, researchers [Shutts (1983a), White and Green (1982)] have tried using non-zonal versions of these parameterizations in an attempt to include some important spatial variability.

Green and White (1982) observed that their parameterized eddies, being diffusive, reduced the baroclinic instability of the long waves. Shutts (1983a) examined the effects of the parameterized eddies on the forced long waves. The effects were not especially notable.

The weakness of most eddy parameterizations is the mixing length hypothesis, which has not been shown to be correct. For example, quasi-geostrophic theory suggests that waves growing on a baroclinically zonal flow must have downgradient potential-temperature and potential-vorticity fluxes (Pedlosky, 1979).

White and Green (1982) and later Shutts (1983a) questioned whether any theoretical basis existed for a synoptic-eddy parameterization. They argued that, if Stone's baroclinic adjustment hypothesis (1978) were correct, parameterizing the heat flux only using the mean flow must be

incorrect. Stone had hypothesized that synoptic-scale eddies dominate the mid-latitude tropospheric flow, and maintain the zonal flow at near baroclinic neutrality. Hence, the large-scale flow should be near neutral stability regardless of the radiative forcing. Since the radiative forcing is balanced principally by the eddy heat flux, parameterizing the eddy heat flux only using the instability properties of the large-scale flow is suspect. (The instability properties will define simple-structure flows.)

Observations of the mid-latitude troposphere are consistent with baroclinic adjustment (Stone, 1978), while results from numerical models are contradictory. For example, most of our simulations strongly support a baroclinic adjustment modified by including friction and curvature of the zonal flow. On the other hand, Vallis and Roads (1984) found little evidence for a modified baroclinic adjustment. These conflicting results are examined in chapter 5. It suffices to state that baroclinic adjustment will hold for some parameters.

We will not examine the objections raised by White, and Green and Shutts. The parameterization developed in this thesis is based on the large-scale flow and an external parameter (synoptic-eddy amplitude); thus, their arguments do not apply.

In summary, a good parameterization of the transient eddies would be useful for theories of planetary-scale waves and climate modeling. Most parameterizations are based on the mixing-length theory which suggests that transient eddies mix conserved quantities like molecular diffusion. Whether this theory applies to the large-scale atmospheric flow is unclear. The transient eddies have a well-defined structure which may have fluxes which are not strictly downgradient.

Parameterization Details
Numerical Model's Modes

The fluxes determined by the numerical model are compared with those determined by the parameterization. In particular, we are interested in the eddy fluxes which affect the numerical model's large-scale modes which are listed below. The other modes in the model have length scales which are comparable with or smaller than the most unstable wavelength, and are of less interest.

Larger scale modes in the numerical model:

$\sin(l_o y)\ \exp(ik_o x)$ $\qquad$ $\sin(l_o y)\ \exp(2ik_o x)$

$\sin(2l_o y)\ \exp(ik_o x)$ $\qquad$ $\sin(2l_o y)\ \exp(2ik_o x)$

Synoptic modes:
(Most unstable modes for uniform flow)

$\sin(l_o y)\ \exp(3ik_o x)$ $\qquad$ $\sin(2l_o y)\ \exp(3ik_o x)$

Meridional Structure

Our WKB analysis has to be extended before it can be used in parameterizing the eddy fluxes. The following example shows a deficiency in the analysis.

Consider a planetary-scale wave with the widest meridional structure, $\sin(l_o y)$. The zonal winds from this basic-state wave are opposite in the northern and southern halves of the channel. Therefore, terms like Ut'(x) and U'(x) are zero (see below).

Let $\theta_{ps} = \theta_o(x) \sin(l_o y)$

Let $\Psi_{ps} = \Psi_o(x) \sin(l_o y)$

By (3.44), Ut' for the $\sin(j \cdot l_o y)$ is

$$Ut' = - \langle \theta_o l_o \cos(l_o \cdot y) \sin(j l_o \cdot y) \mid \sin(j \cdot l_o \cdot y) \rangle$$

$$= - \langle \theta_o l_o \cos(l_o \cdot y) \mid \frac{1}{2} (1 - \cos(2j \cdot l_o \cdot y)) \rangle$$

$$= 0$$

Similarly U', DU', and DUt' are all zero.

Since Ut', U', DU' and DUt' are zero, synoptic-scale waves should not be spatially modulated.

The problem with the model equations is that the spatial modulation only has a zonal dependence. Consequently, the equations cannot describe a wave that also has a 'y' modulation. For this reason, we will describe a simple modification to include the effects of the $\sin(l_o y)$ long mode.

Synoptic-scale Wave: $\sin(l_o y)$

This section considers the $\sin(l_o y)$ synoptic mode, and shows the values of U', Ut', DU' and DUt'.

Using (3.43-3.46) gives

$$U_1'(x) = \langle -\frac{\partial}{\partial y} \Psi'_{ps} \sin(l_o y) \mid \sin(l_o y) \rangle$$

Define $\Psi'_{ps} = \sum_j a_j(x) \sin(j l_o y)$ (B.1)

$$\theta'_{ps} = \sum_j b_j(x) \sin(j l_o y) \quad \text{(B.2)}$$

From (B.1), $U_1'(x) = l_o \cdot a_2(x)$ + smaller terms (B.3)

1. The $\sin(2l_o y)$ long mode modulates the $\sin(l_o y)$ synoptic mode (B.1).
2. The $\sin(l_o y)$ synoptic modes have a $\sin(2l_o y)$ eddy flux.

By (1) and (2), the $\sin(2l_o y)$ long mode affects the $\sin(l_o y)$ synoptic mode and vice versa. These two modes, therefore, have a mutual interaction, a necessary condition for a feedback and strong interactions.

Some other important terms are:

$$Ut_1' \doteq l_o \cdot b_2(x)$$
$$DU_1' \doteq -4l_o^3 a_2(x)$$
$$DUt_1' \doteq -4l_o^3 b_2(x)$$

Synoptic Mode: $\sin(2l_o y)$

The two other important modes are the $\sin(l_o y)$ long-wave mode and the $\sin(2l_o y)$ synoptic mode. According to our analysis, the $\sin(2l_o y)$ synoptic mode interacts with $\sin(4l_o y)$ long wave and not with the $\sin(l_o y)$ large-scale mode. However in the numerical model, the $\sin(4l_o y)$ long wave has a small meridional-length scale, so it is less important.

The second synoptic/planetary-scale interaction can be best understood by an artificial construction. The $\sin(2l_o y)$ synoptic mode is unaffected by inserting a wall in the center of the channel since that mode's meridional velocity is zero in the middle. Now, insert a wall in the middle of the channel, and then apply our analysis to each subdomain. The $\sin(2l_o y)$ synoptic mode is now modulated by $\sin(l_o y)$ long wave.

The second synoptic/planetary-scale interaction is calculated as if a barrier existed in the middle of the channel. This procedure is equivalent

to assuming the synoptic mode is given by equation B.4. This mode takes advantage of the opposite signs of U', Ut' etc. in the northern and southern regions.

$$\Psi = \sin(2l_o y)\, e^{i\langle k\rangle x + \int^{x} ik'dx - iwt} \qquad 0 < y < \frac{Y}{2} \qquad \text{(B.4)}$$
$$= \sin(2l_o y)\, e^{i\langle k\rangle x - \int^{x} ik'dx - iwt} \qquad \frac{Y}{2} < y < Y$$

Equation B.4 is formally justified for the Galerkin approximation gives considerable freedom for modal expansions. The modal expansions need not be eigenvectors; they only have to satisfy the boundary conditions. A poor expansion only gives a slow convergence. These modes (B.4), while unconventional, do converge to the eigenvectors for small spatial modulation (i.e., $\varepsilon \to 0$, $\delta \to 0$). This suggests that the convergence may be reasonable in this limit.

$$U_2' = \frac{32}{15\pi} l_o\, a_1(x)$$
$$Ut_2' = \frac{32}{15\pi} l_o\, b_1(x)$$
$$DU_2' = -\frac{32}{15\pi} l_o^3\, a_1(x)$$
$$DUt_2' = -\frac{32}{15\pi} l_o^3\, b_1(x)$$

The above values are for the southern half of the channel. The values in the northern half have the opposite sign.

Zonal-Mean Flow

The long wave in our analysis was made stationary by a zonal translation. The $\langle U\rangle$ relative to the surface will be called $\langle U\rangle_s$. It and $\langle Ut\rangle$ were found using (B.4) and (B.5). Generally, $\langle Ut\rangle$ and $\langle U\rangle_s$ depend on

the meridional structure of the perturbation.

$$\langle U\rangle_{s,m} = \langle -\frac{\partial}{\partial y}\psi_{ps}\ \sin(m\cdot l_o\cdot y)\ |\ \sin(m\cdot l_o\cdot y)\rangle \qquad (B.5)$$

$$\langle Ut\rangle_{m} = \langle -\frac{\partial}{\partial y}\theta_{ps}\ \sin(m\cdot l_o\cdot y)\ |\ \sin(m\cdot l_o\cdot y)\rangle \qquad (B.6)$$

$\langle U\rangle_{s,m}$ is the effective zonal-mean wind for the $\sin(m\cdot l_o y)$ synoptic mode measured relative to the ground.

$\langle Ut\rangle_{m}$ is effective thermal wind for the $\sin(m\ l_o y)$ synoptic mode

The above equations can be rewritten.

$$\langle Ut\rangle = \sum \frac{1}{\pi} m\cdot l_o\cdot L^{nm}\ b_{m0} \qquad (B.7)$$

where $\langle\theta\rangle = \sum_m b_{m0}\ \sin(m\cdot l_o\ y)$

$$\langle U\rangle_{s,n} = \sum_m \frac{1}{\pi} m\ l_o\ L^{nm}\ a_{m0} \qquad (B.8)$$

where $\psi = \sum_m a_{m0}\ \sin(m\cdot l_o\ y)$

The expressions for $\langle Ut\rangle_m$ and $\langle U\rangle_{s,m}$ can be approximated by the first term in (B.7) and (B.8). The other terms are neglected since L^{nm} is small, and the model's values of b_{m0} and a_{m0} are small compared with b_{10} and a_{10} (see following table). With this approximation, the zonal-mean winds are only a function of the large-scale fields, and given by (B.9-B.12).

	m=1	m=2	m=3	m=4	m=5
a_{m0}:	.14	.0077	-.0030	-.0037	.0018
b_{m0}:	.14	.0027	.011	-.0027	.0034
L^{1m}:	8/3	0	-23/15	0	62/105
L^{2m}:	32/15	0	14/9	0	-32/45

Time mean values of a_{m0} and b_{m0} are from the control run:

$$\langle Ut\rangle_1 = \frac{8}{3\pi} l_o\ b_{10} \qquad \text{for } \sin(l_o\ y) \text{ synoptic mode} \qquad (B.9)$$

$$\langle U \rangle_{s,1} = \frac{8}{3\pi} l_o \, a_{10} \tag{B.10}$$

$$\langle Ut \rangle_2 = \frac{32}{15\pi} l_o \, b_{10} \quad \text{for } \sin(2l_o y) \text{ synoptic mode} \tag{B.11}$$

$$\langle U \rangle_{s,2} = \frac{32}{15\pi} l_o \, a_{10} \tag{B.12}$$

In our theory, the planetary-scale wave was made stationary by a zonal translation, so <U> is measured relative to the phase speed of that wave. Fortunately, the exact value of the zonal wind is not critical; our analysis suggests that the zonal wind affects the synoptic-scale wave by changing its group velocity. An inexact zonal wind will change the amplitudes of the synoptic-eddy fluxes but not the more important phases. (See equations 3.74, 3.78, 3.80, and 3.82.) A simple estimate of the phase speed of the planetary-scale waves is given below.

Let $c_{n,m} = \langle U \rangle_{s,m} - \beta(K^2 + F) \; / \; K^2(K^2 + 2F)$

where $K^2 = (nk_o)^2 + (ml_o)^2$

$c_{n,m}$ is an crude estimate of the phase speed of a transient planetary-scale wave with the form $\sin(ml_o y) \exp(ink_o x)$

For stationary planetary-scale waves, $c_{n,m} = 0$

Using the above estimates for the phase speed, <U> is given by (B.13) and (B.14). Note that the parameterization uses a different zonal wind for each meridional mode.

$$\langle U \rangle_1 = \langle U \rangle_{s,1} - c_{n,2} \quad \text{for the } \sin(l_o y) \text{ synoptic mode} \tag{B.13}$$

$$\langle U \rangle_2 = \langle U \rangle_{s,2} - c_{n,1} \quad \text{for the } \sin(2l_o y) \text{ synoptic mode} \tag{B.14}$$

Our eddy parameterization has some constants such as F and beta. Since the parameterization will be compared with the results of the numerical model, these values are identical with the numerical model's. (See chapter 5.)

Synoptic-scale Wave

The eddy parameterization depends on the wavenumbers of the synoptic-scale wave. Most of our theoretical analysis is based on the most unstable zonal wavenumber. However, this wave does not exist in the numerical model since the wavenumbers are quantized. So the parameterization uses the most unstable wavenumbers that exist in the numerical model.

$\sin(l_o y)$ mode: $k=3k_o$, $l=l_o$, $K^2 = 4.48$

$\sin(2l_o y)$ mode: $k=3k_o$, $l=2l_o$, $K^2 = 5.84$

$K^2_{critical} = 2^{1/2}F = 4.91$

The synoptic-eddy amplitude of the $\sin(l_o y)$ and $\sin(2l_o y)$ modes is undetermined by our WKB analysis. This amplitude can be determined by either scale analysis (e.g. Green, 1970), numerical simulations, global energetics, or even prognostic equations. In this thesis, the synoptic-eddy amplitude is either a free parameter or determined by the numerical simulations (see the following formulae).

Amplitude of $\sin(l_o y)$ synoptic-scale mode $\approx |\Psi(k=3k_o, l=l_o)|$

Amplitude of $\sin(2l_o y)$ synoptic-scale mode $\approx |\Psi(k=3k_o, l=2l_o)|\ (1 + g)$

$$\text{Where } g = \text{real} \quad \frac{\Psi(k=3k_o, l=3l_o) + \Psi(k=3k_o, l=5l_o)}{\Psi(k=3k_o, l=2l_o)}$$

When the $\sin(2l_o y)$ synoptic mode is zonally modulated, it has the opposite modulation in the northern and southern regions. As a result, its meridional structure will have energy in many meridional modes. The term 'g' tries to include this extra energy by considering the other modes which are in phase with $\sin(2l_o y)$ mode.

Summary

In summary, the numerical model has two large-scale meridional modes, $\sin(l_o y)$ and $\sin(2l_o y)$. The $\sin(2l_o y)$ long-wave mode modulates the $\sin(l_o y)$ synoptic mode, and the fluxes of that synoptic mode will directly force the $\sin(2l_o y)$ long wave. This mutual interaction is necessary for a feedback. As result, strong interactions can occur. The other long-wave mode, $\sin(l_o y)$ has a coupling with the $\sin(2l_o y)$ synoptic mode which is another source of strong interactions. These mutual interactions can produce the feedback which is studied in this thesis.

Appendix C: Energy Fluxes

This appendix defines the baroclinic energy, barotropic energy, and various energy fluxes. When Ψ and θ are used, the baroclinic and barotropic energies are more convenient than traditional kinetic and available potential energies

$$\text{Total Energy} = \sum_{k,\ell} \frac{1}{2} K^2 |\Psi_{k,1}|^2 + \frac{1}{2} (K^2 + 2F) |\theta_{k,1}|^2 \qquad (C.1)$$

$$\text{Kinetic Energy} = \sum_{k,\ell} \frac{1}{2} K^2 |\Psi_{k,1}|^2 + \frac{1}{2} K^2 |\theta_{k,1}|^2 \qquad (C.2)$$

$$\text{APE} = \sum_{k,\ell} F |\theta_{k,1}|^2 \qquad (C.3)$$

$$\text{Barotropic Energy} = \sum_{k,\ell} \frac{1}{2} K^2 |\Psi_{k,1}|^2 \qquad (C.4)$$

$$\text{Baroclinic Energy} = \sum_{k,\ell} \frac{1}{2} (K^2 + 2F) |\theta_{k,1}|^2 \qquad (C.5)$$

Let $\Psi(x,y,t) = \langle\Psi(y,t)\rangle + \Psi'(x,y,t)$

Let $\theta(x,y,t) = \langle\theta(y,t)\rangle + \theta'(x,y,t)$

$\sum \frac{1}{2} K^2 |\langle\Psi_{o,1}\rangle|^2$ = zonal barotropic energy (ZBT)

$\sum \frac{1}{2} K^2 |\Psi'_{k,1}|^2$ = eddy barotropic energy (EBT)

$\sum \frac{1}{2} (K^2 + 2F) \langle\theta_{o,1}\rangle^2$ = zonal baroclinic energy (ZBC)

$\sum \frac{1}{2} (K^2 + 2F) |\theta'_{k,1}|^2$ = eddy baroclinic energy (EBC)

Define $\overline{A(x,y)} = \frac{1}{X \cdot Y} \int_0^Y \int_0^X A(x,y) \cdot dx \cdot dy$

The equation for the vertical mean stream function is

$$\frac{\partial}{\partial t} \nabla^2\Psi = -\beta \frac{\partial\Psi}{\partial x} - J(\Psi, \nabla^2\Psi) - J(\theta, \nabla^2\theta) + D$$

where D = dissipation

The energy fluxes for the above equation are:

$\overline{\langle\Psi\rangle\, J(\Psi', \nabla^2\Psi')}$ = gain of ZBT due to BTW-BTW-BTZ triads

= loss of EBT due to BTW-BTW-BTZ triads

$\overline{\langle\Psi\rangle\, J(\theta', \nabla^2\theta')}$ = gain of ZBT due to BCW-BCW-BTZ triads

$\overline{\Psi' \left[J(\langle\theta\rangle, \nabla^2\theta') + J(\theta', \nabla^2\langle\theta\rangle)\right]}$ = gain of EBT due to BCW-BCZ-BTW triads

$\overline{\Psi'\, J(\theta', \nabla^2\theta')}$ = gain of EBT due to BCW-BCW-BTW triads

The equation for the thermal stream function is

$$\frac{\partial}{\partial t}\,(\nabla^2 - 2F)\,\theta = -\beta\,\frac{\partial\theta}{\partial x} - J(\Psi,\,(\nabla^2 - 2F)\,\theta) - J(\theta,\,\nabla^2\Psi) + Q$$

Q = heating and thermal dissipation

The energy fluxes for the above equation are:

$\overline{\langle\theta\rangle \left[J(\Psi', (\nabla^2 - 2F)\,\theta') + J(\theta', \nabla^2\Psi')\right]}$ =

gain of ZBC from BCW-BCZ-BTW triads

$\overline{\theta'\, J(\Psi', \nabla^2\theta')}$ = gain of EBC from BCW-BCW-BTW triads

$\overline{\theta'\, J(\langle\Psi\rangle, \nabla^2\theta')}$ = gain of EBC from BCW-BCW-BTZ triads

$\overline{\theta' \left[J(\Psi', (\nabla^2 - 2F)\,\langle\theta\rangle) + J(\langle\theta\rangle, \nabla^2\Psi')\right]}$ =

gain of EBC from BCW-BCZ-BTW triads

Appendix D

Parameterization and Energy Fluxes

Energy fluxes were used to analyze the numerical model. These fluxes were compared, in chapter 5, with predictions based the eddy parameterization. This determined the conditions under which the theory does poorly.

The numerical model's energy fluxes was calculated by:

1. Periodically saving the state of the model.
2. Calculating the energy fluxes for each archived state.
3. Averaging over all archived states.
4. Repeating steps (2) and (3) except with with certain components of the flow set to zero. Steps (1) through (4) allow one to calculate the energetics for any triad or group of triads.

Example 1: Find the energy fluxes caused by wave mean-flow interactions

1. Calculate the energetics for the flow.
2. Set the zonal flow to zero.
3. Calculate the energetics for this wavy flow.
   (Step 3 calculates the wave-wave interactions.)
4. Subtract the results of step (3) from step (1).
   (In the thesis, a special program was used instead of steps 1-4.)

Example 2: Find the energy fluxes from the BCZ-BCW-BTW triad

1. Set the barotropic zonal flow to zero.
2. Calculate the energetics of the wave mean-flow interactions.
   (See example 1.)

Example 3: Find the flux involving the $3k_o$ wave

1. Calculate the energetics.
2. Set the $3k_o$ wave to zero.
3. Calculate the energetics with this 'new' flow.
4. Subtract the results of step (3) from step (1).

The synoptic-eddy parameterization was used to find an energy flux by: (1) determining the amplitude of the synoptic eddies for each archived state using the model's output (see Appendix B), (2) finding the eddy fluxes using the eddy parameterization, (3) using these eddy fluxes to find the energy fluxes, and (4) averaging over all archived states.

Appendix E: The Jacobian

We evaluated the jacobian with the collocation or pseudo-spectral method (Gottlieb and Orszag, 1977) because it is faster than the interaction method (i.e. tensor multiplication). The collocation method takes O(n log(n)) operations compared with $O(n^{5/2})$ operations for the interaction method (n is the number of modes).

The spectral expansion is given by (E.1) and (E.2).

$$\text{Let } \Psi_a = \sum_n a_{n0} \cos(nl_o y) + \sum_{n,m} a_{nm} \sin(nl_o y) \exp(imk_o x) \qquad \text{(E.1)}$$

$$\text{Let } \Psi_b = \sum_n b_{n0} \cos(nl_o y) + \sum_{n,m} b_{nm} \sin(nl_o y) \exp(imk_o x) \qquad \text{(E.2)}$$

Through the transformations: $x \rightarrow x' / k_o$, $y \rightarrow y' / l_o$,
we can set k_o and l_o to one.

$$\text{Define } \bar{\Psi}_a = \sum_n a_{n0} \cos(ny)$$
$$\tilde{\Psi}_a = \sum_{n,m} a_{nm} \sin(ny)\, e^{imx}$$
$$\bar{\Psi}_b = \sum_n b_{n0} \cos(ny)$$
$$\tilde{\Psi}_b = \sum_{n,m} b_{nm} \sin(ny)\, e^{imx}$$

J_{nm}, the spectral decomposition of Jacobian is given by:

$$J(\text{real}(\Psi_a), \text{real}(\Psi_b)) = \sum_n J_{n0} \cos(ny) + \sum_{n,m} \text{real}(J_{nm} \sin(ny)\, e^{imx})$$

J_{nm} can be divided into 3 parts: $J = J^1 + J^2 + J^3$.

$$J(\text{real}(\tilde{\Psi}_a), \text{real}(\tilde{\Psi}_b)) = \sum_{n,m} \text{real}(J^1_{nm} \sin(ny)\, e^{imx}) + \sum_n J^2_{n0} \cos(ny)$$
$$J(\tilde{\Psi}_a, \bar{\Psi}_b) + J(\bar{\Psi}_a, \tilde{\Psi}_a) = \sum_{n,m} \text{real}(J^3_{nm} \sin(ny)\, e^{imx})$$

We evaluated the jacobian in three parts, J^1, J^2 and J^3, to prevent numerical error. Such errors would occur if we used a discrete spectral transform to convert from a {sin(ny)} to a {cos(ny)} representation.

Example: Suppose a field is in its sine representation,

$$f(y) \doteq \sum_n s_n \sin(ny)$$

but we want a cosine representation

$$f(y) \doteq \sum_n c_n \cos(ny)$$

The best way to find c_n is by

$$c_n = \langle \cos(ny) \mid \sum_{n'} s_{n'} \sin(n'y) \rangle \qquad \text{(E.3)}$$

Using two discrete spectral transformations gives different results.

$$\{ c'_n \} = \mathfrak{F}_c \tilde{\mathfrak{F}}_s^{-1} \{ s_n \}$$

where $\mathfrak{F}_c$ is the discrete cosine transform

and $\mathfrak{F}_s^{-1}$ is the discrete inverse sine transform

note that $\{c_n\} \neq \{c'_n\}$

$\{c_n\}$ is not equal to $\{c'_n\}$ because the basis functions {sin(ny)} and {cos(ny)} are not orthogonal. Consequently, c'_n depends on the number of points used by the discrete spectral transformations. Since c_n is independent of the number of points, $\{c_n\} \neq \{c'_n\}$.

To avoid this error, we transform between the sine and cosine representations using (E.3), which is equivalent to matrix multiplication. This method forces the jacobian to be evaluated in three parts.

Part I, wave*wave -> wave

J^1 is the interaction of $\tilde{\psi}_a$ and $\tilde{\psi}_b$ producing a wavy field, and it is found by the collocation method. The derivatives of $\tilde{\psi}_a$, and $\tilde{\psi}_b$ are easily and accurately calculated in the spectral representation. They are then projected onto a grid (16 x 9). J^1 is evaluated on this grid, and the values on the grid are then transformed back into spectral space.

Evaluating J^1 takes O(n log(n)) operations where n is the number of modes (25). If the fast Fourier transform were not used, J^1 would take $O(n^2)$ operations.

Steps:

1. find $A(x,y) \doteq \sum_{n,m}$ real[im a_{nm} sin(ny) e^{imx}] by an inverse transform
2. find $B(x,y) \doteq \sum_{n,m}$ real[n b_{nm} cos(ny) e^{imx}] by an inverse transform
3. find $C(x,y) \doteq \sum_{n,m}$ real[n a_{nm} cos(ny) e^{imx}] by an inverse transform
4. find $D(x,y) \doteq \sum_{n,m}$ real[im b_{nm} sin(ny) e^{imx}] by an inverse transform
5. evaluate $E(x,y) = A(x,y)B(x,y) - C(x,y)D(x,y)$ on the grid points
   where grid points are at $x = 2m\pi / 16 \quad m = 0,\ldots,15$
   $y = n\pi / 8 \quad n = 0,\ldots,8$
6. find $\sum_{n,m}$ real[J^1_{nm} sin(ny) e^{imx}] = E(x,y) by a spectral transform

Finding J^1_{nm} in the above equation requires a transformation from spatial to spectral domain using an sine transform in y.

Part II, wave*wave -> zonal

J^2 is the zonally averaged interaction of two wavy fields.

$$J^2 = < J(\text{real}(\tilde{\psi}_a), \text{real}(\tilde{\psi}_b)) >$$
$$= \frac{1}{2} \text{real}(a^*_{nm} b_{pm} \{-im\cdot p\cdot \sin(ny) \cos(py) - im\cdot n\cdot \cos(ny) \sin(py)\})$$
$$= -\frac{1}{2} \text{real}(im \frac{\partial}{\partial y}\{[a^*_{nm} \sin(ny)][b_{pm} \sin(py)]\}) \qquad (E.4)$$

J^2 is evaluated by the collocation method. The terms in the brackets (E.4) are transformed onto grid space. These grid-point values are then multiplied together and transformed back into spectral space using a cosine transform. This result is multiplied by a matrix [L] which takes the y derivative and converts that result from a sine to a cosine representation. (The simpler method of multiplying I_n by n and taking an inverse cosine transform introduces errors.)

Steps:

1. find $F_m(y) = \sum_n a^*_{nm} \sin(ny)$ using an inverse sine transform
2. find $G_m(y) = \sum_n b_{nm} \sin(ny)$ using an inverse sine transform
3. evaluate $H(y) = \text{real}(-im\cdot F_m(y)\cdot G_m(y))$
   on the grid points $y = j\pi/16 \quad j = 0,\ldots,16$
4. find $\sum_n I_n \cos(ny) = [H(y)]$ using a cosine transform
5. evaluate $J^2_{n0} = \sum_p L_{np} I_p$
   where $L_{np} = <j \cos(my) \mid \sin(jy)>$

Part III, wavy*zonal -> wavy

J^3 is the interaction of a wavy field and zonal field, producing a wavy field. J^3, like the other terms is found using the collocation method.

$$J^3 = J(\bar{\Psi}_a, \tilde{\Psi}_b) - J(\bar{\Psi}_b, \tilde{\Psi}_a)$$

$$J^3 = \{[n \cdot a_{n0} \cos(ny)][b_{pl} \sin(py)] - [n \cdot b_{n0} \cos(ny)][a_{pl} \sin(py)]\}\ il \cdot e^{ilx}$$

term: A B C D (E.5)

The terms in the four brackets (E.5) are transformed onto a set of y points using either a inverse cosine (A, C) or inverse sine (B, D) transform, giving equation E.6.

Steps:

1. find $A(y) \doteq \sum_n a_{n0} \cos(ny)$ using an inverse cosine transform
2. find $B_l(y) \doteq \sum_p b_{pl} \sin(py)$ using an inverse sine transform
3. find $C(y) \doteq \sum_n b_{n0} \cos(ny)$ using an inverse cosine transform
4. find $D_l(y) \doteq \sum_p a_{pl} \sin(py)$ using an inverse sine transform
5. evaluate $E_l(y) = A(y)B_l(y) - C(y)D_l(y)$ (E.6)
   on the y points $y = j\,\pi / 16 \quad j = 0,\ldots,16$
6. find $\sum_m F_{ml} \sin(my) = E_l(y)$ using a sine transform (E.7)

$E_l(y)$ is transformed into spectral space using a sine transform, producing matrix [F] (E.7). [F] is the sine representation of J^3. [F] is then converted into a cosine representation by multiplication with constant matrix [G] (E.8).

7. find $G_{m,j} = \langle \cos(my) \mid \sin(jy) \rangle$ (E.8)
8. the final result is $J^3{}_{ml} = G_{m,j} F_{jl}$

Appendix F: Multiple Time-Mean States

The model used in this thesis is a simple, forced dissipative system. For the model parameters, the radiative-equilibrium state is baroclinically unstable, and the model has no obvious stable equilibrium states. Two time-mean states, however, do exist. The two states have a strong symmetry property as shown in figure 30.

Define a transformation T: $T \circ A(x,y) = -A(x, Y - y)$

T has the properties:

1. T is a linear operator
2. $J(T \circ A, T \circ B) = J(-A(x, Y - y), -B(x, Y - y))$
   $= T \circ J(A, B)$
3. $T \circ \theta_e = T \left[- 0.3 \left(\frac{y}{Y} - \frac{1}{2} \right) \right]$
   $= \theta_e$

The properties of operator T insure that if Ψ and θ are nonlinear solutions, then $T \circ \Psi$ and $T \circ \theta$ are also solutions. The system must, therefore, have multiple-time-mean states since if $\langle \Psi(y) \rangle$ and $\langle \theta(y) \rangle$ form a time-mean state, then $\langle T \circ \Psi \rangle$ and $\langle T \circ \theta \rangle$ must also be one. Of course, the time-mean states need not be distinct.

After long integrations, the numerical calculations show two distinct time-mean states which are related by transformation T. These states are probably stable (for the control run's parameters) because the zonal flow remained close to the time-mean state.

The time-mean state is determined by the initial state; thus in this forced-dissipative system, certain aspects of the initial state are never

forgotten. The model may have more than two time-mean states, but the ease with which they were found, suggests otherwise.

The symmetry properties implies that time-mean states must come in pairs. However, the states may be indistinct (i.e., $\Psi = T \circ \Psi$, $\theta = T \circ \theta$). Perhaps entropy considerations are important. If the two time-mean states were identical, some of the zonal modes would have no energy. Common sense, however, suggests the nonlinear terms should put energy in all modes (to increase the entropy of the system). Perhaps, if the variability is small, the time-mean states become distinct.

The existence of two time-mean states does not alter our results or conclusions. The symmetry property of the governing equations implies the time-mean states, energetics and solutions are simply related.

In summary, the nonlinear model has two distinct time-mean states. The symmetry property of the model implies time-mean states must come in pairs, but doesn't suggest why the states are distinct. Fortunately, our conclusions are unaffected by the two time-mean states.

Whether multiple time-mean states can exist in a more realistic model is unanswered. Nevertheless, one can speculate that interannual variations are different time-mean states where seasonal changes 'randomly' choose the state. One can also speculate there are two time-mean states, one with the ITCZ (intertropical convergence zone) in the Northern Hemisphere, and another in the Southern Hemisphere.

Appendix G: Linear instability calculation

The linear growth rate can be calculated for either the instability of the flow represented by the numerical model, or the instability that exists in the numerical model. Since the two are different, we will use the latter which is more relevant.

The equations governing the normal modes are given by (G.1) and (G.2). In these equations, the wave-wave interactions are neglected, and the instability grows like e^{-iwt}.

<..> is the basic state flow which is only a function of y

$$-iw\,\nabla^2\psi' = -\beta\frac{\partial\psi'}{\partial x} - J(\langle\psi\rangle, \nabla^2\psi') - J(\psi', \nabla^2\langle\psi\rangle) \qquad (G.1)$$
$$- J(\langle\theta\rangle, \nabla^2\theta') - J(\theta', \nabla^2\langle\theta\rangle) + g'$$

$$-iw\,(\nabla^2 - 2F)\theta' = -\beta\frac{\partial\theta'}{\partial x} - J(\langle\psi\rangle, (\nabla^2 - 2F)\theta) \qquad (G.2)$$
$$- J(\psi', (\nabla^2 - 2F)\langle\theta\rangle) - J(\langle\theta\rangle, \nabla^2\psi') - J(\theta', \nabla^2\langle\psi\rangle) + h'$$

g', h' are linear functions of ψ' and θ' and include Ekman pumping, eddy viscosity, and Newtonian cooling

The normal modes of the model have the following form.

$$\psi' = \sum_{n=1}^{5} a_n \sin(nl_o y)\, e^{ikx} \qquad (G.3)$$

$$\theta' = \sum_{n=1}^{5} a_{n+5} \sin(nl_o y)\, e^{ikx} \qquad (G.4)$$

where $k = j\cdot k_o \quad j=1,\ldots,5$

Equations G.1 and G.2 can be written as a matrix equation using (G.3) and (G.4).

$$-iw \cdot a_m = \sum_{j=1}^{10} [D]_{m,j}\, a_j \qquad \text{(G.5)}$$

Where [D] is a 10x10 matrix

Matrix [D] is a complicated function of the zonal basic state. It can, however, be evaluated with the wave mean-flow version of the numerical model. Basically, the model is initialized with the zonal basic state, and one of the a_j's is set to one. The model finds the time-derivatives of a_m, which are simply $[D]_{m,j}$. This procedure is repeated for all 10 a_j's which completely determines matrix [D].

The normal modes are the eigenvectors of matrix [D], and the growth rates are the real part of the eigenvalues. These quantities were found using a standard eigenvector finder EIGCFA (National Center for Atmospheric Research Software library).

Appendix H

Detailed Calculations

The main body of the thesis only gives an overview on how (3.41) and (3.42) become (3.51). This appendix contains the details. First, the problem is simplified by assuming that the synoptic-scale wave has a simple meridional structure (3.39 and 3.40).

$$\text{Assume} \quad \psi'(x,y,t) = a(x,t)\cdot\sin(ly) \tag{H.1}$$

$$\theta'(x,y,t) = b(x,t)\cdot\sin(ly) \tag{H.2}$$

The above forms can be inserted into (3.37) and (3.38), and using the Galerkin approximation gives:

$$\begin{aligned}\frac{\partial}{\partial t}(a_{xx} - l^2 a) = &- \beta a_x - \langle \sin(ly) \mid J(\psi_o, (a_{xx} - l^2 a)\sin(ly)) \rangle \\ &- \langle \sin(ly) \mid J(\theta_o, (b_{xx} - l^2 b)\sin(ly)) \rangle \\ &- \langle \sin(ly) \mid J(a\cdot\sin(ly), \nabla^2 \psi_o) \rangle \\ &- \langle \sin(ly) \mid J(b\cdot\sin(ly), \nabla^2 \theta_o) \rangle\end{aligned} \tag{H.3}$$

$$\begin{aligned}\frac{\partial}{\partial t}(b_{xx} - l^2 b - 2Fb) = &- \beta b_x - \langle \sin(ly) \mid J(\psi_o, (b_{xx} - l^2 b)\sin(ly)) \rangle \\ &- \langle \sin(ly) \mid J(\theta_o, (a_{xx} - l^2 a)\sin(ly)) \rangle \\ &+ 2F\cdot\langle \sin(ly) \mid J(\psi_o, b\cdot\sin(ly)) \rangle \\ &- 2F\cdot\langle \sin(ly) \mid J(\theta_o, a\cdot\sin(ly)) \rangle \\ &- \langle \sin(ly) \mid J(a\cdot\sin(ly), \nabla^2 \theta_o) \rangle \\ &- \langle \sin(ly) \mid J(b\cdot\sin(ly), \nabla^2 \psi_o) \rangle\end{aligned} \tag{H.4}$$

where $\langle a \mid b \rangle = \frac{2}{Y}\int_0^Y a\cdot b\cdot dy$

The planetary-scale flow varies on a long length scale, so zonal derivatives of the planetary-scale flow are only $O(\varepsilon)$ quantities. Hence, the jacobians can be simplified by ignoring the x-derivatives of the planetary-scale flow.

ex. $\langle \sin(ly) \mid J(\psi_o, (a_{xx} - l^2 a) \sin(ly)) \rangle$

$$= \langle \sin(ly) \mid -\frac{\partial}{\partial y} \psi_o (a_{xx} - l^2 a)_x \sin(ly) \rangle + \text{smaller terms}$$

$$= (a_{xx} - l^2 a)_x \langle \sin(ly) \mid -\frac{\partial}{\partial y} \psi_o \sin(ly) \rangle$$

define $U(x) = \langle \sin(ly) \mid -\partial\psi_o/dy \cdot \sin(ly) \rangle$

then $\langle \sin(ly) \mid J(\psi_o, (a_{xx} - l^2 a) \sin(ly)) \rangle = U(x) (a_{xx} - l^2 a)_x$

Similarily, Ut(x) DU(x) and DUt(x) are defined by:

$Ut(x) = \langle \sin(ly) \mid -\partial\theta_o/\partial y \sin(ly) \rangle$

$DU(x) = \langle \sin(ly) \mid -\partial^3\psi_o/\partial y^3 \sin(ly) \rangle$

$DUt(x) = \langle \sin(ly) \mid -\partial^3\theta_o/\partial y^3 \sin(ly) \rangle$

U(x) is effective (barotropic) zonal wind.

Ut(x) is the effective thermal zonal wind.

DU is the curvature of U

DUt is the curvature of Ut

From (H.3) and (H.4), we can get (3.41) and (3.42).

$$\frac{\partial}{\partial t}(a_{xx} - l^2 a) = -\beta a_x + U(l^2 a - a_{xx})_x + Ut(l^2 b - b_{xx})_x + DU \cdot a_x + DUt \cdot b_x \qquad \text{(H.5)}$$

$$\frac{\partial}{\partial t}(b_{xx} - l^2 b) = -\beta\, b_x + U[(2F + l^2)\, b - b_{xx}]_x \qquad (H.6)$$
$$- Ut[(2F - l^2)\, a + a_{xx}]_x + DU \cdot b_x + DUt \cdot a_x$$

The above equations have only two independent variables, x and t. If the synoptic-scale wave varies as exp(-iwt), then the above equations are an ODE in x, with non-constant coefficients. The linear system is solved using the WKB technique. Basically, we assume that a(x,t) has the form given below.

$$a(x,t) = \exp\{i\, g_o(X)/\varepsilon + i \cdot g_1(X) + i \cdot \varepsilon \cdot g_2(X) + .. - i \cdot w_o \cdot t - i \cdot \varepsilon \cdot w_1 \cdot t - ..\} \qquad (H.7)$$

Since a(x,t) and b(x,t) have a normal mode structure, they must have the same time dependence. In addition, if we assume that the heat flux only has an X dependence, then the relative phases of a(x,t) and b(x,t) can only vary on the long length scale. Thus, the WKB form of b(x,t) is given by (H.8).

$$b(x,t) = (co(X) + \varepsilon \cdot c_1(X) + ..)\, a(x,t) \qquad (H.8)$$

As a convenience, a local wavenumber is defined by:

$$k(X) = \frac{1}{\varepsilon}\frac{\partial}{\partial x} g_o(X)$$

Therefore $a(x,t) = \exp\left(i \int^x k(X) \cdot dx + \ldots - i \cdot w_o \cdot t - \ldots \right)$

and $\frac{\partial a}{\partial x} \approx ik \cdot a$ + smaller terms

Inserting (H.7) and (H.8) into (H.5) and (H.6), ignoring terms of

$O(\varepsilon)$, one gets two third-order polynomials in k.

$$-i\cdot w_o\cdot[(ik)^2 - l^2] = -ik\,\beta_{eff} - ik\cdot U\,[(ik)^2 - l^2] - ik\cdot co\cdot Ut\,[(ik)^2 - l^2] + ik\cdot co\cdot DUt \qquad (H.9)$$

$$-i\cdot w_o\cdot co\,[(ik)^2 - l^2] = -ik\,co\,\beta_{eff} + ik\cdot co\cdot U\,[2F - (ik)^2 + l^2] - ik\cdot Ut\,[2F + (ik)^2 - l^2] + ik\cdot DUt \qquad (H.10)$$

Where $\beta_{eff} = \beta - DU$

Now the above equations can be rewritten as:

$$\sum_{n=0}^{3} d_n\cdot(ik)^n + e_n\cdot co\cdot(ik)^n = 0 \qquad \text{from H.9} \qquad (H.11)$$

$$\sum_{n=0}^{3} f_n\cdot(ik)^n + g_n\cdot co\cdot(ik)^n = 0 \qquad \text{from H.10} \qquad (H.12)$$

where

$$d_n = \{ -iwl^2, -\beta_{eff} + l^2U, iw, -U \} \qquad (H.13)$$

$$e_n = \{ 0, l^2\,Ut + DUt, 0, -Ut \} \qquad (H.14)$$

$$f_n = \{ 0, (l^2 - 2F)Ut + DUt, 0, -Ut \} \qquad (H.15)$$

$$g_n = \{ -i(l^2 + 2F)\,w, -\beta_{eff} + (l^2 + 2F)\,U, iw, -U \} \qquad (H.16)$$

note that: $e_o = e_2 = f_o = f_2 = 0$

$$f_3 = e_3,\ d_3 = g_3,\ d_2 = g_2$$

co can be eliminated from (H.11) and (H.12) by

$$co = -\left[\sum_{n=0}^{3} d_n \cdot (ik)^n\right] / \left[\sum_{n=0}^{3} e_n \cdot (ik)^n\right]$$
$$= -\left[\sum_{n=0}^{3} f_n \cdot (ik)^n\right] / \left[\sum_{h=0}^{3} g_n \cdot (ik)^n\right]$$

The resulting equation is the order 1 WKB equation.

$$-\left[\sum_{0}^{3} d_n (ik)^n\right]\left[\sum_{0}^{3} g_n (ik)^n\right] + \left[\sum_{0}^{3} f_n (ik)^n\right]\left[\sum_{0}^{3} e_n (ik)^n\right]$$
$$= H(w,k) = \sum_{h=0}^{6} a_n k^n \qquad (H.17)$$

where

$$a_6 = (i)^6 [f_3e_3 - d_3g_3] = -[e_3^2 - d_3^2]$$
$$= U^2 - Ut^2$$

$$a_5 = (i)^5[f_3e_2 + f_2e_3 - d_3g_2 - d_2g_3]$$
$$= i\,[-2d_3d_2]$$
$$= -2Uw$$

$$a_4 = (i)^4\,[f_3e_1 + f_2e_2 + f_1e_3 - d_3g_1 - d_2g_2 - d_1g_3]$$
$$= [f_3(e_1 + f_1) - d_3(g_1 + d_1) - d_2g_2]$$
$$= -Ut\,[l^2Ut + DUt + (l^2 - 2F)Ut + DUt]$$
$$+ U\,[-\beta_{eff} + l^2U - \beta_{eff} + (l^2 + 2F)U\,] - (iw)^2$$
$$= -2Ut\,[DUt + (l^2 - F)\,Ut] - 2U\,[\beta_{eff} - (l^2 + F)U] + w^2$$
$$= w^2 + 2U^2(l^2 + F) - 2\beta_{eff}U + 2Ut^2(F - l^2) - 2Ut\cdot DUt$$

$$a_3 = (i)^3[f_3e_o + f_2e_1 + f_1e_2 + f_oe_3 - d_3g_o - d_2g_1 - d_1g_2 - d_og_3]$$
$$= (-i)[-d_3(g_o + d_o) - d_2(g_1 + d_1)]$$
$$= -(iU)[-i(l^2 + 2F)w - il^2w]$$
$$- w[\beta_{eff} + (l^2 + 2F)U - \beta_{eff} + l^2U]$$
$$= -2iU[-i(l^2 + F)w] - 2w[-\beta_{eff} + (l^2+F)U]$$
$$= 2\beta_{eff}w - 4wU\,(l^2 + F)$$

$$a_2 = (i)^2[f_2e_o + f_1e_1 + f_oe_2 - d_2g_o - d_1g_1 - d_og_2]$$

$$= -[f_1 e_1 - d_2(g_o + d_o) - d_1 e_1]$$

$$= -[DUt + (l^2 - 2F)Ut](l^2 Ut + DUt)$$

$$+ iw[-i(l^2 + 2F)w - il^2 w]$$

$$+ (-\beta_{eff} + l^2 U)[-\beta_{eff} + (l^2 + 2F)U]$$

$$= -l^2(l^2 - 2F)Ut^2 - DUt^2 - 2(l^2 - F)\, Ut \cdot DUt$$

$$+ 2w^2(l^2 + F) + \beta_{eff}{}^2 - 2(l^2 + F)\beta_{eff} U + l^2(l^2 + 2F)\, U^2$$

$$a_1 = (i)[f_1 e_o + f_o e_1 - d_1 e_o - d_o g_1]$$

$$= (i)[-d_1 e_o - d_o e_1]$$

$$= -(-\beta_{eff} + l^2 U)[-i(l^2 + 2F)w] - [-\beta_{eff} + (l^2 + 2F)U](-il^2 w)$$

$$= 2w[\beta_{eff}(l^2 + F) - l^2(l^2 + 2F)U]$$

$$a_o = f_o e_o - d_o g_o = -d_o g_o$$

$$= -[-il^2 w][-i(l^2 + 2F)w]$$

$$= w^2 l^2 (l^2 + 2F)$$

Appendix I: Detailed Calculations

This appendix contains the derivatations of the partial derivatives of H.

$$\frac{\partial H}{\partial U} = \quad \text{(from 3.51, and keeping on the only averaged terms)}$$

$$= 2Uk^6 - 2wk^5 + 4U(l^2+F)k^4 - 2\beta k^4 - 4w(l^2+F)k^3$$
$$- 2\beta(l^2+F)k^2 + 2l^2U(l^2+2F)k^2 - 2wl^2(l^2+2F)k$$

$$= 2Uk^4(K^2+F) - 2wk^3(K^2+F) + 2U(l^2+F)k^4 - 2w(l^2+F)k^3 - 2\beta(K^2+F)k^2$$
$$- 2wl^2(l^2+2F)k + 2l^2U(l^2+2F)k^2$$

$$= 2k^3(Uk-w)(K^2+F) + 2(Uk-w)(l^2+F)k^3 - 2\beta(K^2+F)k^2$$
$$- 2wl^2(l^2+2F)k + 2l^2U(l^2+2F)k^2$$

$$= -2k^3(w-Uk)(K^2 + 2F + l^2) - 2\beta(K^2+F)k^2$$
$$- 2wl^2(l^2+2F)k + 2l^2U(l^2+2F)k^2$$

Now w can be expanded using (3.52).

$$\frac{\partial H}{\partial U} = -2k^3(i\cdot imag(w) - \beta\frac{k}{M}(K^2+F))(K^2 + 2F + l^2) - 2\beta(K^2 + F)k^2$$
$$- 2wl^2(l^2+2F)k + 2l^2U(l^2+2F)k^2$$

$$= - 2k^3\cdot i\cdot imag(w)(K^2 + 2F + l^2) + 2k^4\frac{\beta}{M}(K^2+F)(K^2 + 2F + l^2)$$
$$- 2\beta(K^2+F)k^2 - 2wl^2(l^2+2F)k + 2l^2U(l^2+2F)k^2$$

Expanding w by equation 3.52 gives:

$$= - 2i\cdot k^3\, imag(w)(K^2 + 2F + l^2) - 2i\cdot imag(w)\, l^2(l^2+2F)k$$
$$+ 2k^4\beta(K^2+F)/K^2 + 2k^4\frac{\beta}{M}(K^2+F)\, l^2$$
$$- 2\beta(K^2+F)\, k^2 - 2\cdot real(w)\, l^2(l^2+2F)\cdot k + 2l^2U(l^2+2F)\, k^2$$

$$= - 2i\cdot k^3\, imag(w)(K^2 + 2F + l^2) - 2i\cdot imag(w)\, l^2(l^2+2F)k$$
$$+ 2k^4\beta + 2k^4\beta F\, /\, K^2 + 2k^4\frac{\beta}{M}(K^2+F)\, l^2 - 2\beta(K^2+F)\, k^2$$
$$- 2(real(w) - Uk)l^2(l^2+2F)\, k$$

$$= - 2i\cdot imag(w)\,[k^2(K^2 + 2F + l^2) + l^2(l^2+2F)]\, k$$
$$+ 2k^4\beta + 2k^4\frac{\beta}{M}(K^2+F)l^2 - 2\beta K^2\, k^2 - 2(real(w)-Uk)\, l^2(l^2+2F)\, k$$

$$+ 2\beta F k^2 (k^2/K^2 - 1)$$

$$= - 2i \cdot imag(w) (K^4 + 2FK^2) k - 2k^2 \beta l^2$$

$$+ 2k^4 \frac{\beta}{M} (K^2+F) l^2 - 2(real(w)-Uk) l^2 (l^2+2F) k - 2\beta F k^2 l^2 / K^2$$

$$= - 2i \cdot imag(w) (K^4 + 2FK^2) k + 2k^2 \frac{\beta}{M} [-l^2 M + k^2 (K^2+F) l^2]$$

$$- 2(real(w)-Uk) l^2 (l^2+2F) k - 2\beta F k^2 l^2 / K^2$$

$$= - 2i \cdot imag(w) k M + 2l^2 k^2 \frac{\beta}{M} [-M + k^2 (K^2+F)]$$

$$- 2(real(w) - Uk) l^2 (l^2+2F) k - 2\beta F k^2 l^2 / K^2$$

Expanding in real(w)

$$= - 2i \cdot imag(w) \cdot M \cdot k + 2l^2 k^2 \frac{\beta}{M} [-M + k^2 (K^2+F)]$$

$$+ 2 \frac{\beta}{M} l^2 k^2 (K^2+F) (l^2+2F) - 2\beta F k^2 l^2 / K^2$$

$$= - 2i \cdot imag(w) M k + 2l^2 k^2 \frac{\beta}{M} [-M + k^2 (K^2+F) + (K^2+F)(l^2+2F)]$$

$$- 2\beta F k^2 l^2 / K^2$$

$$= - 2i \cdot imag(w) \cdot M \cdot k + 2l^2 k^2 \frac{\beta}{M} [FK^2 + 2F^2] - 2\beta F k^2 l^2 / K^2$$

Since $M = K^2 (K^2 + 2F)$

$$= - 2i \cdot imag(w) M k + 2l^2 k^2 \frac{\beta}{M} (FK^2 + 2F^2) - 2\beta \frac{F}{M} k^2 l^2 (K^2+2F)$$

$$= - 2i \cdot imag(w) M k + 2l^2 k^2 \frac{\beta}{M} [FK^2 + 2F^2 - F(K^2+2F)]$$

$$= - 2i \cdot imag(w) M k$$

Therefore, we get (4.25), $\frac{\partial H}{\partial U} = -2i \cdot imag(w) M k$

Another term is $\frac{\partial H}{\partial Ut}$.

Using (3.51), and keeping only the zonally averaged terms, one gets:

$$\frac{\partial H}{\partial Ut} = -2Ut k^6 + 4Ut(F-l^2) k^4 - 2Ut l^2 (l^2-2F) k^2$$

$$= 2Utk^2 [-k^4 + 2(F-l^2)k^2 - l^2 (l^2-2F)]$$

$$= 2Utk^2 (-k^4 + -2l^2 k^2 - l^4 + 2FK^2)$$

$$= 2Utk^2 (-K^4 + 2FK^2)$$

$$= 2Utk^2 K^2 (2F - K^2)$$

Therefore, we get (3.57), $\frac{\partial H}{\partial Ut} = 2Ut \cdot k^2 K^2 (2F - K^2)$

Since $\beta_{eff} = \beta - DU$, $\frac{\partial H}{\partial DU} = -\frac{\partial H}{\partial \beta}$

$$\frac{\partial H}{\partial DU} = 2Uk^4 - 2wk^3 - 23k^2 + 2(l^2+F)Uk^2 - 2w(l^2+F)\,k$$

$$= 2Uk^2(K^2+F) - 2wk(K^2+F) - 2\beta k^2$$

$$= 2k(Uk-w)(K^2+F) - 2\beta k^2$$

but $w = Uk - \beta \frac{k}{M}(K^2+F) + i\cdot imag(w)$

$$= 2k\,[-i\cdot imag(w) + \beta k(K^2+F)/M\,](K^2+F) - 2\beta k^2$$

$$= -2i\cdot imag(w)\cdot k\cdot(K^2+F) + 2k^2\beta(K^2+F)^2/M - 2\beta k^2$$

$$= -2i\cdot imag(w)\cdot k\cdot(K^2+F) + 2k^2\beta[(K^2+F)(K^2+F) - M\,] / M$$

$$= -2i\cdot imag(w)\cdot k\cdot(K^2+F) + 2k^2\beta F^2 / M$$

Now $\frac{\partial H}{\partial DUt} = -2Utk^4 - 2(l^2-F)Utk^2$

$$= -2Utk^2(K^2-F)$$

Now $\frac{\partial H}{\partial k}$ is, (retaining only the zonally averaged quantities):

$$\frac{\partial H}{\partial k} = 6k^5(U^2 - Ut^2) - 10k^4Uw$$

$$+ 4k^3[w^2 + 2U^2(l^2+F) - 2\beta U + 2Ut^2(F-l^2)] + 3k^2[2\beta w - 4wU(l^2+F)]$$

$$+ 2k[-l^2(l^2-2F)Ut^2 + 2w^2(l^2+F) + \beta^2 - 2(l^2+F)\beta U + l^2(l^2+2F)U^2]$$

$$+ 2w[\beta(l^2+F) - l^2(l^2+2F)U]$$

Now, collect the imaginary terms.

$$imag(\frac{\partial H}{\partial k}) / 2imag(w) = -5k^4U + 4k^3\,real(w) + 3k^2[\beta - 2U(l^2+F)]$$

$$+ 4k(l^2+F)\,real(w) + \beta(l^2+F) - l^2(l^2+2F)U$$

$$= U\,[-5k^4 - 6k^2\,(l^2+F) - l^2\,(l^2+2F)] + 4k\,real(w)\,(K^2+F) + 2k^2\beta$$

$$+ \beta(K^2+F)$$

$$= -U\,[4k^2(K^2+F) + K^2(K^2+2F)] + 4k\cdot\mathrm{real}(w)\,(K^2+F) + 2k^2\beta + \beta(K^2+F)$$

Since $\mathrm{real}(w) = Uk - \beta\,\frac{k}{M}\,(K^2+F)$, and $M = K^2\,(K^2+2F)$

$$= -U\cdot M - 4\,\frac{\beta}{M}\,k^2(K^2+F)^2 + 2k^2\beta + \beta(K^2+F)$$

$$= -U\cdot M - 4\,\frac{\beta}{M}\,k^2[(K^2+F)^2 - M] - 2k^2\beta + \beta(K^2+F)$$

$$= -U\cdot M - 4\,\frac{\beta}{M}\,k^2\,F^2 - 2k^2\beta + \beta(K^2+F)$$

Therefore, we get (3.60),

$$\mathrm{imag}\,\frac{\partial H}{\partial k} = 2\cdot\mathrm{imag}(w)\,[-\,U\cdot M - 4\,\frac{\beta}{M}\,k^2\,F^2 - 2k^2\beta + \beta(K^2+F)]$$

Now to find real $\frac{\partial H}{\partial k}$.

$$\mathrm{real}(\partial H/\partial k) = 6k^5(U^2 - Ut^2) - 10k^4U\,\mathrm{real}(w)$$
$$+ 4k^3[\mathrm{real}(w^2) + 2U^2(l^2+F) - 2\beta U + 2Ut^2(F-l^2)]$$
$$+ 6k^2\,\mathrm{real}(w)[\beta - 2U(l^2+F)]$$
$$+ 2k[-l^2(l^2-2F)Ut^2 + 2\,\mathrm{real}(w^2)(l^2+F) + \beta^2 - 2(l^2+F)\beta U + l^2(l^2+2F)U^2]$$
$$+ 2\,\mathrm{real}(w)[\beta(l^2+F) - l^2(l^2+2F)U]$$

Defining $w = Uk + N$, and collecting terms $U^2\,k^5$, $U^2\,k^3$ gives,

$$\mathrm{real}(\partial H/\partial k) = 0\cdot k^5\,U^2 + 0\cdot k^3\,U^2 - 6k^5Ut^2 - 10k^4U\,\mathrm{real}(N)$$
$$+ 4k^3[\mathrm{real}(2UkN + N^2) - 2\beta U + 2Ut^2(F-l^2)]$$
$$+ 6k^2\,\mathrm{real}(Uk + N)\beta - 12k^2\,\mathrm{real}(N)U(l^2+F)$$
$$+ 2k[-l^2(l^2-2F)Ut^2 + 2\cdot\mathrm{real}(2UkN + N^2)(l^2+F) + \beta^2 - 2(l^2+F)\beta U$$
$$+ l^2(l^2+2F)U^2] + 2\cdot\mathrm{real}(Uk + N)[\beta(l^2+F) - l^2(l^2+2F)U]$$

Collecting terms of $\beta\cdot U$, and $k\cdot l^2(l^2+2F)\,U^2$

$$= -2k(K^2+F)\,\beta\,U + 0\cdot k\cdot l^2\,(l^2+2F)\,U^2 - 6k^5Ut^2 - 10k^4U\,\mathrm{real}(N)$$
$$+ 4k^3[\mathrm{real}(2UkN + N^2) + 2Ut^2(F-l^2)]$$
$$+ 6k^2\,\mathrm{real}(N)\beta - 12k^2\,\mathrm{real}(N)U(l^2+F)$$

$$+ 2k[-l^2(l^2-2F)Ut^2 + 2\,\mathrm{real}(2UkN + N^2)(l^2+F) + \beta^2]$$

$$+ 2\,\mathrm{real}(N)[\beta(l^2+F) - l^2(l^2+2F)U]$$

Collect terms of U real(N),

$$= - 2M\cdot U\,\mathrm{real}(N) - 2k(K^2+F)\,\beta\cdot U - 6k^5Ut^2$$

$$+ 4k^3[\mathrm{real}(N^2) + 2Ut^2(F-l^2)] + 6k^2\,\mathrm{real}(N)\beta$$

$$+ 2k[-l^2(l^2-2F)Ut^2 + 2\,\mathrm{real}(N^2)(l^2+F) + \beta^2]$$

$$+ 2\,\mathrm{real}(N)\beta(l^2+F)$$

But $\mathrm{real}(N) = -\beta\,\frac{k}{M}\,(K^2+F)$; therefore, the first two terms sum to zero.

$$= - 6k^5Ut^2 + 4k^3[\mathrm{real}(N^2) + 2Ut^2(F-l^2)] + 6k^2\,\mathrm{real}(N)\beta$$

$$+ 2k[-l^2(l^2-2F)Ut^2 + 2\cdot\mathrm{real}(N^2)(l^2+F) + \beta^2] + 2\,\mathrm{real}(N)\beta\,(l^2+F)$$

Since $N = - \beta\,\frac{k}{M}\,(K^2+F) + i\cdot\mathrm{imag}(w)$; therefore,

$$= - 6k^5Ut^2 + 4k^3[\,\beta^2k^2(K^2+F)^2/M^2 - \mathrm{imag}(w)^2 + 2Ut^2(F-l^2)]$$

$$- 6k^3\,\beta^2\,(K^2+F)/M - 2k\cdot l^2(l^2-2F)Ut^2$$

$$+ 4k\,[\,\beta^2k^2(K^2+F)^2/M^2 - \mathrm{imag}(w)^2]\,(l^2+F)$$

$$+ 2k\beta^2 - 2\beta^2\,\frac{k}{M}\,(K^2+F)(l^2+F)$$

Collecting terms of $\mathrm{imag}(w)^2$

$$= -4k\,(K^2+F)\,\mathrm{imag}(w)^2 - 6k^5Ut^2$$

$$+ 4k^3[\,\beta^2k^2(K^2+F)^2/M^2 + 2Ut^2(F-l^2)] - 6k^3\,\beta^2\,(K^2+F)/M$$

$$- 2k\,l^2(l^2-2F)Ut^2 + 4k^3\,\beta^2\,(K^2+F)^2\,(l^2+F)\,/\,M^2$$

$$+ 2k\beta^2 - 2\beta^2\,\frac{k}{M}\,(K^2+F)(l^2+F)$$

$$= -4k\cdot(K^2+F)\,\mathrm{imag}(w)^2$$

$$- 6k^5Ut^2 + 8k^3Ut^2(F-l^2) - 2k\,Ut^2\,l^2(l^2-2F)$$

$$+ 4k^5\,\beta^2\,(K^2+F)^2/M^2 - 6k^3\,\beta^2\,(K^2+F)/M + 4k^3\,\beta^2\,(K^2+F)^2\,(l^2+F)\,/\,M^2$$

$$+ 2k\beta^2 - 2\,\beta^2\,\frac{k}{M}\,(K^2+F)\,(l^2+F)$$

$$= -4k\,(K^2+F)\,\mathrm{imag}(w)^2$$

$$+ 2k\,Ut^2\,[-\,3k^4 + 4k^2\,(F-l^2) - l^2(l^2-2F)\,]$$

$$+ 2k\,\beta^2\,[\,2k^4\,(K^2+F)^2/M^2 - 3k^2\,(K^2+F)/M$$

$$+ 2k^2 (K^2+F)^2 (l^2+F) / M^2 + 1 - (K^2+F)(l^2+F)/M \ ]$$

$$= -4k (K^2+F) \, \mathrm{imag}(w)^2$$
$$+ 2k \, Ut^2 \, [\, (2k^2 + 2K^2)F - 3k^4 - 4k^2 l^2 - l^4 \ ]$$
$$+ 2k \, \beta^2 \, [\, 2k^4 (K^2+F)^2/M^2 - 3k^2 (K^2+F)/M$$
$$+ 2k^2 (K^2+F)^2 (l^2+F) / M^2 + 1 - (K^2+F)(l^2+F)/M \ ]$$

$$= -4k (K^2+F) \, \mathrm{imag}(w)^2$$
$$+ 2k \, Ut^2 \, [\, 2k^2(F - K^2) - K^2(K^2 - 2F) \ ]$$
$$+ 2 \frac{k}{M} \beta^2 \, [\, 2k^4 (K^2+F)^2/M - 3k^2 (K^2+F)$$
$$+ 2k^2 (K^2+F)^2 (l^2+F) / M + M - (K^2+F)(l^2+F) \ ]$$

$$= -4k (K^2+F) \, \mathrm{imag}(w)^2 + 2k \, Ut^2 \, [\, 2k^2(F - K^2) - K^2(K^2 - 2F) \ ]$$
$$+ 2 \frac{k}{M} \beta^2 \, [\, 2k^4 (K^2+F)^2/M - 2k^2 (K^2+F)$$
$$+ 2k^2 (K^2+F)^2 (l^2+F) / M + M - (K^2+F)(K^2+F) \ ]$$

$$= -4k (K^2+F) \, \mathrm{imag}(w)^2 + 2k \, Ut^2 \, [\, 2k^2(F - K^2) - K^2(K^2 - 2F) \ ]$$
$$+ 2 \frac{k}{M} \beta^2 \, [\, 2k^4 (K^2+F)^2/M - 2k^2 (K^2+F) + 2k^2 (K^2+F)^2 (l^2+F) / M - F^2 \ ]$$

$$= -4k (K^2+F) \, \mathrm{imag}(w)^2 + 2k \, Ut^2 \, [\, 2k^2(F - K^2) - K^2(K^2 - 2F) \ ] - 2\frac{k}{M} \beta^2 F^2$$
$$+ 4k^3 \beta^2 (K^2+F) \, [\, k^2 (K^2+F) - M + (K^2+F) (l^2+F)] / M^2$$

$$= -4k (K^2+F) \, \mathrm{imag}(w)^2 + 2k \, Ut^2 \, [\, 2k^2(F - K^2) - K^2(K^2 - 2F)]$$
$$- 2 \frac{k}{M} \beta^2 F^2$$
$$+ 4k^3 \beta^2 (K^2+F) \, [\, F^2 + (k^2 - 2K^2 + K^2 + l^2) F$$
$$+ k^2 K^2 - K^4 + K^2 l^2] / M^2$$

$$= -4k (K^2+F) \, \mathrm{imag}(w)^2 + 2k \, Ut^2 \, [\, 2k^2(F - K^2) - K^2(K^2 - 2F)]$$
$$- 2 \frac{k}{M} \beta^2 F^2 + 4k^3 \beta^2 (K^2+F) F^2 / M^2$$

Therefore, $\mathrm{real}(\frac{\partial H}{\partial k}) = -4k (K^2+F) \, \mathrm{imag}(w)^2$
$$+ 2k \, Ut^2 \, [\, 2k^2(F - K^2) - K^2(K^2 - 2F)]$$
$$+ 2 \frac{k}{M} \beta^2 F^2 \, [\frac{2}{M} k^2 (K^2+F) - 1]$$

REFERENCES

Ahlquist, J. E., 1985: Climatology of Normal Mode Rossby Waves. J. Atmos. Sci., 42, 2059-2068.

Baer, F., 1974: Hemispheric spectral statistics of available potential energy. J. Atmos. Sci., 29, 649-664.

Baines, P. G., and J. S. Frederiksen, 1978: Baroclinic instability in two-layer models. Quart. J. Roy. Meteor. Soc., 104, 45-68.

Barker, W. E., E. C. Kung, and R. C. J. Somerville, 1977: Energetics diagnosis of the NCAR general circulation model. Mon. Wea. Rev., 105, 1364-1401.

Bender, C. M., and S. A. Orszag, 1978: Advanced mathematical methods for scientists and engineers. McGraw Hill, New York.

Blackmon, M., 1976: A climatological spectral study of the 500 mb geopotential height of the Northern Hemisphere. J. Atmos. Sci., 33, 1607-1623.

Boer, G. J., and T. G. Shepperd, 1983: Large-scale two-dimensional turbulence in the atmosphere. J. Atmos. Sci., 40, 164-184.

Blackmon, M., and G. H. White, 1982: Zonal wavenumber characteristics of Northern Hemisphere transient eddies. J. Atmos. Sci., 39, 1985-1998.

Boville, B. A, 1980: Amplitude vacillation on an f-plane. J. Atmos. Sci., 37, 1413-1423.

Branscome, L. E., 1983: A parameterization of transient eddy heat flux on a beta-plane. J. Atmos. Sci., 40, 2508-2521.

Burger, A. P., 1958: Scale considerations of planetary motions of the atmosphere. Tellus, 10, 195-205.

Charney, J. G., 1947: The dynamics of long waves in a baroclinic westerly current. J. Meteor., 4, 135-162.

Charney, J. G., 1971: Geostrophic Turbulence. J. Atmos. Sci., 28, 1087-1095.

Charney, J. G., and J. G. DeVore, 1979: Multiple flow equilibria in the atmosphere and blocking. J. Atmos. Sci., 36, 1205-1216.

Charney, J. G., and A. Eliassen, 1949: A numerical method for predicting the perturbations of middle latitude westerlies. Tellus, 1, 38-54.

Charney, J. G., and M. E. Stern, 1962: On the stability of internal baroclinic jets in a rotating atmosphere. J. Atmos. Sci., 19, 159-172.

Clark, J. H. E., 1978: The stability of ultralong waves on a mid-latitude beta-plane. Quart. J. Royal Meteor. Soc., 104, 429-445.

Dickinson, R. E., 1968: Planetary Rossby waves propagating vertically through weak Westerly wind wave guides. J. Atmos. Sci., 25, 984-1002.

Frederiksen, J. S., 1978: Instability of planetary waves and zonal flows on the regions of cyclogensis. Quart. J. Royal Meteor. Soc., 104, 841-872.

Frederiksen, J. S., 1979: The effects of long planetary waves on the regions of cyclogensis: linear theory. J. Atmos. Sci., 36, 195-204.

Frederiksen, J. S., 1979: Baroclinic instability of zonal flows and planetary waves in multilevel models on a sphere. J. Atmos. Sci., 36, 2320-2335.

Frederiksen, J. S., 1980: Zonal and meridional variations of eddy fluxes by long planetary waves., Quart. J. Royal Meteor. Soc., 106, 195-204.

Frederiksen, J. S., 1981: Scale selection and energy spectra of disturbances in Southern Hemisphere flows. J. Atmos. Sci., 38, 2573-2584.

Frederiksen, J. S., 1982: A unified three-dimensional instability theory of the onset of blocking and cyclogensis. J. Atmos. Sci., 39, 962-982.

Frederiksen, J. S., 1983: Disturbances and eddy fluxes in Northern Hemsphere flows: Instability of three-dimensional January and July flows. J. Atmos. Sci., 40, 836-855.

Frederiksen, J. S., 1983: A unified three-dimensional instability theory of the onset of blocking and cyclogensis. II: Teleconnection Patterns, J. Atmos. Sci., 40, 2724-2731.

Gall, R., 1976: Structural changes of growing baroclinic waves. J. Atmos Sci., 33, 374-390.

Gall, R., R. Blakeslee, and R. C. J. Somerville, 1979a: Baroclinic instability and the selection of the zonal scale of the transient eddies of middle latitudes. J. Atmos. Sci., 36, 767-784.

Gall, R., R. Blakeslee, and R. C. J. Somerville, 1979b: Cyclone-scale forcing of ultra-long waves. J. Atmos. Sci., 36, 1692-1698.

Geisler, J. E., and R. R. Garcia, 1977: Baroclinic Instability at long wavelengths on a beta plane. J. Atmos. Sci., 34, 311-321.

Gent, P. R., 1974: Baroclinic instability of a slowly varying zonal flow. J. Atmos. Sci., 31, 1983-1994.

Gill, A. E., 1974: The stability of planetary waves on an infinite beta-plane. Geophysical Fluid Dyn., 6, 29-47.

Gill, A. E., 1982: Atmosphere-Ocean Dynamics. Academic Press, New York.

Golub, G. H., and C. F. Van Loan, 1983: Matrix Computations. The John Hopkins University Press, Baltimore.

Gottlieb, D., and S. A. Orszag, 1977: Numerical Analysis of Spectral Methods: Theory and Applications. Society for Industrial and Applied Mathematics (SIAM), Philadelphia.

Green, J. S. A., 1970: Transfer properties of the large scale eddies and the general circulation of the atmosphere. Quart. J. Royal Meteor. Soc., 96, 157-185.

Gutowski, W. J., Jr., 1983: Vertical eddy heat fluxes and the temperature structure of the mid-latitude troposphere. Ph.D. Thesis, Massachusetts Institute of Technology.

Gutowski, W. J., Jr., 1985: A simple model for the interaction between vertical eddy heat fluxes and static stability. J. Atmos. Soc., 42, 346-358.

Gutowski, W. J., Jr., 1985: Baroclinic Adjustment and Midlatitude Temperature Profiles. J. Atmos. Soc., 42, 1733-1745.

Haidvogel, D. B., I. M. Held, 1980: Homogenous quasi-geostrophic turbulence driven by a uniform temperature gradient. J. Atmos. Sci., 37, 2644-2660.

Hasselman, K., 1967: A criterion for nonlinear wave stability. J. Fluid Mech., 30, 737-739.

Hayashi, Y., and D. G. Golder, 1983: Transient Planetary Waves Simulated by GFDL Spectral General Circulation Models. Part I: Effects Mountains. J. Atmos. Sci., 40, 941-950.

Hayashi, Y., and D. G. Golder, 1983: Transient Planetary Waves Simulated by GFDL Spectral General Circulation Models. Part II: Effects of Nonlinear Energy Transfer. J. Atmos. Sci., 40, 951-957.

Held, I. M., 1975: Momentum transport by quasi-geostrophic eddies. J. Atmos. Sci., 35, 572-576.

Held, I. M., 1978: The vertical scale of an unstable baroclinic wave and its importance for eddy heat flux parameterizations. J. Atmos. Sci., 35, 572-576.

Held, I. M., 1983: Stationary and quasi-stationary eddies in the extra-tropical troposphere: theory. Large-Scale Dynamical Processes in the Atmosphere, Ed. B. Hoskins, and R. Pearce, Academic Press, New York.

Holopainen, E. O., 1970: An observational study of the energy balance of the stationary disturbances in the atmosphere. Quart. J. Roy. Meteor. Soc., 96, 626-644.

Holopainen, E. O., 1978: On the dynamic forcing of the long-term mean flow by large scale Reynold's stresses. J. Atmos. Sci., 35, 1596-1604.

Holopainen, E. O., 1983: Transient eddies in mid-latitudes: observations and interpretation. Large-Scale Dynamical Processes in the

Atmosphere, Ed. B. Hoskins, and R. Pearce, Academic Press, New York.

Holopainen, E. O., L. Rontu, and N.-C. Lau, 1982: The effect of large-scale transient eddies on the time-mean flow in the atmosphere. J. Atmos. Sci., 39, 1972-1984.

Holton, J. R., 1972: An Introduction to Dynamic Meteorology. Academic Press, New York.

Hoskins, B. J, and D. J. Karoly, 1981: A steady linear response of a spherical atmosphere to thermal and orographic forcing. J. Atmos. Sci., 38, 1179-1196.

Hoskins, B. J, and I. N. James, G. H. White, 1983: The shape, propagation of large scale weather systems. J. Atmos. Sci., 40, 1595-1612.

Hoskins, B. J, and M. J. Revell, 1981: The most unstable long wavelength baroclinic instability modes. J. Atmos. Sci., 38, 1498-1503.

Kalnay-Rivas, E., and L.-O. Merkine, 1981: A simple mechanism for blocking. J. Atmos. Sci., 38, 2077-2091.

Karoly, D. J., and B. J. Hoskins, 1982: Three dimensional propagation of planetary waves. J. Meteor. Soc. Japan, 60, 109-123.

Kao, S. K., and J. F. Sabendoef, 1970: The large-scale meridional transport of sensible heat in wavenumber-frequency space. Tellus, 22, 172-185.

Kasahara, A., 1980: Effect of zonal flows on the free oscillations of a barotropic atmosphere. J. Atmos. Sci., 37, 917-929. Corrigendum, 1981: J. Atmos. Sci., 38, 2284-2285.

Kim, K, 1978: Instability of baroclinic Rossby waves; energetics in a two-layer ocean. Deep-Sea Res., 25, 795-814.

Kirkwood, E., and J. Derome, 1977: Some effects of the upper boundary condition and vertical resolution on modeling forced planetary waves. Mon. Wea. Rev., 105, 1239-1251.

Kung, E. C., 1977: Energy sources in middle latitude synoptic disturbances. J. Atmos. Sci., 34, 1352-1365.

Lau, N.-C., 1979a: The structure and energetics of transient disturbances in the Northern Hemisphere wintertime circulation. J. Atmos. Sci., 36, 982-995.

Lau, N.-C., 1979b: The observed structure of tropspheric stationary waves and the local balances of vorticity and heat. J. Atmos. Sci., 36, 996-1016.

Lau, N.-C., G. H. White, and R. L. Jenne, 1981: Circulation statistics for the extratropical Northern Hemisphere based on NMC analyses. NCAR Tech. Note 171+STR, April 1981. Available from the National Center for Atmospheric Reasearch, Boulder, Colorado.

Lau, N.-C., and E. O. Holopainen, 1984: Transient eddy forcing of the time-mean flow as identified by geopotential tendencies. J. Atmos. Sci., 41, 313-328.

Lau, N.-C., and J. M. Wallace, 1979: On the distribution of horizontal transports by transient eddies in the northern hemisphere wintertime circulation. J. Atmos. Sci., 36, 1844-1861.

Lin, C. A., 1980: Eddy heat fluxes and stability of planetary waves. Part I. J. Atmos. Sci., 37, 2353-2372.

Lin, C. A., 1980: Eddy heat fluxes and stability of planetary waves. Part II. J. Atmos. Sci., 37, 2373-2380.

Lindzen, R. S., 1967: Planetary waves on beta planes. Mon. Wea. Rev., 95, 441-451.

Lindzen, R. S., and A. J. Rosenthal, 1981: A WKB asymptotic analysis of baroclinic instability. J. Atmos. Sci., 38, 619-629.

Lindzen, R. S., B. Farrell, and K.-K. Tung: The concept of wave overreflection and its application to baroclinic instability. J. Atmos. Sci., 37, 44-63.

Lindzen, R. S., D. M. Straus, and B. Katz, 1984: An observational study of large-scale atmospheric Rossby waves during FGGE. J. Atmos. Sci., 41, 1320-1335.

Lindzen, R., S., E. S. Batten, and J.-W. Kim, 1968: Oscillations in Atmospheres with Tops. Mon. Wea. Rev., 96, 133-140.

Lindzen, R. S., T. Aso, and D. Jacqmin, 1982: Linearized calculations of stationary waves in the atmosphere. J. Meteor. Soc. Japan, 60, 66-77.

Lorenz, E. N., 1971: N-cycle time-differencing for stepwise numerical integration. Mon. Wea. Rev., 644-648.

Lorenz, E. N., 1972: Barotropic instability of Rossby wave motion. J. Atmos. Sci., 29, 258-269.

MacVean, M. K., 1985: Long-wave growth by baroclinic processes. J. Atmos. Sci., 42, 1089-1101.

Mesinger, F, and A. Arakawa, 1976: Numerical methods used in atmospheric models. Vol. 1, Garp Publications Series No. 17, World Meteor. Organization.

Mudrick, S. E. 1982: A study of the adequace of quasi-geostrophic dynamics for modeling the effects of cyclone waves on the larger scale flow. J. Atmos. Sci., 39, 2414-2430.

Niehaus, M. C. W., 1980: Instability of non-zonal baroclinic flows. J. Atmos. Sci., 37, 1447-1463.

Niehaus, M. C. W., 1981: Instability of non-zonal baroclinic flows: Multiple-scale analysis. J. Atmos. Sci., 38, 974-987.

Nigam, S., 1983: On the structure ond forcing of tropospheric stationary waves., Ph.D. thesis, Princeton University, Princeton, New Jersey.

Nigam, S., I. M. Held and S. Lyons, 1986: Simulation of the stationary eddies in a GCM. (In preparation.)

North, G. R., R. F. Cahalan, and J. A. Coakley Jr., 1981: Energy balance climate models. Rev. of Geophysics and Space Physics, 19, 91-121.

Opsteegh, J. D., and A.-D. Verneker, 1982: A simulation of the January standing wave pattern including the effects of transient eddies. J. Atmos. Sci., 39, 734-744.

Pedlosky, J., 1975: On secondary baroclinic instabiliy and the meridional scale of motion in the ocean. J. Phys. Ocean., 5, 603-607.

Pedlosky. J., 1979: Geophysical Fluid Dynamics. Springer-Verlag, New York.

Petterssen, S., 1956: Weather Analysis and Forecasting. Vol. 1. Motion and Motion systems. McGraw Hill, New York.

Petterssen, S., and S. J. Smebye, 1971: On the development of extratropical cyclones. Quart. J. Royal Meteor. Soc., 97, 457-482.

Phillips, N. A., 1954: Energy transformations and meridional circulations associated with simple baroclinic waves in a two-level, quasi-geostrophic model. Tellus, 6, 27 3-286.

Phillips, N. A., 1959: An example of non-linear computational instability. The Atmosphere and the Sea in Motion, Rossby Memorial Volume, Rockefeller Institute Press, New York.

Pierrehumbert, R. T., 1984: Local and Global Baroclinic Instability of Zonally Varying Flow. J. Atmos. Sci., 41, 2141-2162.

Pratt, R. W., and J. M. Wallace, 1976: Zonal propagation characteristics of large-scale fluctuations in the mid-latitude troposphere. J. Atmos. Sci., 33, 129-146.

Rienhold, B. B., and R. T. Pierrehumbert, 1982: Dynamics of Weather Regimes: Quasi-stationary waves and blocking. Mon. Wea. Rev., 110, 1105-1145.

Roads, J. O., 1980: Climatic anomaly experiments in middle-latitudes. Tellus, 32, 410-427.

Roads, J. O., 1982: Forced, stationary waves in a linear, stratified, quasi-geostrophic atmosphere. J. Atmos. Sci., 39, 2431-2449.

Salmon, R., 1980: Baroclinic instability and geostrophic turbulence. Geophys. Astrophys. Fluid Dyn., 15, 167-211.

Salmon, R., 1982: Geostrophic Turbulence. Topics in Ocean Physics, Corso LXXX, 30-78. Soc. Italiana di Fisica, Bologna, North-Holland

Salmon, R., M. C. Hendershott, 1976: Large scale air-sea interactions with a simple general circulation model. Tellus, 28, 228-242.

Saltzman, B., 1970: Large-scale atmospheric energetics in the wave-number domain. Rev. Geophys. Space Phys., 8, 289-302.

Saltzman, B., 1978: A survey of statistical-dynamical models of the terrestial climate. Adv. Geophysics, Vol. 20, Academic Press, New York.

Shepherd, T. G., 1984: A barotropic study of waves and turbulence in the presence of a large-scale zonal jet. Ph.D. thesis, Mass. Inst. of Technology, Cambridge, Massachusetts.

Shutts, G. J., 1983: Parameterization of traveling weather systems in a simple model of large-scale atmospheric flow. Adv. Geophysics, Vol. 25, Academic Press, New York.

Shutts, G. J., 1983: The propagation of eddies in diffluent jetstreams: Eddy vorticity forcing of 'blocking' flow fields. Quart. J. Roy. Meteor. Soc., 109, 737-761.

Simmons, A. J., and B. J. Hoskins, 1978: The life cycles of some nonlinear baroclinic waves. J. Atmos. Sci., 35, 414-432.

Simmons, A. J., and B. J. Hoskins, 1980: Barotropic influences on the growth and decay of nonlinear baroclinic waves. J. Atmos. Sci., 37, 1679-1684.

Smagorinsky, J., 1953: The dynamical influence of large-scale heat sources on the quasi-stationary mean motions of the atmosphere. Quart. J. Royal Meteor. Soc., 79, 342-366.

Smith, R. B., 1979: The influence of mountains on the atmosphere. Adv. Geophysics, Vol. 21, Academic Press, New York.

Stone, P. H., 1974: The meridional variations of the eddy heat fluxes by baroclinic waves and their parameterizations. J. Atmos. Sci., 31, 444-456.

Stone, P. H., 1978: Baroclinic Adjustment. J. Atmos. Sci., 35, 561-571.

Stone, P. H., and J. H. Carlson, 1979: Atmospheric lapse rates and their parameterization. J. Atmos. Sci. 36, 415-423.

Stone, P. H., and D. A. Miller, 1980: Empirical relations between seasonal changes in meridional temperature gradients and meridional fluxes of heat. J. Atmos. Sci., 37, 1708-1721.

Tsay, C. Y., and S.-K. Kao, 1978: Linear and nonlinear contributions to the growth and decay of the large-scale atmospheric waves and jet stream. Tellus, 3, 1-14.

Tenenbaum, J., 1979: Spectral and spatial energetics of the GISS model atmosphere. Mon. Wea. Rev., 104, 15-30.

Tomatsu, K., 1979: Spectral energetics of the troposphere and lower stratosphere. Advances in Geophysics, Vol. 21, Academic Press, New York.

Vallis, G. K., and J. O. Roads, 1984: Large-scale stationary and turbulent flow over topography. J. Atmos. Sci., 41, 3255-3271.

Wallace, J. M., 1983: The climatological mean stationary waves: observational evidence. Large-Scale Dynamical Processes in the Atmosphere, Ed. B. Hoskins, and R. Pearce, Academic Press, New York.

Wallace, J. M., and M. L. Blackmon, 1983: Observations of low-frequency variability. Large-Scale Dynamical Processes in the Atmosphere, Ed. B. Hoskins, and R. Pearce, Academic Press.

White, A. A., 1982: Zonal translation properties of two quasi-geostrophic systems of equations. J. Atmos. Sci., 39, 2107-2118.

White, A. A., and J. S. A. Green, 1982: A non-linear atmospheric long wave model incorporating parameterizations of transient baroclinic eddies. Quart. J. Royal Meteor. Soc., 108, 55-85.

Yao, M.-S., 1980: Maintenance of quasi-stationary waves in a two level quasi-geostrophic spectral model with topography. J. Atmos. Sci., 37, 29-43.

Yeh, T.-C., 1949: On energy dispersion in the atmosphere. J. Meteor., 6, 1-16.

Young, R. E., and G. L. Villere, 1985: Nonlinear forcing of planetary scale waves by amplifying unstable baroclinic eddies generated in the troposphere. J. Atmos. Sci., 42, 1991-1990.

Youngblut, C., and T. Sasamori, 1980: The nonlinear effects of transient and stationary eddies on the winter mean circulation, Part I diagnostic analysis. J. Atmos. Sci., 37, 1944-1957.